

STAR-FORMATION BIMODALITY IN EARLY-TYPE GALAXIES

A. AMBLARD^{1,2}, L. RIGUCCINI^{1,2}, P. TEMI¹, S. IM^{1,2}, M. FANELLI^{1,2}, P. SERRA³

Draft version July 29, 2021

ABSTRACT

We compute the properties of a sample of 221 local early-type galaxies with a spectral energy distribution (SED) modelling software, CIGALEMC. Concentrating on the star forming activity and dust contents, we derive parameters such as the specific star formation rate, the dust luminosity, dust mass and temperature. 52% of our sample is composed of elliptical (E) galaxies and 48% of lenticular (S0) galaxies. We find a larger proportion of S0 galaxies among galaxies with a large specific star formation rate (sSFR) and large specific dust emission. The stronger activity of S0 galaxies is confirmed by larger dust masses. We investigate the relative proportion of active galactic nuclei (AGN) and star-forming (SF) galaxies in our sample using spectroscopic SDSS data and near-infrared selection techniques, and find a larger proportion of AGN dominated galaxy in the S0 sample than the E one. This could corroborate a scenario where blue galaxies evolve into red ellipticals by passing through a S0 AGN active period while quenching its star formation. Finally, we find a good agreement comparing our estimates with color indicators.

Subject headings: galaxies : elliptical and lenticular; galaxies: ISM; infrared: galaxies; infrared: ISM

1. INTRODUCTION

Elliptical (E) and lenticular (S0) galaxies, early-type galaxies (ETGs), are among the most massive galaxies today. Their poorly known formation is subject to much debate.

The two main scenarios of ETG formation are the monolithic and hierarchical models. In the monolithic view, ETGs assembled most of their mass quite early on ($z > 2\text{-}3$) as they merge with smaller substructures, they are characterized by a strong early star formation (SF) and then evolve passively into galaxies we see today. In the hierarchical view, ETGs are formed by mergers of galaxies either rich (“wet” merger) or poor (“dry” merger) in gas. In this picture, it is not clear which merging path(s) ETGs follow.

ETGs constitute the majority of the red galaxies ($\sim 75\%$ Driver et al. 2006) in the bimodal color distribution of galaxies, their stellar population already transitioned from blue to red as their star-formation ceased (Faber et al. 2007; Hughes & Cortese 2009). Indeed the most massive ($> 10^{10} M_{\odot}$) ETGs are red and with little star formation (Temi et al. 2009b); their stellar content formed at an early epoch (Trager et al. 2000; Cimatti et al. 2004; Thomas et al. 2005; Temi et al. 2005a,b) and passively evolved to their present form.

However, multi-frequency observations in recent years have revealed that on closer inspection many E galaxies and even more S0 galaxies do in fact contain dust and cold gas in amounts that cannot be ignored (Young et al. 2011; Temi et al. 2007b,a), sufficient to generate appreciable star formation at rates as large as several $M_{\odot} \text{ yr}^{-1}$ (Temi et al. 2009a,b).

Recent ultra-violet (UV) observations of large samples of ETGs present clear evidence of current star-formation (Yi et al. 2005; Schawinski et al. 2007a; Kaviraj et al. 2007, 2008; Kaviraj 2010; Salim et al. 2012; Fang et al. 2012; Barway et al. 2013). Using UV-optical colors, Kaviraj et al. (2007) show that at least $\sim 30\%$ of UV-selected early-type

galaxies at $z < 0.11$ have evidence of recent star-formation within the last 1 Gyr. The contribution from old stars to the UV flux is however uncertain.

The remarkable diversity of nearby ETG galaxies is most clearly expressed in infrared emission where many S0 galaxies exhibit a range of unusual properties not often found in ellipticals. Temi et al. (2009a,b) showed a banana-shaped mid ($24\mu\text{m}$) and far ($70\mu\text{m}$) correlation containing only early-type galaxies. While S0 galaxies are spread along the entire correlation, most elliptical galaxies, for which star formation is negligible, occupy an extended region with a nearly flat $\log(L_{24}/L_K) \approx 30.2$. S0 galaxies have a star-forming diversity that mimics infrared colors of galaxies of any type. The SAURON survey (Bacon et al. 2001; de Zeeuw et al. 2002) found that E and S0 can be separated into slow and fast rotators, the slow rotator group being composed mostly of ellipticals (Cappellari et al. 2007; Emsellem et al. 2007). Building in part on this finding, the ATLAS^{3D} project (Cappellari et al. 2011a) observed a sample of 260 local early-type galaxies (complete within 42 Mpc at -21.5 K band magnitude) in a large number of wavelengths, including optical integral-field spectroscopy (IFS). Emsellem et al. (2011) showed that most ETGs are fast rotators ($86 \pm 2\%$) and Cappellari et al. (2011b) showed that slow rotators are in general round ellipticals (E4 or rounder). They also showed that the slow/fast rotators classification improves the kinematic morphology-density T - Σ relation over the E/S0 classification and argue that the kinematic classification may be more accurate than the morphologic classification which is plagued by projection effects.

Lenticular S0 galaxies differ morphologically from E galaxies having stellar distributions in bulges and rotating disks that are somewhat less concentrated than E galaxies. In this paper, we investigate differences between Elliptical and Lenticular local galaxy populations. Although the distinction between E and S0 morphologies is not always easy, many local S0 galaxies are quite distinct from ellipticals, having attributes consistent with recent star formation: significantly larger mid and far infrared luminosities, large masses of molecular gas, and younger stellar ages as inferred from optical absorption line spectra. Since S0 galaxies at higher

¹ NASA Ames Research Center, Moffett Field, CA, USA

² BAER Institute, Sonoma, CA, USA

³ IAS, CNRS (UMR8617), Université Paris-Sud 11, Bâtiment 121, F-91400 Orsay, France

redshift are difficult to distinguish from E galaxies, particularly if the S0s are face-on, the two types of galaxies are often combined. Therefore results from large surveys of “early-type” galaxies that combine S0 and E galaxies will be misleading if applied only to E. However, the distribution of old population starlight in low redshift S0s, which are of interest here, define a unique and rather large fraction of early type galaxies.

As our main tool, we use a SED fitter, CIGALEMC (Serra et al. 2011), capable of modeling our galaxy SED from UV to mm wavelength, which allows us to determine the stellar mass, dust luminosity, stellar population age, bolometric luminosity and star formation rate of our galaxies in a less ambiguous manner than single-band photometric indicators. In the second part of the paper, we concentrate on the far-infrared emission and estimate the dust mass and temperature of our sample. We compare these quantities with the ones estimated from the full SED and distinguish the two sub-population. In the third part, we investigate the proportion of AGN in both the E and S0 population using SDSS spectroscopic and NIR selection criteria. In the last part, we compare our analysis with optical, UV and Far-Infrared colors.

2. THE DATA

We base our work on a sample of 225 Early-Types Galaxies (ETGs) from Temi et al. (2009b). As pointed out in their work, a few sources present an uncertain morphological classification, in particular galaxies NGC 3656 and NGC 5666. We use the morphological type T from the HyperLeda database⁴ (Paturel et al. 2003) and exclude the 2 following sources: NGC3656 and NGC5666 because of the positive value of their T parameter, indicating that they are not ETGs as expected. Our sample is composed of 116 ellipticals (52 % of the sample), 35 E-S0 (16%), 48 S0 (22%) and 22 S0-a (10%), which is roughly the same distribution as in Temi et al. (2009b). In order to perform a reliable SED-fitting for each source, we need to have access to a large fraction of their SED from the UV to the FIR. To facilitate the data analysis we concentrate primarily on 6 instruments which span these wavelengths and have extensive sky coverage : GALEX for the UV part, SDSS for the optical, 2MASS and IRAC-Spitzer for the near-Infrared (NIR) and mid-Infrared (MIR), and MIPS-Spitzer and IRAS for the mid and far-IR. We also use public data from Herschel-SPIRE(Griffin et al. 2010) when available.

We address the representativeness of our sample using the wide (2 deg^2) equatorial COSMOS field (Scoville et al. 2007). With a large statistic and multi wavelength datasets, and in particular an optical catalog with morphological indexes and a $24\mu\text{m}$ sources catalog, it is a good source to answer this question. We select 4 605 “local” sources ($z < 0.09$, about $D < 400 \text{ Mpc}$) in the COSMOS optical catalog(Illert et al. 2009). 3 873 of these sources are in the morphological catalog of Tasca et al. (2009) (i.e. 84%), and 994 are classified as ETGs (i.e. 26 %)). In the $24\mu\text{m}$ catalog (Le Floc'h et al. 2009) 236 sources are lying at $D < 400 \text{ Mpc}$, 206 are in the morphological catalog (i.e. 87%), and 64 sources are classified as ETGs (i.e. 31%). The percentage of $24\mu\text{m}$ selected ETGs is slightly larger than the optical selected one, but it is not statistically significant, a $24\mu\text{m}$ selection does not bias much an ETG sample.

We also compared the absolute B magnitude distribution

of these three ETGs samples (COSMOS optical, COSMOS $24\mu\text{m}$ and our sample). The comparison between the distribution of our sample of ETGs in absolute B magnitude with the one from the optically selected ETGs in COSMOS shows that they cover the same range of M_B but the COSMOS distribution is slightly shifted towards brightest sources than the distribution of our sources, similarly to the COSMOS $24\mu\text{m}$ sample. We conclude that our ETGs sample is quite representative of the overall distribution of ETGs in the local Universe.

2.1. UV Observations

To cover the UV part of the spectrum we use GALEX GR6 data release⁵ , since it covers $25,000 \text{ deg}^2$ of the sky with a sensitivity down to $m_{AB}=21$ for the All Sky Imaging Survey (AIS) and $m_{AB}=25$ for the Deep Imaging Survey (DIS) (Morrissey et al. 2007). GALEX is a NASA satellite, equipped with two microchannel plate detectors imaging in the near-UV (NUV) at 2316 \AA and far-UV (FUV) at 1539 \AA (Morrissey et al. 2007) and a grism to disperse light for low resolution spectroscopy. The source position accuracy is about 0.34 arcseconds and the angular resolution of FUV and NUV is respectively 4.3 and 5.3 arcseconds. We find a match in GALEX catalog for 199 sources of our sample in the FUV band and 198 sources in the NUV band. We apply a galactic dust extinction correction, $A(\text{FUV})/E(\text{B-V})=8.376$ $A(\text{NUV})/E(\text{B-V})=8.741$, to GALEX data, assuming Milky Way dust with $R_v=3.1$ (Cardelli et al. 1989; Marino et al. 2011), and using NASA/IPAC Extragalactic Database (NED) E(B-V) values. The UV emission is a good indicator of the dust content and star formation rate of galaxies in our sample when compared with the optical data.

2.2. Optical and NIR Observations

We choose SDSS data to cover the optical range of the SED of our galaxies, given the large part of the sky covered by SDSS ($14,555 \text{ deg}^2$). The SDSS data have an angular resolution of about 1.5 arcseconds. We retrieve SDSS data through the Imaging Query Form interface⁶. 147 sources from our sample have an optical counterpart in the 5 bands of the Sloan Digital Sky Survey (SDSS), u, g, r, i and z (respectively $0.335 \mu\text{m}$, $0.469 \mu\text{m}$, $0.616 \mu\text{m}$, $0.748 \mu\text{m}$ and $0.893 \mu\text{m}$). At Near-Infrared wavelength, we use the extended source catalog of the Two Micron All Sky Survey (2MASS) data , which contains 1,647,599 sources. 2MASS resolution is about 2 arcseconds and its source position accuracy is about 0.5 arcseconds. The $10-\sigma$ limit magnitude in the 3 filters J, H, K_s is about 14.7, 13.9, 13.1⁷. 220 Galaxies in our sample have counterparts in the 3 different filters, J, H and K_s bands, at $1.24 \mu\text{m}$, $1.66 \mu\text{m}$ and $2.16 \mu\text{m}$ respectively.

2.3. InfraRed Observations

The *Spitzer* Space Telescope provides data in the near-IR and mid-IR with the IRAC camera with 4 channels imaging at 3.6, 4.5, 5.6 and $8 \mu\text{m}$ with about 2 arcsecond angular resolution and in the mid and far-IR with the MIPS instrument observing at 24, 70 and $160 \mu\text{m}$ at angular resolution of 6, 18 and 40 arcseconds (Rieke et al. 2004). We download data for our galaxies from the NASA/IPAC Infrared Science

⁵ <http://galex.stsci.edu/GR6/>

⁶ <http://skyserver.sdss3.org/dr9/en/tools/search/IQS.asp>

⁷ http://www.ipac.caltech.edu/2mass/releases/allsky/doc/sec4_5.html

Archive⁸. Reduction of the data follows Temi et al. (2009b) for MIPS and a similar treatment is applied on IRAC data to produce maps. The Mosaicing and Pointsource Extraction (MOPEX)⁹ is used to process BCD data into corrected images and to co-add them into a mosaic. To compute IRAC fluxes, a number of packages in the Image Reduction and Analysis Facility (IRAF)¹⁰ are used for unit conversion, to remove artifacts, and to perform aperture photometry. We use the centroid sky fitting algorithm of the PHOT function (part of the APPHOT IRAF package) with an appropriate annulus and dannulu value and a constant photometric weighting scheme for wphot. For MIPS, flux densities are extracted from apertures that cover the entire optical disk (R25). Sky subtraction is performed by averaging values from multiple apertures placed around the target, avoiding any overlap with the faint extended emission from the galaxy. Foreground stars and background galaxies present in the original mosaiced images are deleted before flux extraction is performed. These are identified by eye and cross-checked using surveys at other wavelengths (Digital Sky Survey and 2MASS). Fluxes of each IRAC and MIPS channel are obtained in mJy unit. We obtain a flux measurement for 165, 173, 164, 171, 204, 121, 93 of our galaxies at 3.6, 4.5, 5.6, 8, 24, 70, 160 μm respectively. In order to have better constraints on the peak of the SED in the IR, to derive for example the dust temperature of our sources, we also include the observations from the *Infrared Astronomical Satellite* (IRAS). We obtain the IRAS dataset for our sample using the Scan Processing and Integration tool (Scanpi) which gives us the fluxes and errors in the 4 IRAS bands: 12, 25, 60 and 100 μm . The larger errors and the poor angular resolution (4 arcminutes at 100 μm) of the IRAS observations compared with the rest of the available data encouraged us to check if the IRAS data agree well with the other data points. After removing the IRAS observations in case of conflict, we finally have a detection in the 12 μm -band for 154 sources, in the 25 μm -band for 124 sources, in the 60 μm -band for 135 sources and in the 100 μm -band for 141 sources.

The launch of the *Herschel*¹¹ telescope allows unprecedented precisions at FIR wavelength. We use public level2 data, which are maps of Astronomical Observation Requests (AORs), from the SPIRE instrument, downloaded from the Herschel Science Archive¹². The SPIRE instrument observes at 250, 350 and 500 μm with an angular resolution of about 18, 25, 36 arcseconds (Griffin et al. 2010). Level2 maps are combined into a single map for each object using a simple pixel co-addition technique (several AORs were requested for most objects). We subtract a background level from each image, the background is estimated by taking a median at 3 arcminutes around the source. We compute the size of each galaxy on our 250 μm map by grouping neighboring pixels with a signal to noise ratio greater than 2 around the source location using a friend-of-friend algorithm. We then perform an aperture photometry of this angular size at each wavelength. The size of galaxies, which surface brightness is too low to perform this measurement (no pixels with a S/N larger than

2), is taken to be the major axis diameter from the NED. The aperture size is inspected by eyes to check for multiple sources or complex morphology. We obtained data for 75 galaxies and detected at the 5 σ confidence level 31 sources at 250 μm , 31 at 350 μm and 25 at 500 μm .

3. SED FITTING

To fit the spectral energy distribution (SED) of our galaxies, we use CIGALEMC¹³ (Serra et al. 2011) which is a modified version of the Code Investigating GALaxy Emission (CIGALE Noll et al. 2009; Giovannoli et al. 2011). CIGALEMC uses a Markov Chain Monte Carlo sampling of the CIGALE parameters which allows to increase the size of the parameter space covered and a more efficient sampling of it. CIGALEMC uses the Maraston (2005) stellar population model and we use the Salpeter initial mass function (IMF) (Salpeter 1955). The Salpeter IMF is in general a better match for massive early-type galaxies as has been found previously (Grillo et al. 2009; Auger et al. 2010; Treu et al. 2010; Spinelli et al. 2011) using stellar dynamics and gravitational lensing. The Maraston (2005) stellar population model includes a realistic treatment of the thermally pulsating asymptotic giant branch (TP-AGB). The TP-AGB phase modelling is important to derive an accurate stellar mass (Maraston et al. 2006; Ilbert et al. 2010). When fitting the data, we assume an exponentially decreasing star formation rate (SFR) for both the old and new star population following Giovannoli et al. (2011). The age of the old stellar population is fixed to 10 Gyr and the e-folding time of the new population is fixed to 20 Gyr, which corresponds effectively to a constant bursting time (Giovannoli et al. 2011; Serra et al. 2011). We use the Calzetti et al. (1994); Calzetti (1997) attenuation to describe the dust absorption of star light. We do not add any modification to the Calzetti curve, like a 2175 Å UV bump or a change of slope. The attenuation is modelled independently for the old and young star populations, the attenuation factor for the young population is A_{ySP} (V band attenuation) and there is a reduction factor f_V for the old stellar population ($A_{ySP} \times f_V$). The IR emission from the dust is computed using Dale & Helou (2002) model, which is composed of 64 templates parametrized by a slope α . This slope represents the power-law slope of the dust mass over the heating intensity. Dale & Helou (2002) followed Desert et al. (1990) approach by dividing their dust emission sources into large grains, small grains and PAHs. They normalized these components using observations from IRAS, ISO and SCUBA. CIGALEMC also includes a model for the AGN emission, using the AGN templates from Siebenmorgen et al. (2004b,a) and a parameter for its amplitude f_{AGN} .

The eight free parameters of the fit, τ_{old} , t_{new} , f_{ySP} , A_{ySP} , f_V , α , f_{AGN} , M_{gal} , are described in table 1 along with their priors.

In the analysis of the SEDs, we use some derived parameters : SFR, age_{D4000} , L_{bol} , L_{dust} , M_* ; these are computed either from the fitted parameters and/or from the fitted SED. The SFR is computed from the contribution of the young and old star populations, however the young star population gives in general the dominant contribution. Therefore the SFR is mostly depending on the fitted parameters M_{gal} the normalization, f_{ySP} the fraction of young star and t_{new} the age of young star population. SFR increases with M_{gal} and f_{ySP} , it decreases slightly as young stellar population ages, i.e. as

⁸ <http://sha.ipac.caltech.edu/applications/Spitzer/SHA>

⁹ <http://irsa.ipac.caltech.edu/data/SPITZER/docs/dataanalysis/tools/tools/mopex/mopexusersguide/>

¹⁰ <http://iraf.noao.edu>

¹¹ Herschel is an ESA space observatory with science instruments provided by European-led Principal Investigator consortia and with important participation from NASA.

¹² http://hereschel.esac.esa.int/Science_Archive.shtml

¹³ <http://cigale.oamp.fr/>

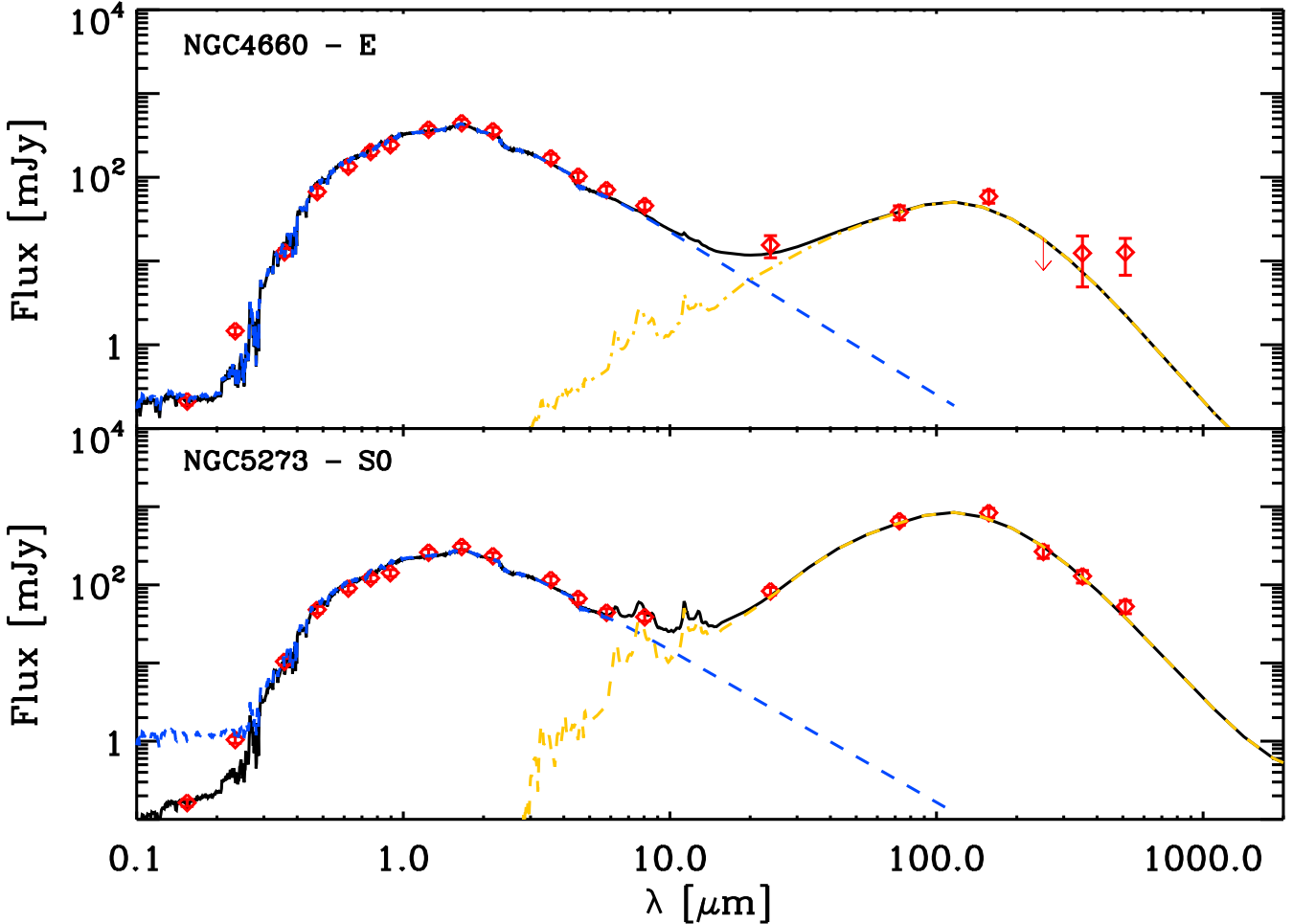


FIG. 1.— Example of fit of SED fit performed with CIGALEMC. For each galaxy, the data are : 2 GALEX, 5 SDSS, 3 2MASS, 4 IRAC, 3 MIPS and 3 SPIRE bands. The top panel shows the fit (black solid line) of NGC4660 (Elliptical galaxy) data (red diamond) with its unabsorbed stellar component (blue dashed line) and the dust emission model (orange dotted dashed line). The bottom panel shows the fit (black solid line) of NGC5273 (lenticular galaxy) data (red diamond) with its unabsorbed stellar component (blue dashed line).

TABLE 1
PARAMETERS FITTED BY CIGALEMC TO THE GALAXY SEDS,
WITH PRIORS CHOSEN.

Parameters	Priors	Description
τ_{old}	$0 < \tau_{old} < 10$ Gyr	old star population e-folding time
t_{new}	$0 < t_{new} < 5$ Gyr	age of the new stellar population
f_{ySP}	$0 < f_{ySP} < 1$	fraction of young stars
A_{ySP}	$0 < A_{ySP} < 5$ mag.	dust extinction for young stars
f_V	$0 < f_V < 1$	factor for dust extinction of old stars
α	$0.06 < \alpha < 4$	slope of the dust mass over heating
f_{AGN}	$0 < f_{AGN} < 1$	AGN fraction of the dust luminosity
M_{gal}	$6 < M_{gal} < 13$	logarithm of the galaxy mass

t_{new} gets larger. Apart from its M_{gal} dependency, the SFR is constrained by the UV, optical and NIR part of the spectrum via the stellar population synthesis (SPS) of Maraston (2005). The age_{D4000} is calculated on the unreddened fitted SED by taking the ratio of the average flux per frequency unit of the wavelength ranges 4000-4100 Å (red continuum) and 3850-3950 Å (blue continuum) and matching this ratio to the age calculated on Maraston models (Maraston 2005). L_{dust} is composed of an AGN contribution fitted with a Siebenmorgen et al. (2004b,a) and a dust component, the dust

component part of L_{dust} is constrained by the fitted absorption in UV and optical and the FIR emission consistently. M_* is calculated by integrating over the evolution track of the Maraston (2005) model, and depends primarily on the UV, optical and NIR part of the spectrum, except for the overall normalization defined by M_{gal} . L_{bol} is the total luminosity, it is computed by integrating the fitted spectrum and therefore depends on the full SED.

Figure 1 shows the SED fit of one elliptical galaxy NGC4660 and one lenticular galaxy NGC5273. The red diamonds represent our data points, the black solid line represents the model spectrum, the blue dashed line represents the unabsorbed stellar spectrum and the orange dotted-dashed line represents the dust emission. Modelled spectra are in pretty good agreement with measurements from 1539 Å GALEX to 500 μ m Herschel-SPIRE. Dust absorption and emission are significantly larger in the lenticular galaxy NGC5273.

Typical constraints provided by CIGALEMC are depicted in figure 2 (NGC4660, corresponding SED is at the top of figure 1). Diagonal elements of this figure show the marginalized (integrated over all the other parameters) probability distri-

bution function (PDF) of each parameter. The off-diagonal elements show the 2-dimensional marginalized PDF for pairs of parameters and allow to quantify the level of degeneracy between pairs of parameters. Parameters age_{D4000} , L_{bol} , M_* , SFR, L_{dust} are constrained respectively at the 11, 14, 16, 53, 87 % level (median of the relative 68% confidence interval). Among these parameters, the correlation is fairly small except for the pair (L_{bol} , M_*) because they depend both mostly on the normalization parameter M_{gal} .

Out of a sample of 221 galaxies (116 E and 105 S0), our model converges to a solution for 193 galaxies. The reduced χ^2 of the fit is between 0.2 and 42, the overall reduced χ^2 is well fitted by a Gaussian distribution centered on 2.5 with a standard deviation of 4.5. We decide to reduce the sample by removing 38 poorly fitted galaxies (reduced $\chi^2 > 10$). Finally, in order to include only strongly constrained galaxy, we select the sub-sample where the galaxy mass is constrained by better than a factor 10 at 68% c.l., this removes 12 additional galaxies. We check that this last cut does not bias the selection by selecting only massive galaxies. Our reduced sample is composed of 75 elliptical galaxies (type < -3) and 68 lenticular galaxies (type > -3), with a respective average reduced χ^2 of 4.7 ± 2.6 and 3.9 ± 2.4 , lenticular galaxies are a better fit to our model on average.

To check our CIGALEMC estimate of SFR in our galaxy sample, we use the SFR estimate at $24 \mu\text{m}$ of Calzetti et al. (2007):

$$\text{SFR}(M_\odot \text{yr}^{-1}) = 1.27 \times 10^{-38} [L_{24\mu\text{m}}(\text{erg s}^{-1})]^{0.8850} \quad (1)$$

We find a good agreement with the 143 galaxies for which we obtain a SFR as indicated by figure 3 (left).

Given that CIGALEMC SFR is constrained by the UV/optical/NIR part of the SED, the agreement with the $24 \mu\text{m}$ estimate give us good confidence in CIGALEMC SFR estimates. Using DR9 SDSS spectrometric measurement of $\text{H}\alpha$ obtained for 50 of our galaxies, we use Calzetti et al. (2007) relation between the $\text{H}\alpha$ flux and SFR to compare with the CIGALEMC SFR estimate :

$$\text{SFR}(M_\odot \text{yr}^{-1}) = 5.3 \times 10^{-42} L(\text{H}\alpha)(\text{erg s}^{-1}) \quad (2)$$

Using $\text{H}\alpha$ to estimate the SFR, we see a large difference with our estimate (blue dashed line on the right fig.3 compared to the data points), the $\text{H}\alpha$ SFR estimate is about a factor 10 time smaller than our SED SFR estimate. Calzetti et al. (2007) proposed to add a correction with the $24\mu\text{m}$ luminosity ($5.3 \times 10^{-42} 0.031 L_{24\mu\text{m}}$) but this correction is larger than the $\text{H}\alpha$ contribution in our sample. It is in fact about the same amplitude as the $24\mu\text{m}$ SFR estimate itself (similar to conclusions of Temi et al. (2009a) on $\text{H}\beta$ estimate), and would only reduce the $\text{H}\alpha$ SFR estimate whereas our plot indicates this estimate needs to be increased. The difference could be explained by the small aperture of SDSS spectroscopic data (around 3 arcseconds) and the fact that Calzetti et al. (2007) relation was estimated on starburst whose star-formation is dominated by the central bulge. Our sources might have a more extended star formation distribution, which is captured by our SED and $24 \mu\text{m}$ estimates but underestimated by the SDSS spectroscopic data and the Calzetti et al. (2007) relation. If this difference of aperture was corrected for, the $\text{H}\alpha$ SFR estimate might, on the contrary, overestimate the true SFR due to the gas photo-ionization by post-AGB stars (Yan & Blanton 2012; Sarzi et al. 2010) and an additional correction would be required. Indeed Yan & Blanton (2012) found a variation

of the emission line ratio as a function of radius in early-type galaxies that could potentially be explained by post-AGB stars (Binette et al. 1994) if they are more abundant or more closely distributed with respect to the gas than expected. Previously, Sarzi et al. (2010) also concluded that post-AGB stars are their favorite candidate to power the ionised-gas emission in ETGs based on the correlation of the $\text{H}\beta$ line and the stellar surface brightness. Nevertheless $\text{H}\alpha$ luminosities correlate well with our SFR estimates and changing the relation to $\text{SFR}(M_\odot \text{yr}^{-1}) = 5.3 \times 10^{-41} L(\text{H}\alpha)(\text{erg s}^{-1})$ leads to a good agreement with our sample (red dotted dashed line on the right of fig. 3). This implies that the star formation mechanism in the central part of our galaxies and in their outskirt is related and that most likely the star formation is distributed relatively homogeneously.

The distribution of the value of our parameters in our reduced sample of galaxies is shown on figure 4. Ellipticals have more massive galaxies than lenticulars, about 40% of ellipticals are heavier than $10^{11} M_\odot$ but only 12% of lenticulars are. The distribution of age_{D4000} fitted on our galaxies is heavily clustered around 10 Gyr for both type, however there is more young ($\text{age}_{D4000} < 8$ Gyr) lenticulars (46% of S0) than ellipticals (23% of E). When normalizing the SFR and dust luminosity by the stellar mass of each galaxy, the lenticular galaxies are on average brighter and producing more stars. The proportion of E galaxies with a sSFR greater than $10^{-11.5} M_\odot/\text{yr}/M_\odot$ about 16%, and the proportion of E galaxies with a dust luminosity to stellar mass ratio greater than 10^{-2} is about 15%. For S0 galaxies, these proportions are respectively about 35% and 47%. These results are in agreement with previous studies using FIR photometric indicators (Temi et al. 2009a,b), which showed that lenticulars are on average more star-forming and contain more dust. We also compared the sSFR with the slow/fast rotator classification of Emsellem et al. (2011), which classified galaxies with an angular momentum λ_R greater than $0.31\sqrt{\epsilon_e}$ as fast rotators. The number of galaxies, common to ATLAS^{3D} and our reduced sample of reasonably fitted galaxies (cf. previous χ^2 and galaxy mass constraints) is 46, with 11 slow rotators and 35 fast rotators. All the slow rotators except for one galaxy are ellipticals, 24 fast rotators are lenticulars. Among the 46 galaxies, only 3 galaxies have a sSFR greater than $10^{-11.5} M_\odot/\text{yr}/M_\odot$. All of these galaxies are fast rotators (3/35), however the small size of this sample does not allow to make a strong conclusion.

4. DUST MASS AND TEMPERATURE

To understand better the dust content of our sample, we decide to fit the far-infrared part of the spectrum with a variety of models parametrized by dust emissivity, temperature and mass. Since CIGALEMC does not provide a direct estimate of the dust mass nor temperature, we apply two additional approaches to measure these quantities : i) we run another SED modeling software MAGPHYS¹⁴ (da Cunha et al. 2008), and ii) we fit some modified black-body spectra to the Far-Infrared portion of our data ($\lambda > 60 \mu\text{m}$).

4.1. Full spectrum fit : MAGPHYS

Multi-wavelength Analysis of Galaxy Physical Properties (MAGPHYS) is a model able to interpret simultaneously the

¹⁴ <http://www.iap.fr/magphys/magphys/MAGPHYS.html>

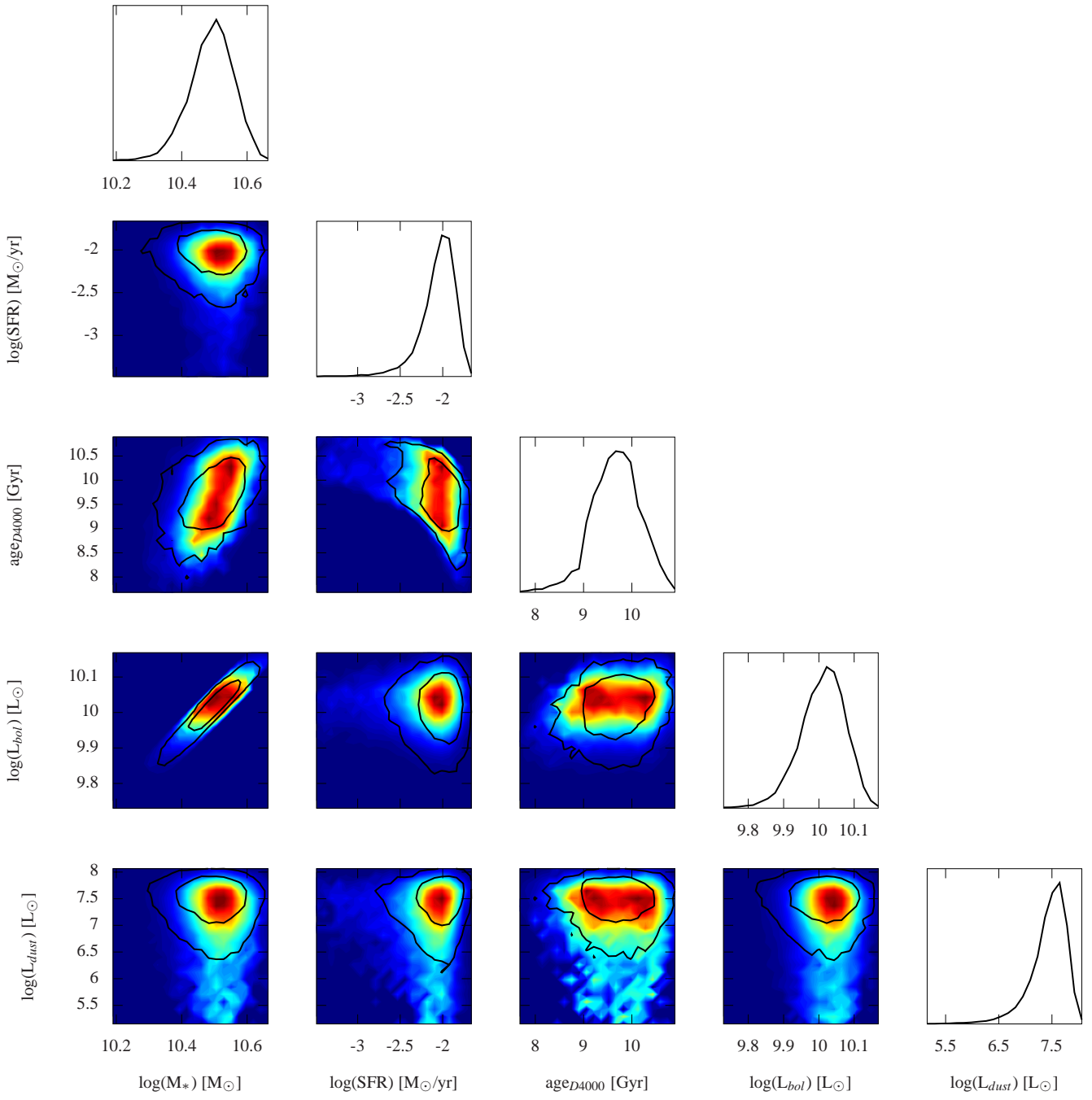


FIG. 2.— Constraints on some of the CIGALEMC parameters (M_* , SFR , age_{D4000} , L_{bol} , L_{dust}) for NGC4660. The diagonal (solid black line) plots show the PDFs of each parameter, the rainbow-color plots show the 2-dimension PDFs of one parameter versus another (solid black contours represent the 68 and 95 % confidence intervals).

ultraviolet, optical and IR emission from galaxies and determine the dust temperature. It separates contribution from dust in stellar birth clouds (BCs) and the ambient interstellar medium (ISM). The dust emission is decomposed in three

components for the BCs. One models the PAHs and the NIR emission. The second corresponds to the hot mid-IR continuum emission, described as the sum of two greybodies of temperature of 130 K and 250 K respectively. The last component

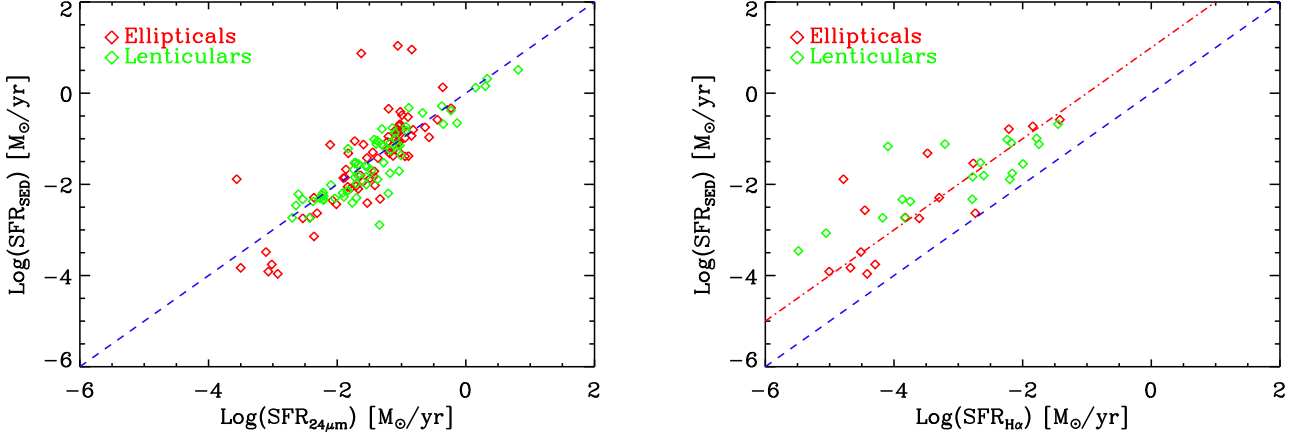


FIG. 3.— **Left :** CIGALEMC estimate of the SFR of our 143 galaxy sample versus the 24 μm estimate as calibrated in Calzetti et al. (2007). **Right :** CIGALEMC estimate of SFR for a 50 galaxy subset compared to the SFR calculated from SDSS spectrometric measurements of the H α flux and the Calzetti et al. (2007) relation. The blue dashed line indicates where the 2 estimates are equal and the red dotted dashed line indicates when CIGALEMC estimate is ten times larger. Our SFR estimate is clearly correlated to the H α luminosity, but the conversion coefficient in the Calzetti et al. (2007) would need to be multiply by 10 for our sample.

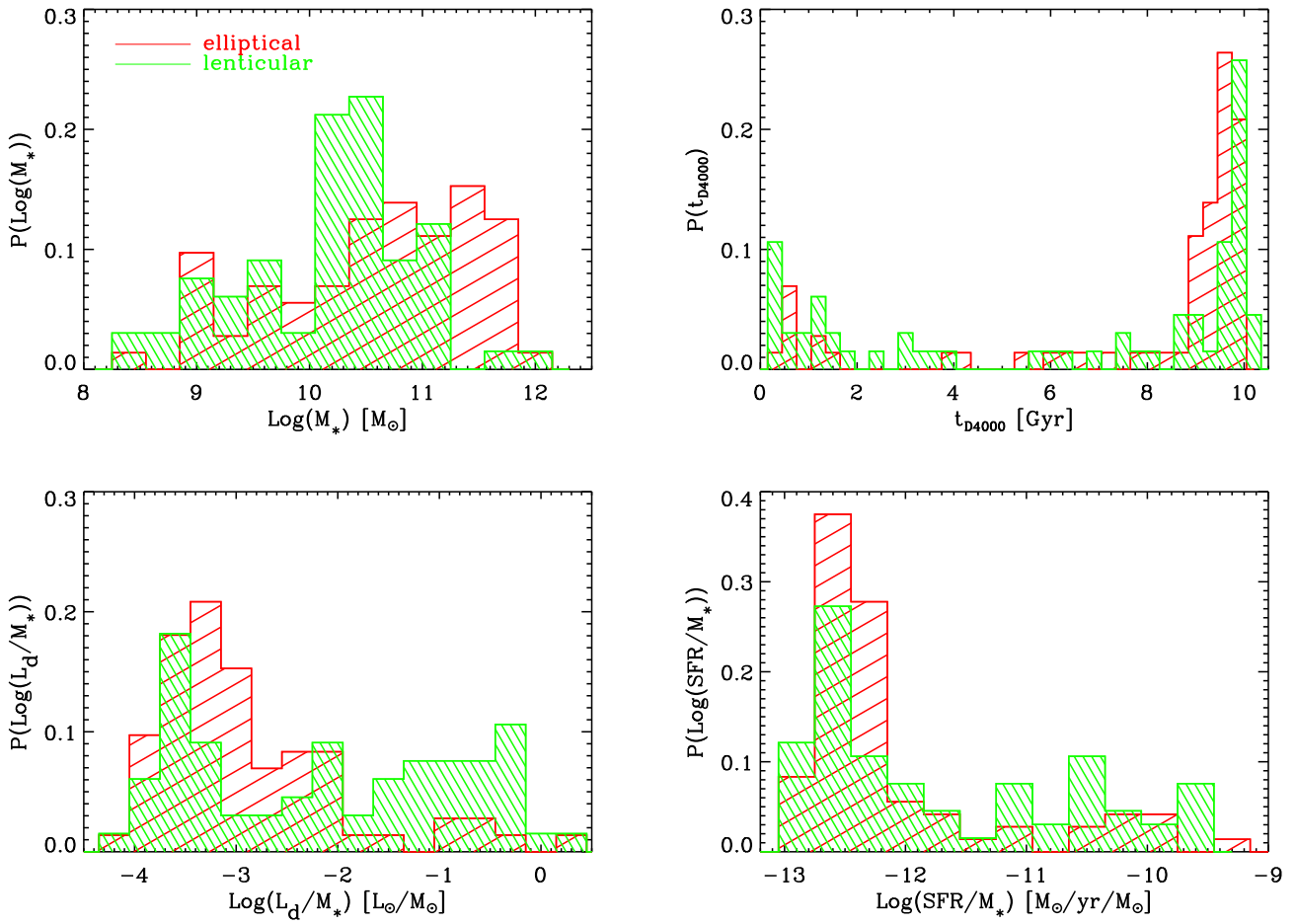


FIG. 4.— Distribution (renormalized to one) of the fitted parameters (from top to bottom and left to right : M_* , $t_{\text{d}400}$, L_d/M_* , SFR/M_*) for our galaxy sample

is dust grains in thermal equilibrium, with a temperature allowed to vary between 30 and 60 K. For the ambient ISM, to

keep the number of free parameters manageable, the proportions of these three components are fixed and the temperature

of the warm dust in the thermal equilibrium is fixed to 45 K. da Cunha et al. (2008) added a cold grain component in the ISM with a temperature that can varies from 15 to 25 K.

Whereas MAGPHYS fits a lot of parameters, our goal is to compute the cold dust temperature and mass of our sample and we concentrate on these two parameters. All the galaxies in our sample are fitted using MAGPHYS, but several parameters are sometimes not well constrained even if the reduced χ^2 of the fit seems acceptable. For instance, among the 221 sources without SPIRE data, 158 sources have good constraint on M_{dust} , 132 on L_{dust} and only 36 (16% of the sample) on T_C^{ISM} , hereafter T_{dust} . Sources with SPIRE data available return similar results except for the temperature : among 75 sources in the initial SPIRE sample, 45 constrain the M_{dust} parameter, 30 constrain L_{dust} and 20 constrain T_{dust} . FIR-data are important to constrain T_{dust} accurately. 50% of the sources are constrained when the full FIR spectrum is available and less than 25% are constrained when SPIRE data are missing. This emphasizes the critical need of FIR data when determining the dust temperature using the MAGPHYS model.

Among the galaxies constrained in temperature, we compare the value of T_{dust} obtained with MAGPHYS with and without SPIRE data. There is a huge discrepancy between these estimates and they do not correlate with each other. This result underlines the fact that values of T_{dust} will not be reliable without observations at FIR wavelengths. We estimate that in our sample, only the temperature of the 20 sources with SPIRE data are accurate enough when using MAGPHYS. This encouraged us to explore other methods to determine the dust temperature of our sample, as detailed in the following sub-section.

4.2. Far-Infrared fit

Using only the Far-Infrared part of our data ($\lambda > 40\mu m$), contrarily to MAGPHYS fitting method, we perform two types of fit on our sources :

- a 2 temperature fit with a standard emissivity β for big dust grain of 1.5 or 2.0 (Draine & Lee 1984; Agladze et al. 1996; Mennella et al. 1998; Reach et al. 1995; Boulanger et al. 1996; Dunne & Eales 2001), on IRAS 60, 100 μm , MIPS 70, 160 μm and 250, 350, 500 μm SPIRE data, the luminosity is then :

$$L(\nu) \propto \alpha B(\nu, T_d^1) \nu^\beta + (1-\alpha) B(\nu, T_d^2) \nu^\beta \quad (3)$$

where $B(\nu, T)$ represents a blackbody spectrum of temperature T at frequency ν , α gives the luminosity ratio of the two dust species. T_d^1 is constrained between 10 and 45 K, T_d^2 between 45 and 95 K.

- a single temperature fit with emissivity β , either 1.5 or 2.0, on IRAS 60, 100 μm , MIPS 70, 160 μm and 250, 350, 500 μm SPIRE data. T_d is constrained between 10 and 95 K, and the luminosity is then expressed as :

$$L(\nu) \propto B(\nu, T_d) \nu^\beta \quad (4)$$

We compute fluxes in each band by integrating over the various instrument filters f_i , which have been normalized so that $\int f_i(\nu) d\nu = 1$. We normalize fluxes with the total dust luminosity defined as $L_d = \int L(\nu) d\nu$. Fluxes in each band, F_i

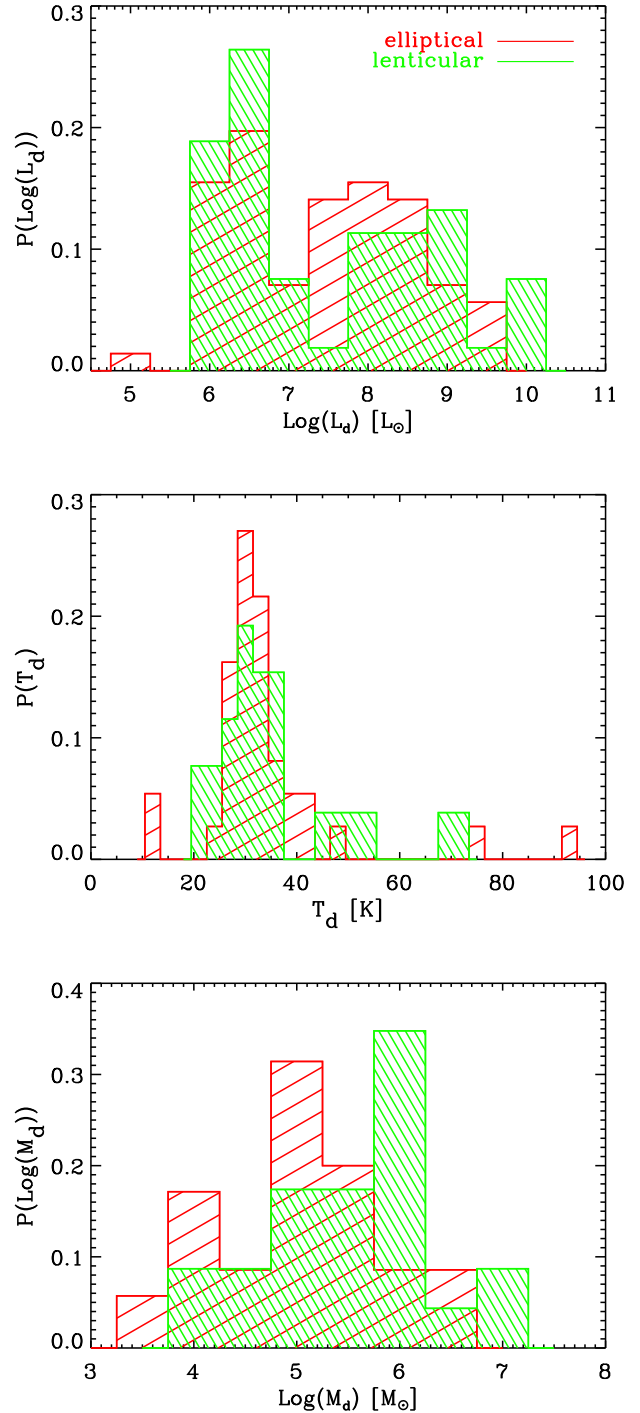


FIG. 5.— Distribution of the dust luminosity (top), temperature (middle) and mass (bottom), obtained by fitting our one temperature model with $\beta=1.5$ to our data. The elliptical and lenticular galaxy histograms are respectively in solid black line and dashed blue line, they both are normalized to one. A few more lenticulars than ellipticals reach a dust mass of $10^6 M_\odot$.

are then defined as :

$$F_i = \frac{L_d}{4\pi D_l^2} \frac{\int L(\nu) f_i(\nu) d\nu}{\int L(\nu) d\nu} \quad (5)$$

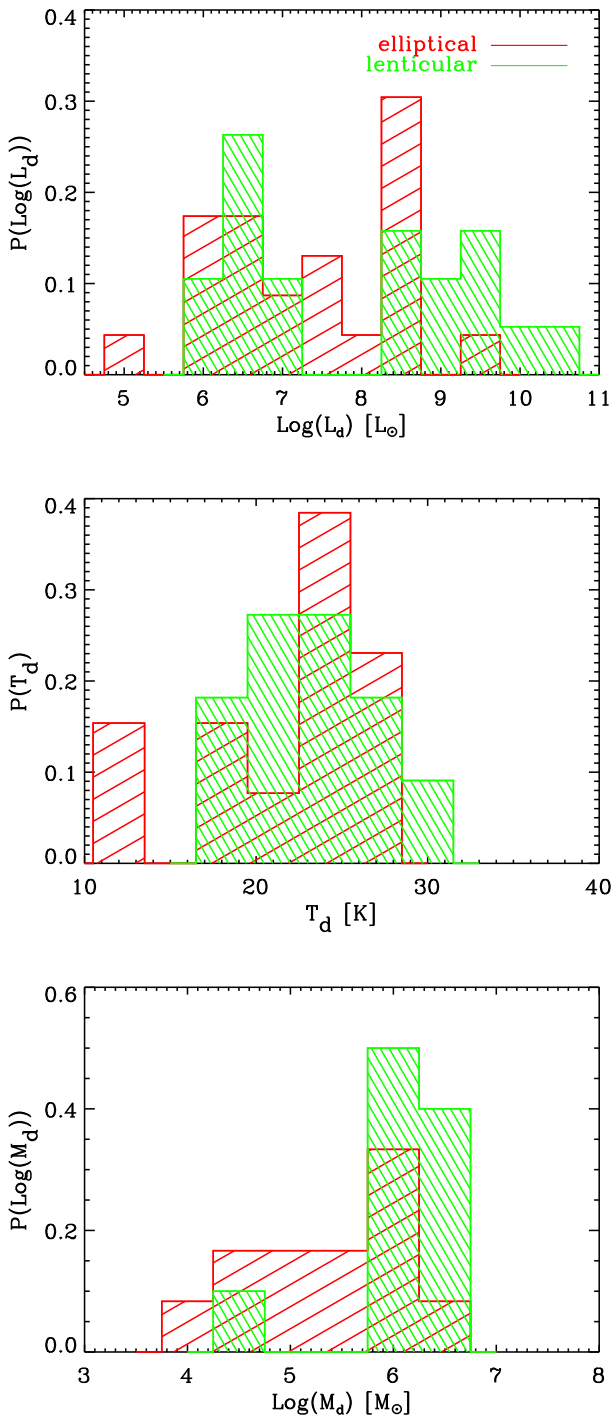


FIG. 6.— Distribution of the dust luminosity (top), cold temperature (center) and mass (bottom), obtained by fitting our two temperature model with $\beta=2.0$ to our data. The elliptical and lenticular galaxy histograms are respectively in solid black line and dashed blue line, they both are normalized to one. Lenticulars appear slightly more dusty and more luminous.

To obtain the mass of the dust we assume that dust grains are in thermal equilibrium and use the Hildebrand (1983) formula, which gives a relation between the dust temperature (T_d), the dust luminosity (L_d) and its mass (M_d):

$$L_d(\lambda) = 4\pi M_d \kappa(\lambda) B(\lambda, T_d) \quad (6)$$

We use the same hypothesis as Dunne et al. (2000) and take κ at $850\text{ }\mu\text{m}$, $\kappa(850\text{ }\mu\text{m})$, to be equal to $0.077\text{ kg}^{-1}/\text{m}^2$ (based on the calculations of Draine & Lee 1984; Hughes et al. 1993). We assume the emissivity to follow the relation $\kappa(\lambda) = \kappa(850\text{ }\mu\text{m})(\lambda/850\text{ }\mu\text{m})^{-\beta}$, the dust mass can then be expressed as :

$$M_d = L_d / \int 4\pi \kappa(\lambda) B(\lambda, T) d\lambda \quad (7)$$

The results of the fit can be found in figures 5 & 6 and tables 8 & 9. When fitting with a two temperature model, our algorithm manage to converge on 42 galaxies (23 E and 19 S0), when using the single temperature model we constrain 124 galaxies (71 E and 53 S0) with a reduced χ^2 of 10 or better. The average reduced χ^2 of our two temperature fit is 3.4, the reduced χ^2 for our single temperature fit is 3.3. Introducing a more complex model does not improve our fit on average, although our frequency coverage is limited in the Far-IR. Some of our galaxies are known to have a strong synchrotron emission (NGC4267 & NGC4486 for instance) as indicated in di Serego Alighieri et al. (2013), they only represent a small fraction of the sample and most of them have a very large reduced χ^2 and are therefore not included in the following analysis.

The fit is slightly better on average for an 2.0 emissivity than 1.5 in the two temperature but it is the opposite for the single temperature. Changing the emissivity in the two temperature fit from 1.5 to 2, increases the luminosity by 20%, decreases the cold temperature by 10% and increases the dust mass by a factor 3. In our single temperature case, we compare the fit with an emissivity β of 1.5 and 2 and find that the temperature and mass change respectively by $\sim -10, -40\%$ when using 2 instead of 1.5, but the luminosity is barely changed. In the following, we will only discuss our fit with an emissivity 2.0 for the 2 temperature model and 1.5 for the single temperature model.

The distributions in figures 5 & 6 show that galaxies fitted by the 2 temperature model have a lower temperature than the one fitted with the single temperature model (22.4 K versus 32.3 K). This can be explained by the fact that our 2 temperature model containing four free parameters, it requires 5 data points. This means that at least one data point from Herschel-SPIRE is required to fit the 2 temperature model, whereas the one temperature fit does not require Herschel data with only two free parameters. The 2 temperature model is only possible on galaxies with colder dust. This result is in agreement with Skibba et al. (2011) where they find higher dust to stellar flux ratio for Herschel-detected galaxies, because Herschel is tracing additional cold dust that was not detected with Spitzer. The 32.3 K average temperature derived on the single temperature model is very close to average temperatures derived from other galaxy selections, like for instance the 35 K estimate from Elbaz et al. (2010) and the 28 K estimate from Amblard et al. (2010). Figure 5 & 6 reveal also that lenticular galaxies have slightly more dust than elliptical (more apparent in 2 temperature model), and slightly higher dust luminosity when their SED is modelled with 2 temperatures.

Fig. 7 shows the evolution of the ratio of dust mass to stellar mass in logarithmic scale versus the stellar mass in elliptical galaxies (in red) and in lenticular ones (in green) with the single temperature model, when selecting only sources with a secure dust mass (less than 50% relative error) and a good fit to the full SED and the FIR spectra (34 sources). We decide to

present results only for the single temperature model, we have similar results but with poorer statistics for the 2 temperature model.

The dashed lines represent the best linear fit obtained with these 34 sources (black), with elliptical galaxies among this sample (red) and with lenticular galaxies (green). The general trend is that the ratio M_{dust} to M_{star} decreases with increasing stellar mass. This relation is stastically identical for both elliptical galaxies (red dashed line) and lenticular ones (green dashed line), the slopes being -1.16 ± 0.16 , -0.97 ± 0.18 , -1.20 ± 0.30 for the whole sample, the elliptical galaxies and for the lenticular galaxies respectively. The decreasing trend is in good agreement with other studies, measurements from Smith et al. (2012) seem compatible with our fit although their stellar mass range is very small (10^{10} to $10^{11} M_\odot$). Agius et al. (2013) found a shallower slope of -0.55 with larger dust-to-stellar mass ratio ($10^{-2.5}$ to 10^{-4}), it uses a sample detected by the shallow H-ATLAS survey which could explain that it selects higher dust-to-stellar mass ratio. (Rowlands et al. 2012) using data from H-ATLAS as well found higher dust masses, around $7 < \log(M_d/M_\odot) < 9$ and higher dust-to-stellar mass ratio. Skibba et al. (2011) measured dust-to-stellar mass ratio in the same range as ours. Cortese et al. (2012) measured dust-to-stellar mass ratio on late-type galaxies ranging from 10^{-2} to 10^{-4} and on early-type galaxies from $10^{-3.5}$ to 10^{-6} .

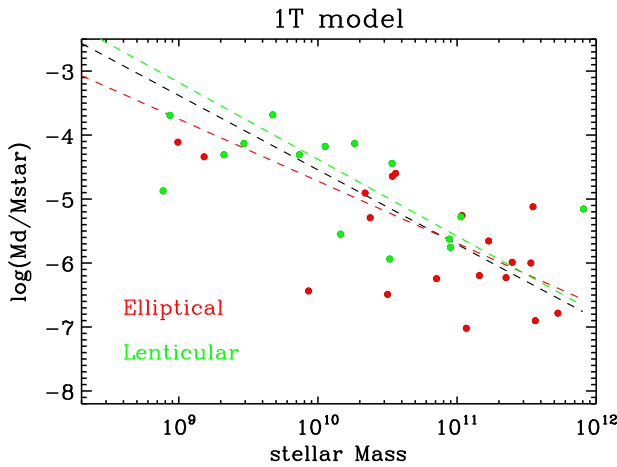


FIG. 7.— Ratio of dust mass to stellar mass in logarithmic scale versus the stellar mass for Elliptical galaxies (in red) and for lenticular ones (in green) for sources with a secure fit (dust mass estimate with a relative error of 50% or less) with the 1T model. The dashed lines represent the best linear fit obtained for the whole sample (black), for elliptical galaxies (red) and for lenticular galaxies (green).

Fig. 8 shows the evolution of the specific star formation rate as a function of the dust-to-stellar mass ratio for Ellipticals (red triangles) and for Lenticulars (green triangles) in logarithmic scale. Fig. 8 is similar in shape to the banana-shaped plots of Temi et al. (2009b) which show the relationship between $\log(L_{24}/L_K)$ and $\log(L_{FIR}/L_K)$, and the information it contains is correlated with our plot. However Fig. 8 permits a better distinction of SFR and dust mass than the 24 μm and FIR (70 or 160 μm) luminosities could.

The sSFR is constant ($\log(\text{sSFR}) \sim -12.5 M_\odot/\text{yr}/M_\odot$) for a dust-to-star mass ratio lesser than 10^{-5} . This part of the diagram is mainly populated by Elliptical galaxies (68% of sources). For a higher dust-to-star mass ratio ($\log(M_d/M_\odot) > -$

5), which mainly contains S0 galaxies (72% of sources), the sSFR rise steeply with the dust to star mass ratio. A single outlier source, NGC4494, lies at $\log(\text{sSFR}) \sim -10$ and $\log(M_d/M_\odot) \sim -6$. This Elliptical galaxy has a high specific star formation rate but a surprisingly small dust-to-star mass ratio. NGC4494 contains an AGN according to the Veron catalog Véron-Cetty & Véron (2010) and could have undergone a recent merger(O’Sullivan & Ponman 2004), which might be able to explain the low dust mass. However, we do not have GALEX or SDSS data for this galaxy, so the fit might have converged to an unphysical solution.

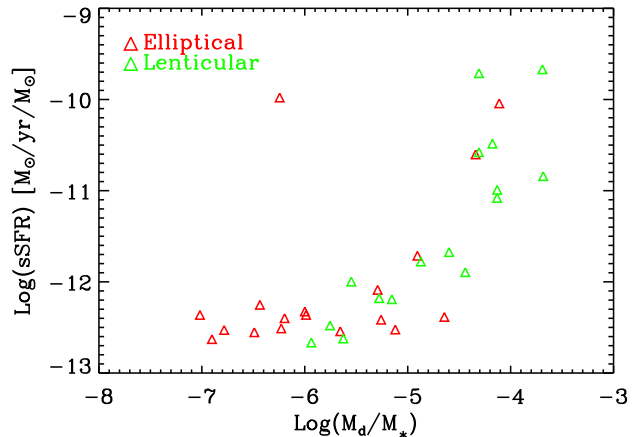


FIG. 8.— Specific star Formation estimated with our CIGALEMC fit versus the dust mass to stellar mass ratio, estimated with the 1 temperature FIR model. We select data with a reduced χ^2 lower than 10, a dust mass error of less than 50% and a dust luminosity logarithm error of less than 1 dex. Elliptical galaxies are indicated with red triangles, Lenticular galaxies with green triangles. The isolate triangle at $\log(\text{sSFR}) \sim -10$ and $\log(M_d/M_\odot) \sim -6$ represents NGC4494.

We compared our E/SO classification with the slow/fast rotator one from Emsellem et al. (2011) and obtained the same sample of 46 galaxies of section 3, that are in *ATLAS^{3D}* and well fitted in our sample. Out of 35 fast rotators, 6 have a $\log(M_d/M_\odot)$ greater than -5.5 but no slow rotator has such a high dust mass. This would indicate that fast rotators are the only one with a large amount of dust, although the small size of this sample does not allow to conclude.

5. AGN ACTIVITY

AGN activity can influence the star formation rate of galaxy. In order to better understand the variability in our sample of ETGs, we try to detect galaxies in our sample with a significant trace of AGN activity.

5.1. Spectroscopic selection

To select AGN, we download the DR9 SDSS spectroscopic line catalog¹⁵ along with the spectroscopic information file and cross-identify it with our 221 galaxy sample. We identify 54 galaxies (27 S0 and 27 E, compared to the 147 galaxies for which we have photometric data), from which we select the ones with at least 4 lines with a signal-to-noise ratio of at least 3 out of the 7 lines that we use to produce the Baldwin, Phillips, Terlevich (BPT) diagrams (Baldwin et al. 1981), namely OIII (5007 Å), NII(6584 Å), SII(6718 and

¹⁵ http://www.sdss3.org/dr9/spectro_access.php

6731 \AA), $\text{H}\alpha$ (6563 \AA), $\text{H}\beta$ (4861 \AA), OI (6300 \AA). We obtain 21 galaxies (13 S0 and 8 E, $\sim 40\%$ of the sample) with enough optical lines detected, about the same rate as Rowlands et al. (2012) (45%) and twice the rate of Schawinski et al. (2007b) ($\sim 20\%$). Our $24\mu\text{m}$ selection and the $250\mu\text{m}$ selection of Rowlands et al. (2012) are more likely to select active ETGs than the optical selection of Schawinski et al. (2007b).

Using the 3 BTP diagrams of figure 9, with Star-Forming (SF), AGN and LINER area defined by Kewley et al. (2001, 2006), we identify 5 AGNs (5 S0), 11 SFGs (7 S0 and 5 E) and 4 (1 S0 and 3 E) undetermined galaxies (with some lines they are identified as AGN and some others as SFG). We obtain a larger proportion (69%) of star forming galaxies than the 57% of the $250\mu\text{m}$ selected sample of Rowlands et al. (2012), although the difference is not statistically significant since both samples are quite small. Schawinski et al. (2007b), using a much larger sample of optically selected ETGs, found 61% of SFGs among sources with optical line detection. Starting with an equal number of E and S0 galaxies in the cross-sample with SDSS spectroscopic data, more S0 galaxies (65% of the detected galaxies) have detected emission lines than E galaxies and all AGN identified with the BPT diagrams are S0. Both Rowlands et al. (2012) and Schawinski et al. (2007b) did not separate their numbers between S0 and E morphology, but Schawinski et al. (2007b) found a time sequence for small to intermediate mass ETGs, going from a star-forming phase to an AGN phase to finish into a quiescent state. Our results would be consistent with such a picture if the S0 dominate the intermediate AGN phase. Overall, our S0 galaxies with SDSS spectroscopic are 52% quiescent, 19% AGN-dominated and 26% SF-dominated, our E galaxies are 70% quiescent, 0% AGN-dominated and 18% SF-dominated. Separating LINERs from other AGNs would not change our results, since our BPT diagrams do not seem to indicate any LINERs in our sample. Two galaxies are potentially borderline LINERS in one BPT diagram but are clearly not LINERs in another one and neither are classified as such in the NED and Hyperleda databases.

We mark, on our BPT diagrams, galaxies for which the $24\mu\text{m}$ morphology is point-source like (red squares). Among galaxies identified with a $24\mu\text{m}$ point-source morphology and for which we have SDSS spectroscopic data, all of them have detected lines. The $24\mu\text{m}$ morphology seems to be a good indicator of galactic activity. They seem to split evenly between AGN emission (2) and SF emission (3), $24\mu\text{m}$ morphology gives a $\sim 50\%$ accuracy in AGN detection in our sample.

5.2. NIR selection

Another powerful way to select AGN is to use NIR selection. Indeed, the UV to MIR continuum for a galaxy is dominated by a black body emission that would dominate at $1.6\mu\text{m}$, while the UV to MIR continuum of an AGN is dominated by a power law. Different criteria have been proposed using IRAC-IRAC colors (e.g., Lacy et al. 2004; Stern et al. 2005) and more recently WISE colors (e.g., Stern et al. 2012). We apply these three criteria to our sample: 9 sources are selected following Lacy et al. (2004), only one source (plus a borderline source) with Stern et al. (2005) criteria, and 4 sources following Stern et al. (2012) using WISE filters. Very few sources are selected by these criteria, this might be explained by these criteria being designed in order to select highly obscured quasars and our sample of ETGs is quite poor in dust.

Assef et al. (2013) underline the incompleteness and the unreliability of these criteria, stating a reliability of only

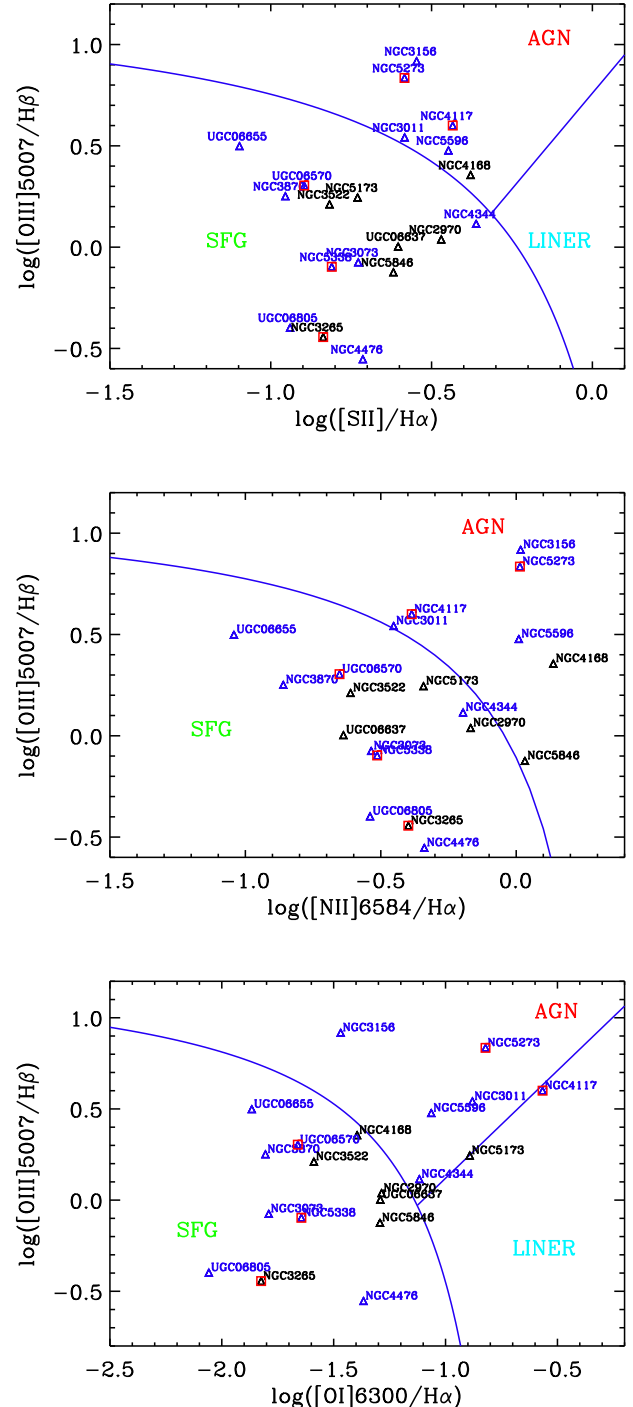


FIG. 9.—BPT diagrams of galaxies in our sample for which we have SDSS spectroscopic data and at least for emission lines detected. Lenticular galaxies are represented by blue triangles, Elliptical galaxies by black triangles. The blue solid line separates the Star Forming Galaxy (SFG) region from the AGN one. The red square indicates galaxies which $24\mu\text{m}$ morphology is point-like.

36% for the selection of Lacy et al. (2004) and a completeness of 79%, a 67% reliability/ 51% completeness for Stern et al. (2005) and a 45% reliability/ 70% completeness for Stern et al. (2012). This leads us to the conclusion that we should combine the 3 criteria to increase the reliability

of the NIR selection on our sample. We finally have only 2 sources selected as AGN via the NIR-methods: NGC1377 and IC5063. We do not have any SDDS spectra for these two sources so we cannot correlate this NIR classification with the BPT spectral classification. Both of these sources have a high f_{agn} fraction from the SED-fitting which could confirm their AGN activity. IC5063 is also detected in X-ray and has a luminosity $L_X > 10^{41} \text{ erg.s}^{-1}$, pointing to some AGN activity. NGC1377 is a power-law source, i.e. presenting $\text{Fl}_{IRAC4} > \text{Fl}_{IRAC3} > \text{Fl}_{IRAC2} > \text{Fl}_{IRAC1}$, once again characterizing an AGN.

Fig. 10 shows the distribution of our sample in the Lacy et al. (2004) diagram. Elliptical galaxies are represented with dots while lenticulars are represented with crosses. We add to this figure the information collected on the BPT diagrams with a color code. Black symbols represent galaxies for which we do not have emission lines or SDSS data, blue symbols represent AGN sources, pink ones represents the potential AGN and green ones represent the star-forming sources. Star-forming sources (green dots and crosses) are mainly distributed in the upper part of the diagram on the outside of the Lacy et al. (2004) box. Sources in this part of the color-color plot, with bluer $S_{5.8}/S_{3.6}$ colors and redder $S_{8.0}/S_{4.5}$ colors than the rest of the sample, are known (Lacy et al. 2004) to be low-redshift galaxies with their 6.2 and 7.7 μm PAH bands redshifted into the IRAC 8 μm filter. The presence of PAHs in these sources shows that they are forming stars and most-likely present emission lines in their spectra. We also notice that AGNs from the BPT diagram (blue dots and crosses) are outside the NIR-selection, showing that these two methods select different types of AGN with different properties. The NIR-selection will select highly obscured quasars. Another trend noticeable on figure 10 is the separation between Ellipticals (dots), concentrated in the left-bottom part, and lenticulars (crosses). This shows that lenticular galaxies have more dust than ellipticals, which goes in the same direction that we have already noticed on Figs.5 & 6.

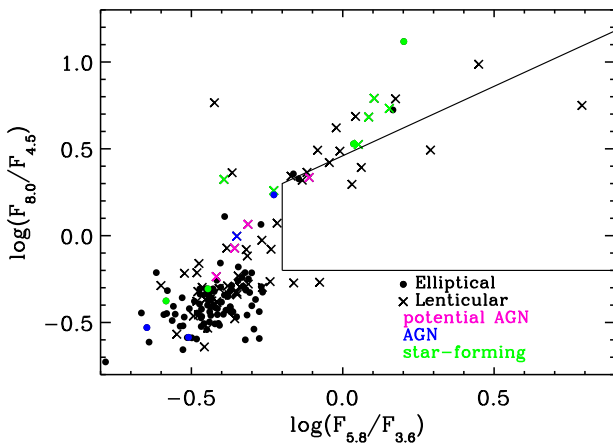


FIG. 10.— Distribution of the sources from our sample in the Lacy et al. (2004) diagram displaying $\log(S_{8.0}/S_{4.5})$ versus $\log(S_{5.8}/S_{3.6})$. Elliptical and Lenticulars are represented by dots and crosses respectively. We also show here the AGN activity versus star-forming activity of our sample from our analysis of the BPT diagram: star forming (green), AGN (blue) and potential AGN (pink). The black quadrilateral shape correspond to the Lacy et al. (2004) box where the highly obscured quasars lie.

Similarly to the BPT diagram, the NIR selected AGNs in

our sample are mainly composed of S0 ($\sim 90\%$). Using this criteria, we find that 12.3% of S0 are AGN-dominated while only 1.1% of Elliptical galaxies are AGN-dominated. As we recalled previously, this estimator is not complete and it could also be biased for our selection, but it qualitatively matches the proportions we find with the BPT diagrams (19% for S0 and 0% for E).

As a comparison in table 2, we indicate sources detected in X-ray with Chandra with a high X-ray luminosity , i.e. $L_X > 10^{41} \text{ erg.s}^{-1}$, believed to be AGN sources as well. We also show if the SED-fit parameter f_{agn} indicates the presence of an AGN. f_{agn} is not strongly constrained by our SEDs, and we chose to report its value by indicating whether its lower 95% confidence level limit is greater than 10% at the 95% confidence level, ie. the AGN luminosity in MIR contributes at least 10% of the total IR luminosity. Galaxies with lower AGN contribution in their SED are reported with a “inc.” for inconclusive, since we could not conclude for these galaxies how large the potential AGN contribution could be.

6. COLORS

Colors can be good and simple indicators of star formation activity in galaxies. Therefore, in this section, we compare our previous results with some typical colors. We compute a color-magnitude diagram (SDSS u-r color versus R magnitude) of galaxies for which we have SDSS data (79 E and 68 S0). In Fig.11, Elliptical and Lenticular galaxies are represented by red and green dots respectively, and as expected most galaxies ($\sim 73\%$) in our sample reside in the red sequence (Strateva et al. 2001; Mignoli et al. 2009). Among the remaining galaxies, 22% (18 E and 15 S0) reside in the green valley and 5% (2 E and 5 S0) in the blue cloud (Strateva et al. 2001). The color-magnitude distribution of ETGs does not seem to depend on the galaxy morphology apart from a statistically poor hint of dominance of S0 in the blue clouds.

In Fig.11, black squares outline a 160 μm MIPS detection, which indicates the presence of cold dust in galaxies. The 160 μm detections (92) are bound to brighter galaxies ($R < -19.5$) (74) or to galaxies in the green valley (14), this distribution is explained by a larger specific dust mass and sSFR in galaxies from the green valley.

Fig. 12 shows the evolution of the dust-to-stellar mass ratio in logarithmic scale versus the (NUV-r) color. The dashed line corresponds to the best fit for our 29 sources with a secure SED fit and detected in the NUV. We find the same trend than (e.g., Smith et al. 2012; Agius et al. 2013), i.e. a decreasing M_{dust}/M_{star} ratio with an increasing (NUV-r) color. We color-code the stellar mass on each point of this plot with red ($\log(M_{star}) < 9.5$), green ($9.5 < \log(M_{star}) < 10.5$), cyan ($10.5 < \log(M_{star}) < 11$) and blue dots ($\log(M_{star}) > 11$). We see that the most massive galaxies (in stellar mass), i.e. galaxies with $\log(M_{star}) > 10.5$ (cyan and blue dots), are very red ($(\text{NUV}-r) > 4$). The most massive sources (blue dots) present a very low M_{dust}/M_{star} ratio, which corresponds most preferentially to galaxies with low M_{dust} and massive elliptical galaxies, as seen on Fig. 7. The NUV-r color seems to correlate with the dust mass only for bluer galaxies ($\text{NUV}-r < 4.5$), this result is consistent with the relation between sSFR and M_d/M_* , and the slope (-0.57 ± 0.17) is compatible with our slope in Fig. 7 and results from Rowlands et al. (2012) assuming a linear relation between sSFR and NUV-r. The correlation is more clear for the lower mass range of our sample ($\log(M_*/M_\odot) < 10$).

We test our sSFR estimated using CIGALEMC with the

TABLE 2
AGN CLASSIFICATION FROM THE 4 CRITERIA :
FROM THE BPT DIAGRAM, FROM THE AGN
TEMPLATE IN THE SED FIT, FROM THE NIR
COLOR CRITERIA, FROM X-RAY LUMINOSITY. A
DASH LINE INDICATES THAT WE DID NOT HAVE
DATA AND “INC.” INDICATES DATA WERE
INCONCLUSIVE.

Name	Type	BPT	SED	NIR	Xray
Eso103-35	S0	–	–	yes	–
Eso428-14	S0	–	–	no	yes
IC4296	E	–	inc.	no	yes
IC5063	S0	–	yes	yes	yes
NGC0221	E	–	–	no	yes
NGC0315	E	–	inc.	no	yes
NGC0410	E	–	inc.	no	yes
NGC0507	E	–	inc.	no	–
NGC0533	E	–	inc.	–	–
NGC0596	E	–	yes	no	–
NGC0807	E	–	inc.	–	–
NGC1016	E	–	inc.	no	–
NGC1374	E	–	inc.	yes	–
NGC1377	S0	–	yes	yes	–
NGC1386	S0	–	inc.	yes	no
NGC1407	S0	–	–	–	yes
NGC1439	E	–	yes	no	–
NGC1510	S0	–	inc.	yes	–
NGC2832	E	–	inc.	no	yes
NGC3011	S0	yes	inc.	yes	–
NGC3156	S0	yes	inc.	–	no
NGC3516	S0	–	inc.	yes	–
NGC3593	S0	–	inc.	no	–
NGC3610	E	–	yes	no	no
NGC3706	E	–	yes	no	–
NGC4117	S0	yes	inc.	no	no
NGC4138	S0	–	inc.	yes	–
NGC4168	E	yes	inc.	no	–
NGC4261	E	–	inc.	no	yes
NGC4344	S0	inc.	–	no	–
NGC4382	S0	–	yes	no	no
NGC4460	S0	–	inc.	yes	–
NGC4638	S0	–	yes	no	no
NGC4915	E	–	yes	no	no
NGC5061	E	–	yes	no	–
NGC5173	E	inc.	inc.	no	–
NGC5273	S0	yes	inc.	no	yes
NGC5419	E	–	inc.	no	yes
NGC5596	S0	yes	inc.	no	–
NGC5846	E	inc.	inc.	no	–
NGC6703	S0	–	yes	no	–
NGC7077	E	–	–	yes	–
NGC7626	E	–	inc.	no	yes

ratio F_{24}/F_K , which is in general a good indicator of specific star-formation when its value is larger than 0.1 Temi et al. (2009b). Fig. 13 shows a linear relation between the sSFR versus and the 24 μm color. Most of the galaxies with a large sSFR and 24 μm are S0 ($\sim 80\%$). This confirms our previous finding that S0 are more active in forming stars than E galaxies.

Three elliptical galaxies occupy a peculiar location in Fig. 13, at $\log(\text{sSFR}) \sim 10$ and $F_{24}/F_K \sim 0.05$. These galaxies are IC3370, NGC4494 and NGC5077. They all host an AGN according to the Veron catalog¹⁶ (Véron-Cetty & Véron 2010). According to our SED fitting, their age_{D4000}, determined with the 4000 Å break, is also very low (age_{D4000} < 1.5 Gyr), which would imply they had a recent episod of star formation.

IC3370 geometry has been found to be triaxial (Samurović & Danziger 2005) and Jarvis (1987) classi-

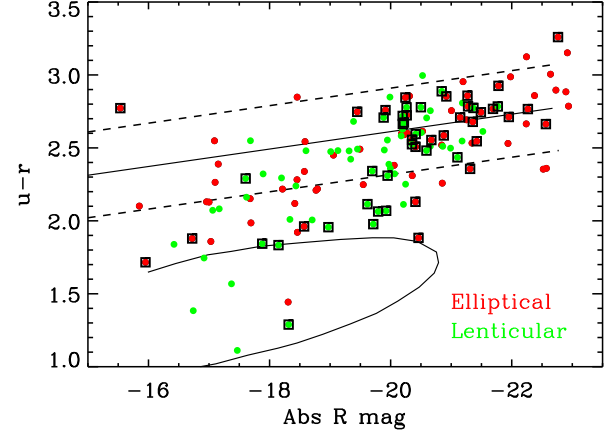


FIG. 11.— Optical color (u-r) versus the absolute R magnitude computed using SDSS data of the 147 sources in our sample for which such data exist. Elliptical and Lenticular galaxies are represented by respectively red and green dots. Sources with a 160 μm MIPS detection have been outlined with a black square. The solid straight line represents the red sequence and the two dashed lines delimit the 3 σ confidence interval. The solid curved line marks the position of the blue cloud. These area were taken from Temi et al. (2009b) and are not derived from the data points.

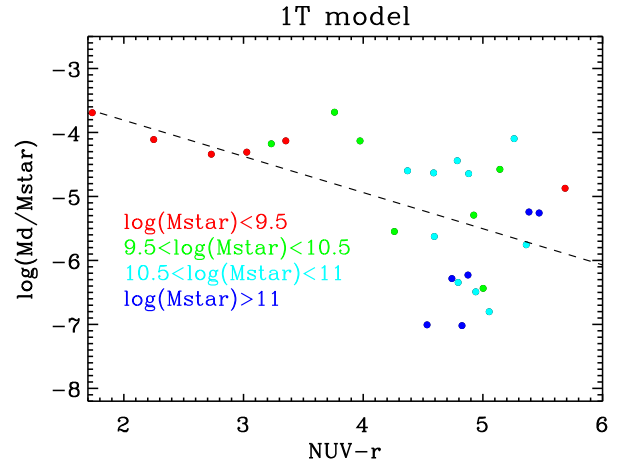


FIG. 12.— M_{dust}/M_{star} versus (NUV-r) color. The dashed line correspond to the best linear fit for all sources detected in NUV and with a relative error on $M_{dust} < 50\%$. The red dots correspond to the least massive galaxies (in terms of stellar mass) of the sample ($\log(M_{star}) < 9.5$) and the most massive sources are represented by the blue dots.

fied it as a peculiar S0pec with a box shape, and found some large isophotal twisting ($\Delta\text{P.A.} \simeq 25\text{deg}$) in its bulge. Jarvis (1987) also argue its peculiar shape could be due to the slow merger of 2 massive disk galaxies following Binney & Petrou (1985) model.

NGC4494 has been found to have an unusually low X-ray flux compared to its B band flux (O’Sullivan et al. 2001a), and this low ratio could be a hint for a recent merger (O’Sullivan & Ponman 2004) since in general it is found to be low for young early-type galaxies (Mackie & Fabbiano 1997; Sansom et al. 2000; O’Sullivan et al. 2001b). We also found earlier that NGC4494 had unusually low dust content for such high star formation rate.

NGC5077 is a LINER, with a H α bright gaseous disk in its central area (Bertola et al. 1991; Pizzella et al. 1997). We have a hint that 2 out of the 3 outliers could be merger, which

¹⁶ <http://heasarc.gsfc.nasa.gov/W3Browse/all/veroncat.html>

could explain their unusual $24\ \mu\text{m}$ color. However, there is also the possibility that our fit converge to a wrong solution for this 3 galaxies, since we do not have UV (GALEX) nor optical data (SDSS) for these galaxies.

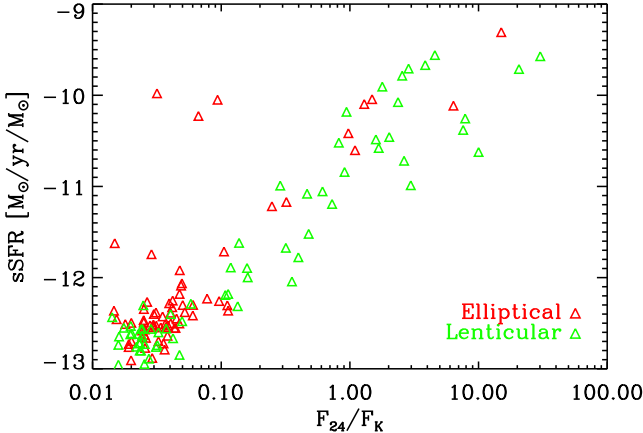


FIG. 13.— Specific SFR estimated with the SED fitting versus the ratio F_{24}/F_K for our elliptical (red) and lenticular (green) galaxies. The sSFR estimate correlate well with the $24\ \mu\text{m}$ color.

Using GALEX and SDSS data, we compute the UV-optical color FUV-r on our sample where data were available (72 E and 65 SO). Galaxies with infrared color F_{24}/F_K less than 0.1 are clustered around a FUV-r color of 7 and F_{24}/F_K of 0.03 on figure 14. Galaxies with larger infrared color are also bluer spreading in FUV-r from 6 to 2. Above a 0.1 F_{24}/F_K color, the logarithm of the infrared color linearly decreases as the FUV-r color increases. Bluer galaxies with $F_{24}/F_K > 0.1$ are composed of 7 Elliptical and 16 Lenticular galaxies. It is another indication that SO galaxies are in proportion more active than Ellipticals and show a clear agreement between infrared and UV star formation estimators.

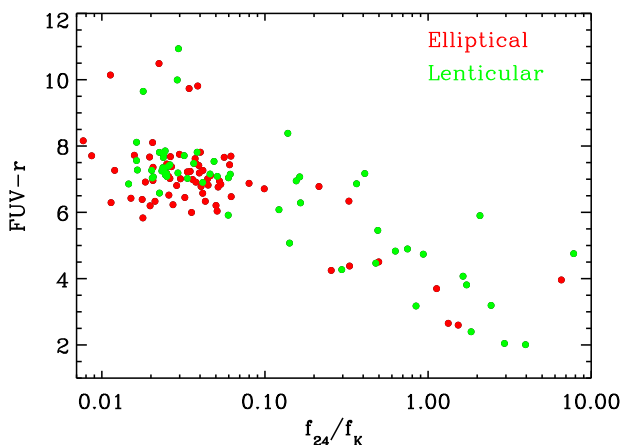


FIG. 14.— Far-UV-R color calculated from GALEX and SDSS data as a function of the infrared color F_{24}/f_K , obtained from MIPS and 2MASS data. Elliptical and Lenticular galaxies are represented by respectively red and green dots.

7. CONCLUSIONS

This paper analyzed a sample of 221 local ETGs to measure their star-formation activity and emphasize differences between Elliptical and Lenticular galaxies. Indeed, most ETGs are red galaxies but studies from past decades (e.g., Faber et al. 2007; Schawinski et al. 2007b) implied an evolution from blue galaxies to red ones through a green phase possibly powered by an AGN. 52% of our sample are Elliptical and 48% are SO. We performed SED-fittings on our galaxies which produced constraints on their physical parameters, we concentrated on their star formation rate, dust luminosity, stellar and dust mass, and dust temperature. Using these parameters, we derived the following conclusions :

- SO have a larger specific star formation rate and larger dust luminosity when renormalized by their stellar mass than elliptical galaxies.
- The average dust temperature of the sample is about 32.3 K fitting with a single temperature model, but it decreases to 22.4 K when using a 2 temperature model. This difference most likely comes from the fact that our 2 temperature model requires at least one Herschel-SPIRE detection, and thus biases the selection towards colder galaxies. We did not find any difference between elliptical and lenticular galaxy dust temperature.
- The dust-to-stellar mass ratio is decreasing with the stellar mass for both elliptical and lenticular galaxies, and these relations are statistically indistinguishable.
- The sSFR does not evolve with the dust-to-stellar mass ratio for $\log(M_d/M_*) < -5$ but steeply increases at higher dust-to-stellar mass ratio. Elliptical galaxies are mainly located at $\log(M_d/M_*) < -5$ with no correlation between their sSFR and dust-to-stellar mass ratio, while SO galaxies are located at higher $\log(M_d/M_*)$, which correlated well with the specific star formation rate.
- According to our BPT and NIR diagrams, a larger fraction ($\sim 12\text{-}19\%$) of SO galaxies show signs of AGN activity when compared to elliptical galaxies ($\sim 0\text{-}1\%$). This observation is consistent with a scenario where blue star-forming galaxies evolve to a red elliptical passing through a SO AGN active phase (Schawinski et al. 2007b).
- far-infrared and UV colors are both in good agreement with our multi-frequency analysis and with each other. All indicators point towards SO being more active at forming stars on average than ellipticals.

These results emphasize the differences between elliptical and lenticular galaxies to possibly explain the transition phase between blue and red galaxies through the green valley. We will focus in the near future on the green and blue early-type galaxies, identified in this paper, to have a better understanding of the star-formation transition phase, using GALEX, IRAC and MIPS data.

We would like to thank our anonymous referee for his/her useful comments which helped improve the original manuscript. This publication makes use of data products from the Two Micron All Sky Survey, which is a joint project of the University of Massachusetts and the Infrared Processing and Analysis Center/California Institute of Technology,

funded by the National Aeronautics and Space Administration and the National Science Foundation. This publication makes use of data from SDSS-III. Funding for SDSS-III has been provided by the Alfred P. Sloan Foundation, the Participating Institutions, the National Science Foundation, and the U.S. Department of Energy Office of Science. The SDSS-III web site is <http://www.sdss3.org/>. SDSS-III is managed by the Astrophysical Research Consortium for the Participating Institutions of the SDSS-III Collaboration including the University of Arizona, the Brazilian Participation Group, Brookhaven National Laboratory, University of Cambridge, Carnegie Mellon University, University of Florida, the French Participation Group, the German Participation Group, Harvard University, the Instituto de Astrofísica de Canarias, the Michigan State/Notre Dame/JINA Participation Group, Johns

Hopkins University, Lawrence Berkeley National Laboratory, Max Planck Institute for Astrophysics, Max Planck Institute for Extraterrestrial Physics, New Mexico State University, New York University, Ohio State University, Pennsylvania State University, University of Portsmouth, Princeton University, the Spanish Participation Group, University of Tokyo, University of Utah, Vanderbilt University, University of Virginia, University of Washington, and Yale University. This work is based in part on observations made with the Spitzer Space Telescope, which is operated by the Jet Propulsion Laboratory, California Institute of Technology under a contract with NASA. This work is based in part on observations made with the NASA Galaxy Evolution Explorer. GALEX is operated for NASA by the California Institute of Technology under NASA contract NAS5-98034.

REFERENCES

- Agius, N. K., Sansom, A. E., Popescu, C. C., et al. 2013, MNRAS, 431, 1929
- Agadzé, N. I., Sievers, A. J., Jones, S. A., Burlitch, J. M., & Beckwith, S. V. W. 1996, ApJ, 462, 1026
- Amblard, A., Cooray, A., Serra, P., et al. 2010, A&A, 518, L9
- Assef, R. J., Stern, D., Kochanek, C. S., et al. 2013, ApJ, 772, 26
- Auger, M. W., Treu, T., Gavazzi, R., et al. 2010, ApJ, 721, L163
- Bacon, R., Copin, Y., Monnet, G., et al. 2001, MNRAS, 326, 23
- Baldwin, J. A., Phillips, M. M., & Terlevich, R. 1981, PASP, 93, 5
- Barway, S., Wadadekar, Y., Vaghmare, K., & Kembhavi, A. K. 2013, MNRAS, 432, 430
- Bertola, F., Bettoni, D., Danziger, J., Sadler, E., Sparke, L., & de Zeeuw, T. 1991, ApJ, 373, 369
- Binette, L., Magris, C. G., Stasińska, G., & Bruzual, A. G. 1994, A&A, 292, 13
- Binney, J., & Petrou, M. 1985, MNRAS, 214, 449
- Boulanger, F., Abergel, A., Bernard, J.-P., et al. 1996, A&A, 312, 256
- Calzetti, D. 1997, in American Institute of Physics Conference Series, Vol. 408, American Institute of Physics Conference Series, ed. W. H. Waller, 403–412
- Calzetti, D., Kennicutt, R. C., Engelbracht, C. W., et al. 2007, ApJ, 666, 870
- Calzetti, D., Kinney, A. L., & Storchi-Bergmann, T. 1994, ApJ, 429, 582
- Cappellari, M., Emsellem, E., Bacon, R., et al. 2007, MNRAS, 379, 418
- Cappellari, M., Emsellem, E., Krajnović, D., et al. 2011a, MNRAS, 413, 813
- . 2011b, MNRAS, 416, 1680
- Cardelli, J. A., Clayton, G. C., & Mathis, J. S. 1989, ApJ, 345, 245
- Cimatti, A., Daddi, E., Renzini, A., et al. 2004, Nature, 430, 184
- Cortese, L., Ciesla, L., Boselli, A., et al. 2012, A&A, 540, A52
- da Cunha, E., Charlot, S., & Elbaz, D. 2008, MNRAS, 388, 1595
- Dale, D. A., & Helou, G. 2002, ApJ, 576, 159
- de Zeeuw, P. T., Bureau, M., Emsellem, E., et al. 2002, MNRAS, 329, 513
- Desert, F.-X., Boulanger, F., & Puget, J. L. 1990, A&A, 237, 215
- di Serego Alighieri, S., Bianchi, S., Pappalardo, C., et al. 2013, A&A, 552, A8
- Draine, B. T., & Lee, H. M. 1984, ApJ, 285, 89
- Driver, S. P., Allen, P. D., Graham, A. W., et al. 2006, MNRAS, 368, 414
- Dunne, L., Eales, S., Edmunds, M., Ivison, R., Alexander, P., & Clements, D. L. 2000, MNRAS, 315, 115
- Dunne, L., & Eales, S. A. 2001, MNRAS, 327, 697
- Elbaz, D., Hwang, H. S., Magnelli, B., et al. 2010, A&A, 518, L29
- Emsellem, E., Cappellari, M., Krajnović, D., et al. 2007, MNRAS, 379, 401
- . 2011, MNRAS, 414, 888
- Faber, S. M., Willmer, C. N. A., Wolf, C., et al. 2007, ApJ, 665, 265
- Fang, J. J., Faber, S. M., Salim, S., Graves, G. J., & Rich, R. M. 2012, ApJ, 761, 23
- Giovannoli, E., Buat, V., Noll, S., Burgarella, D., & Magnelli, B. 2011, A&A, 525, A150
- Griffin, M. J., Abergel, A., Abreu, A., et al. 2010, A&A, 518, L3
- Grillo, C., Göbat, R., Lombardi, M., & Rosati, P. 2009, A&A, 501, 461
- Hildebrand, R. H. 1983, QJRAS, 24, 267
- Hughes, D. H., Robson, E. I., Dunlop, J. S., & Gear, W. K. 1993, MNRAS, 263, 607
- Hughes, T. M., & Cortese, L. 2009, MNRAS, 396, L41
- Ilbert, O., Capak, P., Salvato, M., et al. 2009, ApJ, 690, 1236
- Ilbert, O., Salvato, M., Le Floc'h, E., et al. 2010, ApJ, 709, 644
- Jarvis, B. 1987, AJ, 94, 30
- Kaviraj, S. 2010, MNRAS, 408, 170
- Kaviraj, S., Khochfar, S., Schawinski, K., et al. 2008, MNRAS, 388, 67
- Kaviraj, S., Schawinski, K., Devriendt, J. E. G., et al. 2007, ApJS, 173, 619
- Kewley, L. J., Dopita, M. A., Sutherland, R. S., Heisler, C. A., & Trevena, J. 2001, ApJ, 556, 121
- Kewley, L. J., Groves, B., Kauffmann, G., & Heckman, T. 2006, MNRAS, 372, 961
- Lacy, M., Storrie-Lombardi, L. J., Sajina, A., et al. 2004, ApJS, 154, 166
- Le Floc'h, E., Aussel, H., Ilbert, O., et al. 2009, ApJ, 703, 222
- Mackie, G., & Fabbiano, G. 1997, in Astronomical Society of the Pacific Conference Series, Vol. 116, The Nature of Elliptical Galaxies; 2nd Stromlo Symposium, ed. M. Arnaboldi, G. S. Da Costa, & P. Saha, 401
- Maraston, C. 2005, MNRAS, 362, 799
- Maraston, C., Daddi, E., Renzini, A., et al. 2006, ApJ, 652, 85
- Marino, A., Rampazzo, R., Bianchi, L., et al. 2011, MNRAS, 411, 311
- Mennella, V., Brucato, J. R., Colangeli, L., et al. 1998, ApJ, 496, 1058
- Mignoli, M., Zamorani, G., Scodéglio, M., et al. 2009, A&A, 493, 39
- Morrissey, P., Conrow, T., Barlow, T. A., et al. 2007, ApJS, 173, 682
- Noll, S., Burgarella, D., Giovannoli, E., Buat, V., Marcillac, D., & Muñoz-Mateos, J. C. 2009, A&A, 507, 1793
- O'Sullivan, E., Forbes, D. A., & Ponman, T. J. 2001a, MNRAS, 328, 461
- . 2001b, MNRAS, 324, 420
- O'Sullivan, E., & Ponman, T. J. 2004, MNRAS, 349, 535
- Paturel, G., Petit, C., Prugniel, P., Theureau, G., Rousseau, J., Brouty, M., Dubois, P., & Cambrésy, L. 2003, A&A, 412, 45
- Pizzella, A., Amico, P., Bertola, F., et al. 1997, A&A, 323, 349
- Reach, W. T., Dwek, E., Fixsen, D. J., et al. 1995, ApJ, 451, 188
- Rieke, G. H., Young, E. T., Engelbracht, C. W., et al. 2004, ApJS, 154, 25
- Rowlands, K., Dunne, L., Maddox, S., et al. 2012, MNRAS, 419, 2545
- Salim, S., Fang, J. J., Rich, R. M., Faber, S. M., & Thilker, D. A. 2012, ApJ, 755, 105
- Salpeter, E. E. 1955, ApJ, 121, 161
- Samurović, S., & Danziger, I. J. 2005, MNRAS, 363, 769
- Sansom, A. E., Hibbard, J. E., & Schweizer, F. 2000, AJ, 120, 1946
- Sarzi, M., Shields, J. C., Schawinski, K., et al. 2010, MNRAS, 402, 2187
- Schawinski, K., Kaviraj, S., Khochfar, S., et al. 2007a, ApJS, 173, 512
- Schawinski, K., Thomas, D., Sarzi, M., et al. 2007b, MNRAS, 382, 1415
- Scoville, N., Aussel, H., Brusa, M., et al. 2007, ApJS, 172, 1
- Serra, P., Amblard, A., Temi, P., Burgarella, D., Giovannoli, E., Buat, V., Noll, S., & Im, S. 2011, ApJ, 740, 22
- Siebenmorgen, R., Freudling, W., Krügel, E., & Haas, M. 2004a, A&A, 421, 129
- Siebenmorgen, R., Krügel, E., & Spoon, H. W. W. 2004b, A&A, 414, 123
- Skibba, R. A., Engelbracht, C. W., Dale, D., et al. 2011, ApJ, 738, 89
- Smith, M. W. L., Gomez, H. L., Eales, S. A., et al. 2012, ApJ, 748, 123
- Spinello, C., Koopmans, L. V. E., Trager, S. C., Czoske, O., & Treu, T. 2011, MNRAS, 417, 3000
- Stern, D., Assef, R. J., Benford, D. J., et al. 2012, ApJ, 753, 30
- Stern, D., Eisenhardt, P., Gorjian, V., et al. 2005, ApJ, 631, 163
- Strateva, I., Ivezić, Ž., Knapp, G. R., et al. 2001, AJ, 122, 1861
- Tasca, L. A. M., Kneib, J.-P., Iovino, A., et al. 2009, A&A, 503, 379
- Temi, P., Brightenti, F., & Mathews, W. G. 2005a, ApJ, 635, L25
- . 2007a, ApJ, 660, 1215
- . 2007b, ApJ, 666, 222
- . 2009a, ApJ, 695, 1
- . 2009b, ApJ, 707, 890
- Temi, P., Mathews, W. G., & Brightenti, F. 2005b, ApJ, 622, 235
- Thomas, D., Maraston, C., Bender, R., & Mendes de Oliveira, C. 2005, ApJ, 621, 673
- Trager, S. C., Faber, S. M., Worthey, G., & González, J. J. 2000, AJ, 120, 165
- Treu, T., Auger, M. W., Koopmans, L. V. E., et al. 2010, ApJ, 709, 1195
- Véron-Cetty, M.-P., & Véron, P. 2010, A&A, 518, A10
- Yan, R., & Blanton, M. R. 2012, ApJ, 747, 61
- Yi, S. K., Yoon, S.-J., Kaviraj, S., et al. 2005, ApJ, 619, L111
- Young, L. M., Bureau, M., Davis, T. A., et al. 2011, MNRAS, 414, 940

APPENDIX

TABLE 3
FLUXES (FUV TO z BAND, FROM GALEX AND SDSS DATA) AND REDSHIFTS USED
IN THIS STUDY, DATA WERE COLLECTED ACCORDING TO SECTION 2

Name	Redshift ^a	<i>FUV</i> (μ Jy)	<i>NUV</i> (μ Jy)	<i>u</i> (mJy)	<i>g</i> (mJy)	<i>r</i> (mJy)	<i>i</i> (mJy)	<i>z</i> (mJy)
Eso103-35	0.0133	-	-	-	-	-	-	-
Eso428-14	0.0057	-	-	-	-	-	-	-
Eso462-15	0.0191	76.33 \pm 8.11	351.30 \pm 17.22	-	-	-	-	-
Eso483-13	0.0030	1541.00 \pm 10.35	2364.00 \pm 10.02	-	-	-	-	-
IC0798	0.0047	16.75 \pm 2.97	133.10 \pm 4.56	1.24 \pm 0.02	4.71 \pm 0.01	8.58 \pm 0.02	11.97 \pm 0.03	14.31 \pm 0.10
IC1144	0.0403	1.58 \pm 0.46	184.20 \pm 3.95	1.50 \pm 0.02	6.99 \pm 0.08	13.24 \pm 0.15	17.94 \pm 0.21	22.13 \pm 0.24
IC1459	0.0060	781.10 \pm 8.39	3327.00 \pm 15.47	-	-	-	-	-
IC1639	0.0179	33.79 \pm 1.23	189.70 \pm 2.34	2.03 \pm 0.01	8.81 \pm 0.02	16.26 \pm 0.03	22.03 \pm 0.05	26.80 \pm 0.07
IC3032	0.0040	-	7.90 \pm 3.67	0.91 \pm 0.02	3.56 \pm 0.01	6.18 \pm 0.02	7.36 \pm 0.03	9.59 \pm 0.12
IC3101	0.0048	-	42.70 \pm 7.75	0.61 \pm 0.03	2.24 \pm 0.01	4.14 \pm 0.02	5.91 \pm 0.03	6.72 \pm 0.08
IC3328	0.0034	0.79 \pm 0.28	240.00 \pm 4.81	1.70 \pm 0.04	6.92 \pm 0.02	12.36 \pm 0.03	16.21 \pm 0.04	17.02 \pm 0.15
IC3370	0.0098	-	-	-	-	-	-	-
IC3381	0.0023	8.04 \pm 1.41	231.30 \pm 3.72	1.54 \pm 0.02	7.50 \pm 0.02	13.96 \pm 0.03	19.40 \pm 0.03	23.28 \pm 0.07
IC3383	0.0062	5.95 \pm 3.35	20.37 \pm 7.97	0.71 \pm 0.09	6.41 \pm 0.04	9.82 \pm 0.05	10.75 \pm 0.09	10.86 \pm 0.30
IC3461	0.0034	24.48 \pm 2.86	126.80 \pm 2.64	0.95 \pm 0.03	3.83 \pm 0.02	6.75 \pm 0.02	9.28 \pm 0.04	9.19 \pm 0.12
IC3468	0.0043	-	259.40 \pm 18.57	2.30 \pm 0.05	11.15 \pm 0.02	19.82 \pm 0.06	26.72 \pm 0.12	28.60 \pm 0.27
IC3470	0.0050	32.21 \pm 3.21	183.40 \pm 2.94	1.68 \pm 0.03	6.89 \pm 0.01	13.77 \pm 0.02	19.90 \pm 0.03	23.61 \pm 0.10
IC3487	0.0036	2.03 \pm 0.69	268.80 \pm 3.19	1.14 \pm 0.03	4.39 \pm 0.04	5.69 \pm 0.03	7.84 \pm 0.07	7.72 \pm 0.10
IC3501	0.0055	1.02 \pm 0.94	178.30 \pm 3.71	1.64 \pm 0.03	6.10 \pm 0.02	11.52 \pm 0.03	14.89 \pm 0.04	18.86 \pm 0.11
IC3586	0.0052	8.03 \pm 1.96	307.70 \pm 5.56	1.87 \pm 0.06	7.06 \pm 0.03	11.89 \pm 0.04	14.44 \pm 0.07	17.39 \pm 0.26
IC3602	0.0043	3.33 \pm 0.97	75.50 \pm 3.27	0.44 \pm 0.03	2.09 \pm 0.02	3.83 \pm 0.02	4.79 \pm 0.06	4.21 \pm 0.17
IC3633	0.0068	2.84 \pm 0.70	84.31 \pm 3.05	0.66 \pm 0.02	2.33 \pm 0.01	4.12 \pm 0.02	5.50 \pm 0.02	6.24 \pm 0.08
IC3652	0.0021	10.78 \pm 2.03	204.30 \pm 6.13	1.82 \pm 0.05	7.25 \pm 0.02	12.97 \pm 0.03	17.49 \pm 0.05	22.12 \pm 0.16
IC3653	0.0020	13.84 \pm 1.50	113.10 \pm 3.40	1.54 \pm 0.02	7.60 \pm 0.01	16.08 \pm 0.02	23.01 \pm 0.03	27.82 \pm 0.08
IC3735	0.0063	-	-	2.05 \pm 0.04	6.26 \pm 0.02	10.98 \pm 0.03	15.32 \pm 0.05	15.88 \pm 0.20
IC3773	0.0036	23.38 \pm 2.76	315.60 \pm 5.65	2.43 \pm 0.06	9.70 \pm 0.33	18.77 \pm 0.56	25.52 \pm 0.73	30.42 \pm 0.84
IC3779	0.0039	2.56 \pm 0.34	94.16 \pm 2.84	1.04 \pm 0.04	3.14 \pm 0.01	5.77 \pm 0.02	7.90 \pm 0.03	8.71 \pm 0.13
IC4296	0.0125	288.00 \pm 7.30	1952.00 \pm 13.86	-	-	-	-	-
IC4329	0.0151	256.30 \pm 6.19	623.60 \pm 3.08	-	-	-	-	-
IC5063	0.0113	385.90 \pm 7.07	1151.00 \pm 9.06	-	-	-	-	-
NGC0221	0.0002	1839.00 \pm 20.46	-	-	-	-	-	-
NGC0315	0.0165	220.50 \pm 5.98	816.20 \pm 11.22	5.61 \pm 0.10	49.91 \pm 0.36	113.00 \pm 0.79	172.10 \pm 1.15	224.20 \pm 1.15
NGC0404	0.0009	861.90 \pm 2.73	5439.00 \pm 5.36	-	-	-	-	-
NGC0410	0.0177	154.80 \pm 4.30	902.00 \pm 15.42	6.50 \pm 0.14	39.52 \pm 0.48	93.68 \pm 1.14	144.50 \pm 1.57	179.40 \pm 1.31
NGC0474	0.0078	102.50 \pm 3.38	1231.00 \pm 11.50	8.36 \pm 0.07	39.77 \pm 0.10	82.31 \pm 0.18	120.60 \pm 0.25	143.10 \pm 0.32
NGC0507	0.0165	192.10 \pm 5.92	1394.00 \pm 14.05	6.29 \pm 0.03	25.33 \pm 0.04	100.20 \pm 0.14	150.90 \pm 0.21	192.20 \pm 0.31
NGC0516	0.0082	1.91 \pm 0.89	206.20 \pm 3.95	1.92 \pm 0.05	9.49 \pm 0.18	18.88 \pm 0.28	26.72 \pm 0.22	34.63 \pm 0.60
NGC0526	0.0192	207.40 \pm 4.78	361.70 \pm 4.40	-	-	-	-	-
NGC0533	0.0185	181.80 \pm 11.55	527.70 \pm 18.88	6.30 \pm 0.10	32.15 \pm 0.17	73.34 \pm 0.48	109.30 \pm 0.71	138.70 \pm 0.57
NGC0584	0.0048	230.10 \pm 6.21	1660.00 \pm 11.69	17.02 \pm 0.10	103.50 \pm 1.71	215.60 \pm 3.55	193.20 \pm 1.14	411.90 \pm 5.92
NGC0596	0.0051	146.10 \pm 5.08	1418.00 \pm 10.83	13.61 \pm 0.10	72.51 \pm 0.38	143.20 \pm 0.71	205.60 \pm 1.00	229.90 \pm 0.66
NGC0636	0.0062	90.51 \pm 9.36	760.90 \pm 16.83	9.18 \pm 0.09	49.13 \pm 0.25	100.70 \pm 0.54	150.80 \pm 0.73	178.00 \pm 0.57
NGC0720	0.0058	642.90 \pm 1.09	1840.00 \pm 1.51	-	-	-	-	-
NGC0777	0.0167	242.80 \pm 4.19	716.00 \pm 10.60	5.39 \pm 0.06	32.40 \pm 0.12	75.04 \pm 0.32	115.30 \pm 0.44	149.30 \pm 0.53
NGC0807	0.0159	227.10 \pm 13.97	609.00 \pm 18.61	2.53 \pm 0.40	7.30 \pm 1.62	14.33 \pm 1.29	36.44 \pm 2.67	60.20 \pm 3.39
NGC0814	0.0054	336.30 \pm 6.47	663.80 \pm 4.84	-	-	-	-	-
NGC0821	0.0058	12.92 \pm 2.76	-	-	-	-	-	-
NGC0855	0.0020	1327.00 \pm 12.37	3314.00 \pm 17.30	8.19 \pm 0.20	23.35 \pm 0.40	39.83 \pm 0.66	51.71 \pm 0.60	60.00 \pm 0.78
NGC1016	0.0222	78.17 \pm 12.93	333.50 \pm 20.61	5.24 \pm 0.06	28.36 \pm 0.04	68.29 \pm 0.12	104.00 \pm 0.15	122.00 \pm 0.25
NGC1023	0.0028	759.70 \pm 15.34	3848.00 \pm 21.64	-	-	-	-	-
NGC1199	0.0086	126.30 \pm 5.02	735.10 \pm 7.85	6.65 \pm 0.07	46.67 \pm 0.32	101.20 \pm 0.47	154.90 \pm 0.78	188.60 \pm 0.81
NGC1266	0.0073	22.95 \pm 4.31	372.90 \pm 10.46	-	-	-	-	-
NGC1316	0.0059	1730.00 \pm 16.08	13110.00 \pm 29.48	-	-	-	-	-
NGC1374	0.0043	234.60 \pm 1.12	1007.00 \pm 1.59	-	-	-	-	-
NGC1377	0.0060	-	-	-	-	-	-	-
NGC1386	0.0029	606.20 \pm 1.32	1965.00 \pm 1.62	-	-	-	-	-
NGC1395	0.0057	739.20 \pm 20.96	2447.00 \pm 30.25	-	-	-	-	-
NGC1399	0.0048	2572.00 \pm 2.77	3494.00 \pm 1.86	-	-	-	-	-
NGC1404	0.0065	858.70 \pm 4.33	3510.00 \pm 8.35	-	-	-	-	-
NGC1407	0.0059	1276.00 \pm 14.15	3580.00 \pm 24.28	-	-	-	-	-
NGC1426	0.0048	108.90 \pm 3.75	904.50 \pm 8.74	-	-	-	-	-
NGC1427	0.0046	313.40 \pm 4.18	1917.00 \pm 7.62	-	-	-	-	-
NGC1439	0.0056	111.60 \pm 5.20	958.50 \pm 9.14	-	-	-	-	-
NGC1510	0.0030	4617.00 \pm 15.37	4707.00 \pm 10.98	-	-	-	-	-
NGC1522	0.0030	2751.00 \pm 15.51	3611.00 \pm 8.31	-	-	-	-	-
NGC1533	0.0026	682.40 \pm 12.32	1922.00 \pm 9.28	-	-	-	-	-
NGC1543	0.0039	202.30 \pm 11.90	1363.00 \pm 26.77	-	-	-	-	-
NGC1553	0.0036	828.20 \pm 8.75	5241.00 \pm 17.34	-	-	-	-	-

TABLE 3 — *Continued*

Name	Redshift ^a	FUV (μJy)	NUV (μJy)	<i>u</i> (mJy)	<i>g</i> (mJy)	<i>r</i> (mJy)	<i>i</i> (mJy)	<i>z</i> (mJy)
NGC1700	0.0130	-	-	8.33±0.04	52.68±0.40	110.50±0.85	162.10±1.10	215.50±1.49
NGC2110	0.0078	-	-	-	-	-	-	-
NGC2300	0.0064	349.30±9.11	1284.00±18.69	-	-	-	-	-
NGC2325	0.0073	-	-	-	-	-	-	-
NGC2434	0.0046	475.70±28.16	3738.00±41.46	-	-	-	-	-
NGC2685	0.0029	2103.00±10.52	3655.00±13.79	11.69±0.33	57.18±1.29	116.10±1.94	169.60±2.17	212.90±3.41
NGC2768	0.0046	382.00±9.09	2994.00±25.65	14.68±0.04	86.16±0.12	203.40±0.27	306.60±0.41	422.10±0.61
NGC2778	0.0068	47.42±7.88	276.90±15.79	3.98±0.03	21.27±0.05	43.62±0.09	63.88±0.14	76.47±0.18
NGC2787	0.0023	269.60±24.63	1598.00±42.67	-	-	-	-	-
NGC2832	0.0232	43.16±2.27	150.00±2.71	3.69±0.04	23.77±0.23	52.70±0.58	79.49±0.83	100.80±0.90
NGC2970	0.0054	51.05±2.21	285.90±4.99	2.25±0.03	7.59±0.02	13.21±0.04	17.80±0.06	20.82±0.11
NGC2974	0.0064	394.80±7.32	1882.00±12.86	-	-	-	-	-
NGC2986	0.0077	364.50±25.92	1284.00±27.34	-	-	-	-	-
NGC3011	0.0051	754.00±6.09	1064.00±6.39	1.78±0.03	7.54±0.05	13.98±0.09	18.57±0.13	21.40±0.13
NGC3032	0.0051	1144.00±6.81	2543.00±6.93	7.24±0.06	28.22±0.10	48.49±0.22	33.62±0.05	73.67±0.27
NGC3073	0.0039	311.30±1.33	743.50±1.55	2.90±0.02	10.10±0.02	15.85±0.03	20.57±0.04	23.29±0.09
NGC3115	0.0022	1364.00±14.98	7402.00±26.46	-	-	-	-	-
NGC3125	0.0037	5554.00±16.48	9416.00±12.27	-	-	-	-	-
NGC3156	0.0044	149.60±1.70	990.00±4.69	6.93±0.08	28.30±0.23	48.67±0.36	59.66±0.29	77.63±0.75
NGC3226	0.0038	-	-	7.54±0.07	41.75±0.07	90.76±0.09	139.10±0.11	177.70±0.27
NGC3265	0.0044	521.30±6.97	1067.00±6.77	3.27±0.02	10.76±0.04	19.93±0.07	27.41±0.10	33.49±0.12
NGC3377	0.0022	289.50±6.88	3547.00±17.73	27.49±0.05	139.80±0.19	277.00±0.37	210.20±1.54	514.70±0.73
NGC3379	0.0030	932.80±6.67	3455.00±4.23	29.04±0.08	167.80±0.35	352.30±0.74	300.20±0.20	663.40±1.30
NGC3384	0.0023	416.00±4.76	2253.00±3.33	24.90±0.14	148.30±0.95	301.20±1.96	233.00±0.22	537.80±3.32
NGC3412	0.0028	234.80±2.99	1829.00±3.55	19.95±0.06	117.80±0.47	219.90±0.39	314.40±1.01	362.20±0.87
NGC3489	0.0023	639.60±14.00	3976.00±14.28	25.57±0.13	118.40±0.55	172.10±0.17	258.80±0.66	373.00±1.61
NGC3516	0.0088	1888.00±13.33	3951.00±12.47	-	-	-	-	-
NGC3522	0.0041	42.20±2.18	404.90±6.43	3.40±0.10	14.16±0.20	26.27±0.31	35.94±0.37	39.21±0.17
NGC3557	0.0103	17.44±8.06	1132.00±48.36	-	-	-	-	-
NGC3585	0.0048	494.70±22.99	2980.00±42.40	-	-	-	-	-
NGC3593	0.0021	508.40±7.92	2834.00±13.60	9.80±0.09	50.58±0.09	116.00±0.68	183.20±0.19	254.40±0.34
NGC3607	0.0032	72.00±5.46	3221.00±12.30	34.17±0.08	184.20±0.25	403.30±0.52	618.40±0.80	819.30±1.12
NGC3608	0.0042	255.00±3.38	1384.00±9.22	-	-	-	-	-
NGC3610	0.0057	141.00±2.70	1548.00±7.33	21.35±0.32	99.37±1.65	187.20±2.88	258.40±3.74	304.00±3.33
NGC3640	0.0042	187.90±4.66	2242.00±15.11	19.72±0.09	109.30±0.62	235.70±1.37	360.00±2.16	435.90±2.31
NGC3706	0.0099	142.50±21.31	860.70±42.62	-	-	-	-	-
NGC3773	0.0033	3660.00±49.27	4822.00±32.17	7.07±0.04	15.79±0.03	23.18±0.07	26.75±0.09	27.84±0.14
NGC3870	0.0025	3161.00±16.77	4213.00±11.48	7.43±0.07	15.56±0.15	20.71±0.17	23.79±0.22	25.86±0.15
NGC3923	0.0058	843.00±11.73	5879.00±27.05	-	-	-	-	-
NGC3941	0.0031	12.76±6.03	1276.00±40.19	29.75±0.25	152.50±0.90	300.80±1.50	426.30±1.82	511.70±1.78
NGC3945	0.0042	165.60±20.86	965.90±31.22	9.74±0.05	59.87±0.32	119.40±0.03	196.00±1.13	240.80±1.31
NGC3962	0.0061	275.30±5.41	2190.00±16.29	-	-	-	-	-
NGC4026	0.0031	139.90±9.22	1252.00±19.46	15.96±0.59	90.50±3.65	185.80±7.11	220.30±6.36	340.40±12.87
NGC4073	0.0196	238.40±4.92	593.60±7.20	3.92±0.07	28.90±0.13	71.50±0.58	106.80±0.80	140.70±1.36
NGC4117	0.0031	179.60±3.63	439.20±4.36	3.29±0.10	13.57±0.24	27.20±0.44	39.06±0.63	46.62±0.68
NGC4125	0.0045	242.70±19.46	1929.00±37.41	20.76±0.11	130.50±0.75	288.90±1.91	434.90±3.02	553.30±3.70
NGC4138	0.0030	2309.00±11.31	3726.00±8.56	11.60±0.11	72.73±0.33	140.60±0.52	199.80±0.61	260.40±1.67
NGC4150	0.0034	111.70±2.46	449.20±3.53	9.96±0.04	43.69±0.05	82.15±0.07	118.30±0.11	131.50±0.23
NGC4168	0.0074	175.80±6.73	1636.00±9.66	9.88±0.07	48.61±0.07	101.90±0.16	147.60±0.26	191.50±0.52
NGC4203	0.0036	554.90±12.79	1928.00±18.89	10.92±0.11	61.72±0.59	128.20±0.22	198.80±1.97	249.80±2.29
NGC4251	0.0036	108.80±11.43	1534.00±33.06	16.52±0.34	76.60±0.91	131.50±1.85	216.30±2.50	276.60±4.62
NGC4261	0.0075	599.50±5.27	2069.00±12.97	18.12±0.08	106.60±0.34	231.80±0.75	350.30±1.11	444.20±1.27
NGC4267	0.0034	152.60±6.16	1141.00±13.82	11.38±0.07	61.83±0.16	128.20±0.31	191.70±0.34	236.40±0.34
NGC4278	0.0022	943.10±12.01	3155.00±16.59	23.24±0.07	133.90±0.16	285.70±0.41	424.50±0.58	522.70±0.57
NGC4291	0.0059	-	-	-	-	-	-	-
NGC4308	0.0020	23.60±2.16	198.00±2.89	2.19±0.02	9.30±0.01	17.61±0.02	24.70±0.03	30.03±0.13
NGC4344	0.0038	449.80±6.48	1134.00±7.60	5.80±0.06	19.08±0.09	35.17±0.21	46.93±0.14	54.30±1.06
NGC4350	0.0040	276.80±19.95	1086.00±29.70	12.63±0.08	82.83±3.52	180.70±9.49	268.70±12.75	335.40±16.02
NGC4352	0.0069	30.51±3.25	399.50±4.13	5.76±0.15	21.32±0.26	40.38±0.43	58.77±0.80	71.90±0.94
NGC4365	0.0041	988.40±7.66	4419.00±13.28	28.54±0.07	169.80±0.23	365.60±0.48	537.70±0.71	730.80±1.02
NGC4371	0.0031	254.40±6.57	1413.00±7.76	14.48±0.08	88.37±0.28	187.40±0.54	288.20±0.90	364.10±1.32
NGC4374	0.0035	1311.00±14.20	6867.00±19.68	-	-	-	-	-
NGC4377	0.0046	74.57±13.39	361.60±16.24	7.28±0.04	38.82±0.11	78.56±0.21	114.20±0.29	141.30±0.37
NGC4379	0.0036	135.00±5.93	289.20±5.02	9.13±0.05	45.31±0.13	90.23±0.21	135.30±0.37	165.20±0.40
NGC4382	0.0024	572.40±33.07	5630.00±65.97	23.85±0.64	121.70±1.30	244.30±0.64	334.20±2.16	427.70±2.57
NGC4386	0.0056	-	-	-	-	-	-	-
NGC4406	0.0039	1315.00±16.06	8308.00±23.69	33.49±0.07	216.20±0.28	430.90±0.55	641.20±0.82	861.50±1.15
NGC4417	0.0028	183.20±3.43	1177.00±8.69	12.32±0.29	64.95±1.15	129.60±2.36	190.20±3.47	226.60±4.12
NGC4421	0.0053	48.03±2.74	1079.00±10.75	5.32±0.07	46.04±0.16	84.11±0.25	124.10±0.39	128.40±0.83
NGC4434	0.0036	78.18±2.49	469.50±4.12	6.14±0.04	30.45±0.03	60.98±0.06	87.97±0.08	105.40±0.14
NGC4435	0.0027	187.50±5.12	1780.00±7.10	44.68±0.17	203.80±0.08	421.30±0.12	644.80±0.19	749.70±0.64
NGC4442	0.0018	378.50±4.90	1791.00±9.19	18.56±0.22	119.80±1.54	256.00±3.51	371.40±4.60	481.00±7.19
NGC4458	0.0021	48.66±2.62	596.20±5.26	5.49±0.05	29.21±0.04	57.16±0.07	82.33±0.10	102.30±0.18
NGC4459	0.0040	429.60±7.06	2240.00±12.53	-	-	-	-	-
NGC4460	0.0016	2130.00±13.41	4495.00±8.57	13.10±0.13	42.01±0.13	70.98±1.57	93.35±0.24	100.50±1.88
NGC4464	0.0041	63.19±1.73	252.50±3.01	4.17±0.04	20.36±0.12	40.96±0.24	60.32±0.38	72.86±0.38

TABLE 3 — *Continued*

Name	Redshift ^a	FUV (μJy)	NUV (μJy)	<i>u</i> (mJy)	<i>g</i> (mJy)	<i>r</i> (mJy)	<i>i</i> (mJy)	<i>z</i> (mJy)
NGC4472	0.0033	2605.00±17.86	8820.00±28.03	37.65±0.09	253.40±0.35	557.70±0.76	858.50±1.17	1071.00±1.50
NGC4473	0.0075	434.10±7.14	2366.00±8.47	19.63±0.07	111.20±0.35	228.70±0.72	342.20±1.08	424.90±1.15
NGC4474	0.0053	69.82±4.00	890.90±9.03	7.59±0.05	44.90±0.40	96.14±1.44	134.60±1.34	157.00±1.26
NGC4476	0.0066	155.70±3.17	977.00±4.37	7.46±0.15	28.68±0.45	53.15±0.72	73.84±0.96	88.18±1.14
NGC4477	0.0045	353.20±7.70	1768.00±7.59	18.62±0.12	115.70±0.61	239.80±0.79	350.30±0.90	467.40±2.15
NGC4478	0.0045	215.30±3.87	1050.00±3.89	6.59±0.21	42.97±0.33	91.45±0.51	142.00±0.64	183.10±0.70
NGC4479	0.0029	67.48±4.15	370.50±3.84	3.77±0.05	18.91±0.08	37.12±0.11	51.58±0.10	63.48±0.25
NGC4482	0.0062	14.31±5.26	374.60±21.34	3.29±0.06	13.97±0.07	26.12±0.14	33.67±0.12	36.67±0.20
NGC4483	0.0029	67.64±1.56	408.60±4.39	5.46±0.06	26.44±0.12	53.40±0.26	77.34±0.36	94.69±0.47
NGC4486	0.0044	4771.00±17.30	12200.00±15.87	-	-	-	-	-
NGC4489	0.0032	55.09±2.40	591.20±5.20	5.12±0.08	26.62±0.21	48.96±0.32	70.47±0.47	81.28±0.48
NGC4494	0.0045	-	-	-	-	-	-	-
NGC4515	0.0032	56.97±3.85	449.20±6.92	5.02±0.04	20.24±0.06	38.43±0.11	54.90±0.17	61.56±0.17
NGC4526	0.0015	667.50±7.11	3613.00±16.00	30.95±0.23	186.30±2.26	400.10±4.92	331.90±0.34	799.40±11.30
NGC4528	0.0045	75.13±3.81	529.10±3.58	7.46±0.08	33.79±0.28	67.40±0.54	98.55±0.84	121.60±1.03
NGC4552	0.0037	1193.00±12.74	4166.00±12.78	31.92±0.06	190.90±0.25	405.60±0.51	390.40±2.57	840.10±1.12
NGC4564	0.0038	267.40±4.46	1221.00±5.22	13.12±0.22	68.49±0.17	145.80±0.78	215.30±0.76	259.90±0.92
NGC4570	0.0058	285.70±5.10	1350.00±9.57	16.51±1.19	88.74±5.89	183.40±12.37	270.70±18.07	333.70±20.83
NGC4578	0.0076	11.69±1.12	1089.00±9.91	8.06±0.05	41.12±0.06	84.27±0.15	118.40±0.12	143.30±0.24
NGC4589	0.0066	178.20±3.62	1831.00±11.23	-	-	-	-	-
NGC4612	0.0059	85.07±7.28	1052.00±17.58	10.69±1.11	56.35±0.69	106.80±0.86	149.70±1.25	173.10±3.76
NGC4621	0.0037	701.90±9.00	3069.00±14.66	32.67±0.07	219.50±0.28	449.50±0.57	682.40±0.86	889.00±1.16
NGC4623	0.0063	47.77±5.34	525.60±16.32	4.40±0.05	19.81±0.03	38.71±0.07	55.67±0.10	65.78±0.17
NGC4636	0.0031	750.60±31.02	3341.00±58.03	24.78±0.07	126.20±0.18	268.30±0.37	395.50±0.55	568.30±0.87
NGC4638	0.0039	130.90±4.68	1004.00±5.79	11.67±0.40	63.26±2.50	127.50±5.01	184.20±7.45	220.60±6.50
NGC4649	0.0037	3149.00±19.62	7900.00±16.28	-	-	-	-	-
NGC4660	0.0036	212.20±5.05	1466.00±8.90	12.80±0.30	67.10±1.30	134.90±2.58	202.30±3.79	243.50±4.05
NGC4694	0.0039	794.10±8.84	3710.00±14.88	10.93±0.06	44.24±0.63	67.59±0.32	84.17±0.18	94.77±0.20
NGC4696	0.0099	161.70±26.86	1262.00±78.20	-	-	-	-	-
NGC4697	0.0041	756.40±10.49	6516.00±25.32	-	-	-	-	-
NGC4709	0.0156	132.50±23.48	606.00±48.87	-	-	-	-	-
NGC4754	0.0045	240.10±16.93	1088.00±28.32	15.66±0.15	91.35±0.86	208.10±2.94	309.20±4.29	376.30±5.08
NGC4762	0.0033	203.00±21.87	2556.00±26.90	20.68±0.12	106.50±0.75	209.00±1.15	300.70±1.93	362.40±1.28
NGC4786	0.0155	83.90±10.85	382.70±19.56	-	-	-	-	-
NGC4915	0.0101	47.69±10.07	420.10±12.08	-	-	-	-	-
NGC4936	0.0104	134.50±17.83	1246.00±39.13	-	-	-	-	-
NGC5018	0.0094	171.20±18.23	1949.00±35.43	-	-	-	-	-
NGC5044	0.0093	514.10±11.95	2116.00±21.83	-	-	-	-	-
NGC5061	0.0069	264.80±14.17	2955.00±40.88	-	-	-	-	-
NGC5077	0.0094	-	-	-	-	-	-	-
NGC5173	0.0081	535.90±7.16	1022.00±5.81	3.36±0.03	15.85±0.08	30.15±0.20	42.13±0.36	48.29±0.35
NGC5273	0.0035	163.40±3.55	1045.00±8.34	10.46±0.06	48.17±0.05	90.45±0.08	122.00±0.10	142.20±0.29
NGC5322	0.0059	300.00±7.14	2172.00±11.86	19.85±0.21	101.90±1.09	207.20±1.98	299.00±2.81	378.00±3.06
NGC5338	0.0027	258.50±4.89	872.60±7.54	2.75±0.08	13.43±0.33	23.39±0.58	31.25±0.73	34.83±0.65
NGC5353	0.0078	272.60±19.73	890.60±22.04	12.01±0.33	72.57±1.48	156.20±3.08	242.30±5.29	296.30±3.79
NGC5419	0.0138	307.10±27.32	782.60±33.38	-	-	-	-	-
NGC5481	0.0071	-	-	3.79±0.04	18.13±0.04	39.97±0.09	65.93±0.31	63.21±0.16
NGC5557	0.0107	12.74±1.14	1001.00±6.98	9.64±0.06	52.65±0.46	99.23±0.99	185.50±1.92	184.30±1.81
NGC5576	0.0050	181.00±3.51	2064.00±10.88	13.68±0.07	70.77±0.47	139.40±0.79	200.90±1.19	247.00±1.49
NGC5596	0.0104	176.70±2.33	314.70±2.84	2.21±0.02	9.24±0.02	18.79±0.03	27.03±0.05	33.18±0.11
NGC5813	0.0066	391.60±7.09	2638.00±19.84	10.23±0.08	59.72±4.10	133.10±0.83	199.60±1.16	256.50±5.64
NGC5831	0.0055	116.00±4.06	1078.00±8.34	6.36±0.04	33.00±0.13	69.19±0.30	102.70±0.37	131.10±0.38
NGC5845	0.0048	85.48±2.39	275.60±3.63	3.43±0.02	19.94±0.08	43.14±0.19	64.77±0.30	84.54±0.35
NGC5846	0.0057	844.60±8.43	2751.00±15.17	16.80±0.05	96.80±0.14	210.60±0.29	316.00±0.43	462.20±0.70
NGC5866	0.0022	501.60±7.90	4212.00±16.53	40.00±0.44	168.60±1.13	336.00±2.42	481.70±3.06	615.10±2.54
NGC5982	0.0101	214.50±5.62	1434.00±9.97	10.21±0.09	59.32±0.42	124.20±0.96	182.90±1.24	220.50±1.49
NGC6482	0.0131	98.41±4.30	36.19±1.20	-	-	-	-	-
NGC6684	0.0029	-	-	-	-	-	-	-
NGC6703	0.0082	4.25±1.79	-	-	-	-	-	-
NGC6776	0.0183	49.83±8.86	342.10±18.64	-	-	-	-	-
NGC6849	0.0201	21.12±4.59	-	-	-	-	-	-
NGC7077	0.0032	1310.00±8.56	1849.00±7.49	2.52±0.02	9.27±0.02	14.27±0.03	18.39±0.05	22.48±0.09
NGC7176	0.0084	-	-	-	-	-	-	-
NGC7360	0.0156	284.70±3.39	518.30±5.19	1.69±0.04	6.92±0.06	14.18±0.11	20.43±0.13	27.52±0.43
NGC7457	0.0027	90.41±4.55	1686.00±10.25	9.90±0.03	53.61±0.08	103.70±0.14	147.50±0.21	195.10±0.31
NGC7619	0.0125	179.30±6.24	1013.00±16.85	7.39±0.08	57.18±0.14	131.60±0.43	208.50±0.83	255.50±0.59
NGC7626	0.0114	203.60±6.79	851.80±12.51	8.24±0.03	55.52±0.08	129.30±0.17	202.20±0.26	265.70±0.39
NGC7785	0.0127	-	-	8.05±0.24	41.58±0.80	92.26±1.61	139.30±2.12	184.70±3.32
UGC01503	0.0170	-	-	1.76±0.02	5.51±0.06	9.90±0.10	15.49±0.29	19.45±0.45
UGC06570	0.0053	203.70±3.85	613.40±4.89	2.55±0.06	9.11±0.18	16.17±0.33	21.33±0.43	24.93±0.48
UGC06637	0.0061	777.00±7.91	1186.00±6.52	2.36±0.02	6.01±0.03	8.91±0.06	11.00±0.09	12.25±0.11
UGC06655	0.0025	903.90±6.82	1257.00±5.61	2.29±0.02	5.40±0.02	8.19±0.03	9.98±0.04	11.02±0.07
UGC06805	0.0039	483.50±6.45	879.80±5.75	2.15±0.02	5.77±0.02	9.11±0.04	11.02±0.06	12.56±0.10
UGC07436	0.0033	14.87±2.52	205.50±5.57	1.70±0.05	6.81±0.02	12.49±0.03	16.91±0.06	20.82±0.25
UGC07580	0.0021	27.84±1.41	45.86±1.28	1.43±0.03	4.66±0.02	7.79±0.06	10.31±0.12	11.64±0.09
UGC07854	0.0034	-	-	1.04±0.04	3.96±0.01	7.05±0.04	9.65±0.06	11.06±0.13

TABLE 3 — *Continued*

Name	Redshift ^a	FUV (μJy)	NUV (μJy)	<i>u</i> (mJy)	<i>g</i> (mJy)	<i>r</i> (mJy)	<i>i</i> (mJy)	<i>z</i> (mJy)
UGC08876	0.0069	28.18±1.83	141.90±3.03	2.26±0.12	10.63±0.43	21.03±0.83	30.78±1.24	37.89±1.39

^a For a few galaxies (mainly very nearby galaxies), the redshift was calculated using the distance from NED.

TABLE 4
FLUXES (2MASS J TO K BAND AND SPITZER IRAC 3.6 TO 8 μM) USED IN THIS STUDY, DATA WERE COLLECTED ACCORDING TO SECTION 2

Name	<i>J</i> (mJy)	<i>H</i> (mJy)	<i>Ks</i> (mJy)	<i>i</i> 3.6 (mJy)	<i>i</i> 4.5 (mJy)	<i>i</i> 5.8 (mJy)	<i>i</i> 8.0 (mJy)
Eso103-35	46.14±1.02	58.98±1.58	50.70±1.64	-	-	-	-
Eso428-14	197.20±2.36	252.50±3.02	213.30±4.52	121.60±6.08	81.35±4.07	119.10±5.96	249.40±12.47
Eso462-15	197.60±2.37	242.50±3.80	205.20±3.78	138.20±6.91	73.53±3.68	54.14±2.71	22.39±1.12
Eso483-13	35.33±1.53	36.47±2.39	31.67±2.86	13.53±0.68	8.80±0.44	7.26±0.36	10.22±0.51
IC0798	17.54±0.63	21.24±1.12	15.21±1.05	-	-	-	-
IC1144	33.96±0.88	43.21±1.43	37.20±1.27	20.56±1.03	11.88±0.59	7.67±0.38	5.87±0.29
IC1459	1373.00±24.03	1573.00±30.43	1301.00±29.95	591.90±29.60	290.40±14.52	156.00±7.80	140.10±7.01
IC1639	38.35±0.60	46.17±0.94	38.42±1.03	19.10±0.96	11.38±0.57	8.12±0.41	5.48±0.27
IC3032	12.24±0.73	12.22±0.89	9.29±0.83	-	-	-	-
IC3101	4.82±0.52	5.25±0.71	4.67±0.89	-	-	-	-
IC3328	26.63±1.40	27.14±1.98	20.65±2.35	-	5.92±0.30	-	1.36±0.07
IC3370	482.70±5.78	599.70±7.73	493.20±9.54	266.90±13.35	158.70±7.94	123.90±6.20	91.30±4.57
IC3381	35.30±1.69	43.33±2.48	26.12±2.87	-	8.47±0.42	-	1.90±0.09
IC3383	9.57±0.63	10.59±0.91	5.10±1.07	-	-	-	-
IC3461	11.59±0.61	13.10±0.93	7.42±1.04	-	-	-	-
IC3468	45.76±2.62	52.52±4.02	42.83±4.47	-	9.26±0.46	-	2.46±0.12
IC3470	27.63±1.07	29.95±1.35	23.19±1.50	-	-	-	-
IC3487	9.27±0.67	15.56±1.00	8.84±1.15	-	-	-	-
IC3501	24.42±0.70	25.02±1.22	21.87±1.15	-	-	-	-
IC3586	10.20±0.44	10.94±0.77	9.63±0.72	-	-	-	-
IC3602	10.00±0.53	12.27±0.77	12.62±0.91	-	-	-	-
IC3633	3.53±0.30	4.53±0.45	2.74±0.52	-	-	-	-
IC3652	29.85±1.76	33.76±2.40	26.12±3.06	-	-	-	-
IC3653	42.63±1.06	51.14±1.46	40.34±1.86	-	-	-	-
IC3735	17.84±0.94	20.21±1.68	19.27±1.48	-	-	-	-
IC3773	34.30±1.11	36.07±1.46	29.17±1.88	-	-	-	-
IC3779	4.76±0.37	9.36±0.67	5.16±0.60	-	-	-	-
IC4296	663.30±7.94	826.30±9.89	684.50±13.24	271.60±13.58	132.70±6.63	58.72±2.94	47.60±2.38
IC4329	433.00±6.78	483.40±10.69	411.30±9.85	161.70±8.09	103.20±5.16	69.40±3.47	38.04±1.90
IC5063	215.20±2.77	259.40±3.82	216.90±4.00	155.10±7.75	145.00±7.25	302.50±15.12	451.10±22.55
NGC0221	5060.00±74.56	7536.00±111.10	6283.00±98.39	2460.00±123.00	1440.00±72.00	1230.00±61.52	879.70±43.98
NGC0315	431.80±4.77	550.50±8.11	451.00±6.65	249.80±12.49	120.70±6.03	68.89±3.44	47.28±2.36
NGC0404	713.40±11.83	830.10±15.29	665.90±14.72	442.80±22.14	209.00±10.45	152.10±7.60	105.30±5.27
NGC0410	290.60±3.48	363.00±5.35	304.90±5.90	182.00±9.10	83.59±4.18	41.71±2.08	20.37±1.02
NGC0474	263.10±6.30	317.90±9.96	259.50±9.32	-	70.93±3.55	44.25±2.21	22.99±1.15
NGC0507	335.50±4.95	353.50±7.49	327.60±6.94	196.40±9.82	126.90±6.35	104.10±5.21	32.46±1.62
NGC0516	46.44±1.07	53.06±1.42	42.56±1.73	22.04±1.10	13.91±0.70	8.45±0.42	5.81±0.29
NGC0526	-	-	-	-	-	-	-
NGC0533	278.30±4.10	345.40±6.04	287.50±7.15	-	-	-	-
NGC0584	827.40±14.48	1071.00±20.72	821.50±18.92	353.30±17.67	186.70±9.34	159.20±7.96	102.60±5.13
NGC0596	466.10±5.15	560.70±8.78	442.80±9.38	209.90±10.50	120.90±6.04	84.68±4.23	42.63±2.13
NGC0636	307.40±4.25	358.40±5.61	289.30±6.66	157.10±7.85	76.97±3.85	60.52±3.03	27.02±1.35
NGC0720	873.60±14.48	1046.00±19.27	846.80±18.72	-	-	-	-
NGC0777	288.00±3.18	360.00±4.97	308.90±5.12	157.90±7.89	82.38±4.12	53.71±2.69	27.71±1.39
NGC0807	118.00±1.85	145.30±2.94	123.60±2.62	-	-	-	-
NGC0814	24.44±0.68	30.36±1.09	23.11±1.11	13.54±0.68	11.13±0.56	38.07±1.90	107.90±5.40
NGC0821	495.40±5.93	586.10±7.02	474.40±8.30	185.90±9.30	103.10±5.16	48.73±2.44	36.72±1.84
NGC0855	84.75±2.03	99.07±3.10	80.06±3.32	35.93±1.80	22.11±1.11	24.68±1.23	50.18±2.51
NGC1016	250.10±3.46	305.90±4.79	254.60±5.63	136.00±6.80	81.35±4.07	37.16±1.86	26.40±1.32
NGC1023	2248.00±35.19	2681.00±44.45	2193.00±42.41	993.70±49.68	574.00±28.70	833.50±41.67	309.30±15.46
NGC1199	238.40±1.32	302.50±1.95	259.30±2.15	-	98.60±4.93	-	42.37±2.12
NGC1266	106.40±2.74	118.00±4.24	110.80±4.80	52.06±2.60	34.88±1.74	43.01±2.15	108.30±5.42
NGC1316	4334.00±67.87	4729.00±78.40	3994.00±69.89	2003.00±100.20	987.20±49.36	502.80±25.14	509.50±25.48
NGC1374	394.60±4.00	476.80±6.15	372.70±7.21	185.10±9.25	102.90±5.15	59.88±2.99	43.12±2.16
NGC1377	93.01±2.31	110.20±3.15	89.00±3.77	53.95±2.70	77.34±3.87	333.00±16.65	434.90±21.74
NGC1386	421.60±3.50	497.00±4.58	407.20±5.25	224.00±11.20	176.90±8.84	258.00±12.90	436.80±21.84
NGC1395	1207.00±22.24	1441.00±29.21	1198.00±30.91	-	-	-	-
NGC1399	2150.00±37.63	2512.00±48.58	2060.00±51.22	-	-	-	-
NGC1404	1284.00±20.10	1546.00±25.63	1283.00±24.81	617.90±30.89	347.00±17.35	232.40±11.62	165.50±8.27
NGC1407	1442.00±25.23	1686.00±31.05	1430.00±32.93	-	-	-	-
NGC1426	244.20±2.70	291.80±3.49	233.20±4.51	143.80±7.19	83.11±4.16	44.77±2.24	31.57±1.58
NGC1427	402.30±4.45	494.20±6.83	380.70±7.71	207.80±10.39	117.90±5.89	74.31±3.71	46.90±2.35
NGC1439	275.80±4.06	316.20±5.53	255.70±6.83	150.90±7.55	85.24±4.26	55.25±2.76	33.09±1.66

TABLE 4 — *Continued*

Name	<i>J</i> (mJy)	<i>H</i> (mJy)	<i>Ks</i> (mJy)	<i>i3.6</i> (mJy)	<i>i4.5</i> (mJy)	<i>i5.8</i> (mJy)	<i>i8.0</i> (mJy)
NGC1510	50.27±1.76	90.52±2.50	49.41±2.91	15.39±0.77	9.72±0.49	11.73±0.59	22.49±1.12
NGC1522	15.66±1.13	24.27±1.68	19.22±1.70	9.72±0.49	6.46±0.32	6.56±0.33	14.22±0.71
NGC1533	626.50±7.50	757.80±10.47	611.20±11.82	2303.00±115.10	-	108.50±5.43	-
NGC1543	767.90±14.15	898.50±19.04	719.40±18.56	462.80±23.14	273.00±13.65	152.70±7.63	167.00±8.35
NGC1553	2200.00±32.43	2654.00±41.56	2108.00±34.94	-	-	-	-
NGC1700	404.50±3.73	492.00±4.98	399.00±6.62	203.20±10.16	120.30±6.01	107.70±5.38	43.94±2.20
NGC2110	325.20±3.59	430.50±5.55	379.00±6.63	-	-	-	-
NGC2300	597.70±10.46	718.40±14.56	610.60±12.37	-	-	-	-
NGC2325	500.90±6.92	593.10±9.29	478.40±11.90	-	-	-	-
NGC2434	462.70±6.39	583.40±10.21	480.60±10.62	-	-	-	-
NGC2685	328.80±6.06	389.40±8.61	312.30±7.48	151.30±7.56	87.96±4.40	65.24±3.26	202.60±10.13
NGC2768	1102.00±23.34	1359.00±33.79	1090.00±31.12	547.60±27.38	255.30±12.76	260.50±13.03	156.40±7.82
NGC2778	113.60±1.88	136.80±2.52	107.30±2.87	52.43±2.62	30.44±1.52	17.63±0.88	12.31±0.62
NGC2787	848.20±5.47	1039.00±8.62	853.10±8.64	377.20±18.86	249.90±12.49	157.10±7.86	128.20±6.41
NGC2832	222.30±2.87	267.10±4.43	227.50±4.82	87.94±4.40	79.43±3.97	26.07±1.30	17.51±0.88
NGC2970	28.74±0.74	34.35±1.17	26.27±1.09	17.51±0.88	7.00±0.35	6.28±0.31	3.46±0.17
NGC2974	2073.00±3.82	1902.00±7.01	2159.00±9.94	463.20±23.16	308.20±15.41	177.70±8.88	170.60±8.53
NGC2986	632.30±12.81	764.10±15.48	603.40±17.23	-	-	-	-
NGC3011	29.06±0.48	30.79±0.77	23.41±0.71	13.06±0.65	8.23±0.41	10.12±0.51	17.81±0.89
NGC3032	105.70±1.56	121.80±1.79	94.84±2.10	55.78±2.79	34.74±1.74	53.10±2.65	145.10±7.26
NGC3073	31.31±1.33	41.68±2.23	32.70±2.32	21.15±1.06	8.60±0.43	8.57±0.43	18.12±0.91
NGC3115	3157.00±46.53	3767.00±55.51	3041.00±47.61	1281.00±64.06	699.60±34.98	624.70±31.24	368.20±18.41
NGC3125	46.61±1.25	48.93±1.85	42.36±2.11	29.44±1.47	20.64±1.03	43.13±2.16	109.30±5.46
NGC3156	114.00±2.21	125.00±3.22	104.00±3.54	52.17±2.61	28.70±1.44	22.92±1.15	24.31±1.22
NGC3226	283.00±6.00	294.80±8.42	256.00±8.72	197.10±9.85	79.79±3.99	47.72±2.39	48.88±2.44
NGC3265	46.27±0.90	56.38±1.14	45.77±1.22	26.39±1.32	17.39±0.87	41.98±2.10	228.00±11.40
NGC3377	796.00±13.93	937.40±19.00	724.10±19.34	310.00±15.50	192.10±9.60	138.20±6.91	65.45±3.27
NGC3379	2227.00±32.82	2679.00±41.95	2129.00±35.30	829.10±41.46	452.90±22.64	354.00±17.70	164.60±8.23
NGC3384	1406.00±20.73	1672.00±26.17	1368.00±23.95	571.50±28.57	354.00±17.70	310.30±15.51	178.10±8.91
NGC3412	634.00±3.50	755.70±4.87	586.40±5.94	262.70±13.13	161.40±8.07	87.75±4.39	56.48±2.82
NGC3489	807.10±3.72	1005.00±5.56	773.00±6.41	343.00±17.15	205.40±10.27	166.10±8.31	157.00±7.85
NGC3516	252.90±4.66	282.10±6.50	270.00±6.71	164.20±8.21	134.70±6.73	176.20±8.81	265.90±13.30
NGC3522	54.52±0.90	63.15±1.57	48.55±1.48	27.80±1.39	15.74±0.79	7.25±0.36	6.62±0.33
NGC3557	893.10±8.23	1057.00±12.65	901.50±14.12	449.40±22.47	271.10±13.55	215.20±10.76	132.40±6.62
NGC3585	1482.00±23.21	1772.00±29.37	1429.00±27.64	655.60±32.78	380.00±19.00	352.80±17.64	193.20±9.66
NGC3593	711.40±13.11	936.60±19.84	740.30±19.09	390.00±19.50	245.30±12.26	582.90±29.14	1504.00±75.22
NGC3607	1125.00±18.66	1298.00±25.10	1093.00±23.15	517.10±25.86	253.10±12.66	203.90±10.20	176.00±8.80
NGC3608	431.00±3.57	471.10±5.64	396.10±5.47	217.60±10.88	114.90±5.75	77.33±3.87	33.05±1.65
NGC3610	479.60±3.53	570.60±6.31	471.00±5.21	243.80±12.19	141.30±7.06	116.70±5.83	68.58±3.43
NGC3640	691.40±8.28	805.30±10.38	674.50±14.29	374.20±18.71	197.20±9.86	111.00±5.55	59.68±2.98
NGC3706	476.10±4.82	563.30±7.26	473.60±8.29	256.20±12.81	153.30±7.66	108.80±5.44	59.47±2.97
NGC3773	41.05±1.29	37.67±1.84	36.12±2.10	20.08±1.00	10.95±0.55	22.14±1.11	53.18±2.66
NGC3870	36.35±0.77	40.77±1.43	32.22±1.25	22.75±1.14	13.43±0.67	27.71±1.39	64.72±3.24
NGC3923	1766.00±34.15	2095.00±42.45	1723.00±47.60	688.90±34.44	366.40±18.32	298.80±14.94	133.50±6.68
NGC3941	832.80±4.60	1002.00±7.38	812.40±7.48	379.40±18.97	223.70±11.18	173.40±8.67	113.50±5.67
NGC3945	644.00±11.27	951.40±18.40	669.60±15.42	333.30±16.67	186.80±9.34	193.30±9.66	156.00±7.80
NGC3962	615.60±5.67	737.80±7.47	588.00±10.29	361.20±18.06	213.10±10.65	-	-
NGC4026	644.00±10.08	809.70±13.42	634.70±11.11	291.20±14.56	179.70±8.99	167.70±8.38	97.69±4.88
NGC4073	270.70±4.74	346.40±6.06	275.80±7.62	157.00±7.85	94.03±4.70	51.91±2.60	33.71±1.69
NGC4117	69.91±1.22	77.54±2.00	65.67±1.88	34.05±1.70	21.11±1.06	16.56±0.83	24.53±1.23
NGC4125	1277.00±21.17	1523.00±26.66	1242.00±26.32	655.50±32.78	356.40±17.82	273.60±13.68	163.80±8.19
NGC4138	368.90±2.72	453.70±5.01	359.20±4.63	188.20±9.41	118.60±5.93	138.30±6.92	247.30±12.36
NGC4150	176.10±1.78	210.80±2.91	174.20±2.73	102.00±5.10	66.14±3.31	61.96±3.10	78.07±3.90
NGC4168	295.20±3.26	352.50±5.52	289.30±5.60	164.20±8.21	75.26±3.76	37.01±1.85	22.25±1.11
NGC4203	776.50±6.44	932.30±9.45	747.80±9.64	350.00±17.50	214.90±10.75	105.00±5.25	130.50±6.52
NGC4251	557.90±3.60	667.90±4.92	556.40±5.64	270.00±13.50	159.00±7.95	121.00±6.05	72.91±3.65
NGC4261	859.20±15.04	1046.00±20.23	853.10±22.00	417.10±20.86	242.40±12.12	142.10±7.11	72.67±3.63
NGC4267	530.80±6.36	627.40±9.25	500.50±10.60	240.00±12.00	131.60±6.58	77.13±3.86	45.32±2.27
NGC4278	957.00±6.17	1142.00±9.46	917.50±9.29	428.20±21.41	248.70±12.44	169.20±8.46	125.50±6.28
NGC4291	294.10±2.98	366.10±3.71	294.70±4.07	124.80±6.24	82.33±4.12	62.51±3.12	32.50±1.62
NGC4308	42.47±0.86	46.72±1.51	38.71±1.35	20.06±1.00	9.97±0.50	7.27±0.36	4.65±0.23
NGC4344	47.09±0.61	56.75±0.99	44.24±0.98	39.98±6.12	23.19±4.86	-	-
NGC4350	512.10±2.83	661.20±4.26	513.10±3.78	246.10±12.30	145.30±7.26	111.20±5.56	85.08±4.25
NGC4352	91.73±2.11	100.50±2.78	77.59±3.22	-	22.23±1.11	-	5.54±0.28
NGC4365	1578.00±29.07	1895.00±38.39	1514.00±40.45	647.70±32.38	400.70±20.04	303.40±15.17	205.10±10.26
NGC4371	594.50±7.12	694.30±10.23	561.00±11.89	300.40±15.02	171.40±8.57	104.90±5.25	39.23±1.96
NGC4374	2319.00±38.45	2729.00±55.29	2225.00±47.14	886.80±44.34	490.00±24.50	291.80±14.59	124.50±6.22
NGC4377	210.50±1.94	251.20±3.24	201.60±2.97	-	-	-	-
NGC4379	226.00±2.50	275.10±4.05	213.90±3.55	-	-	-	-
NGC4382	2462.00±38.55	2862.00±52.73	2389.00±46.21	944.50±47.22	567.50±28.37	422.70±21.14	268.00±13.40
NGC4386	272.00±3.01	346.10±4.14	274.30±4.29	88.34±4.42	77.56±3.88	60.85±3.04	41.43±2.07
NGC4406	2583.00±49.96	3110.00±74.48	2483.00±64.04	1426.00±71.30	887.90±44.39	234.70±11.74	166.40±8.32
NGC4417	393.50±6.52	452.00±5.83	369.00±9.52	-	-	-	-
NGC4421	214.20±2.76	254.90±4.23	207.90±4.02	117.50±5.88	65.13±3.26	39.09±1.96	31.05±1.55
NGC4434	153.20±2.40	176.70±3.09	141.80±3.79	-	-	-	-
NGC4435	702.30±8.41	1445.00±13.31	826.80±12.18	285.00±14.25	156.00±7.80	136.90±6.84	129.80±6.49

TABLE 4 — *Continued*

Name	<i>J</i> (mJy)	<i>H</i> (mJy)	<i>K_s</i> (mJy)	<i>i3.6</i> (mJy)	<i>i4.5</i> (mJy)	<i>i5.8</i> (mJy)	<i>i8.0</i> (mJy)
NGC4442	849.00±14.86	1059.00±19.50	829.10±18.33	402.60±20.13	231.50±11.58	151.00±7.55	92.51±4.63
NGC4458	134.40±1.73	157.00±2.75	128.90±2.61	67.89±3.40	37.78±1.89	25.80±1.29	14.54±0.73
NGC4459	940.40±6.93	1155.00±10.64	944.90±9.57	504.10±25.20	255.00±12.75	168.90±8.45	176.20±8.81
NGC4460	168.60±3.11	202.60±4.11	163.60±4.97	90.83±4.54	55.99±2.80	82.04±4.10	147.50±7.38
NGC4464	108.60±1.60	125.90±2.44	101.00±2.60	-	29.20±1.46	-	10.43±0.52
NGC4472	4564.00±67.26	5315.00±78.33	4303.00±67.38	2662.00±133.10	1048.00±52.42	682.80±34.14	368.00±18.40
NGC4473	997.50±16.54	1162.00±22.47	940.60±19.93	415.60±20.78	238.20±11.91	160.20±8.01	90.57±4.53
NGC4474	233.80±3.02	273.40±4.03	227.10±3.14	-	-	-	-
NGC4476	115.80±1.60	136.50±2.14	112.30±2.07	-	-	-	-
NGC4477	799.70±7.37	963.70±10.65	785.90±9.41	411.60±20.58	223.10±11.15	135.80±6.79	93.48±4.67
NGC4478	327.90±2.42	397.30±4.03	312.00±3.74	154.50±7.72	92.11±4.61	76.11±3.81	43.34±2.17
NGC4479	91.31±1.60	103.40±2.76	84.53±2.34	-	24.21±1.21	-	9.58±0.48
NGC4482	52.06±1.73	51.14±2.64	40.12±3.00	-	13.99±0.70	-	3.50±0.17
NGC4483	148.40±2.60	167.20±3.54	132.20±3.90	-	-	-	-
NGC4486	3368.00±52.73	3926.00±65.09	3246.00±56.81	1772.00±88.62	1153.00±57.67	670.20±33.51	358.30±17.91
NGC4489	131.50±2.30	153.60±3.68	123.10±3.17	-	-	-	-
NGC4494	1131.00±19.79	1330.00±28.18	1089.00±24.07	482.20±24.11	273.40±13.67	162.60±8.13	134.90±6.74
NGC4515	86.48±1.03	99.80±1.75	76.03±1.61	-	20.97±1.05	-	6.04±0.30
NGC4526	1711.00±26.80	2204.00±36.54	1766.00±32.53	991.90±49.60	526.30±26.31	410.80±20.54	445.90±22.30
NGC4528	184.00±2.20	233.50±3.23	177.40±3.60	-	-	-	-
NGC4552	1470.00±24.37	1762.00±35.70	1396.00±30.87	781.10±39.05	445.90±22.30	303.40±15.17	139.30±6.97
NGC4564	464.40±5.56	613.70±7.91	458.60±8.87	204.80±10.24	113.50±5.67	75.54±3.78	49.52±2.48
NGC4570	592.80±4.37	713.70±5.92	574.60±6.88	265.10±13.25	157.80±7.89	117.90±5.89	74.85±3.74
NGC4578	299.90±5.52	373.90±7.92	298.30±9.07	140.30±7.01	80.34±4.02	51.84±2.59	33.82±1.69
NGC4589	541.20±9.47	683.50±13.22	540.70±11.46	264.00±13.20	162.10±8.10	136.00±6.80	69.53±3.48
NGC4612	280.10±3.87	313.30±4.91	257.90±6.18	99.16±4.96	75.72±3.79	43.60±2.18	25.16±1.26
NGC4621	1431.00±25.05	1725.00±31.77	1373.00±32.89	571.50±28.58	340.70±17.04	207.80±10.39	124.20±6.21
NGC4623	123.70±2.39	147.80±2.99	112.10±3.82	-	-	-	-
NGC4636	1956.00±41.43	2430.00±60.43	1851.00±59.68	628.60±31.43	358.10±17.90	182.50±9.13	107.70±5.39
NGC4638	367.20±3.72	435.30±4.81	356.90±6.25	185.80±9.29	102.40±5.12	71.44±3.57	42.07±2.10
NGC4649	3523.00±55.16	4203.00±65.81	3472.00±67.16	1381.00±69.07	784.10±39.21	495.70±24.79	334.60±16.73
NGC4660	373.70±2.75	446.20±3.70	357.90±5.60	169.80±8.49	102.60±5.13	70.84±3.54	45.78±2.29
NGC4694	184.40±3.06	214.20±3.75	179.60±4.80	165.40±8.27	63.50±3.17	62.34±3.12	370.20±18.51
NGC4696	944.80±15.66	1179.00±19.55	953.70±21.08	503.10±25.16	270.50±13.53	206.80±10.34	100.70±5.03
NGC4697	2094.00±36.64	2432.00±44.80	1947.00±48.43	784.20±39.21	563.30±28.17	378.70±18.93	196.50±9.83
NGC4709	404.50±4.84	501.60±6.01	427.90±8.67	269.30±13.46	162.30±8.11	128.30±6.42	40.79±2.04
NGC4754	778.60±15.06	925.40±18.75	742.30±20.51	334.80±16.74	205.70±10.28	119.90±6.00	60.32±3.02
NGC4762	863.20±16.70	1093.00±21.15	825.30±22.05	378.60±18.93	215.20±10.76	160.10±8.01	98.03±4.90
NGC4786	221.10±3.05	273.90±4.54	223.60±5.56	129.60±6.48	70.07±3.50	52.68±2.63	31.86±1.59
NGC4915	211.90±2.34	259.90±3.11	212.10±4.49	101.70±5.09	60.41±3.02	43.24±2.16	23.55±1.18
NGC4936	552.20±6.10	677.90±8.12	554.40±10.21	373.70±18.68	233.30±11.66	182.40±9.12	131.40±6.57
NGC5018	558.90±5.15	643.80±7.71	552.80±7.13	297.60±14.88	171.90±8.60	134.50±6.72	113.60±5.68
NGC5044	560.90±5.17	673.50±6.82	565.20±10.41	321.60±16.08	173.60±8.68	111.90±5.60	54.09±2.71
NGC5061	866.40±6.38	1032.00±11.40	832.90±10.74	425.00±21.25	267.40±13.37	231.00±11.55	126.40±6.32
NGC5077	344.30±3.49	422.60±4.67	354.60±6.21	183.50±9.18	87.64±4.38	54.09±2.71	38.48±1.92
NGC5173	72.66±1.27	83.24±1.53	65.73±1.76	36.92±1.85	20.85±1.04	21.87±1.09	35.85±1.79
NGC5273	259.70±3.11	308.10±4.54	234.50±5.18	116.20±5.81	66.79±3.34	44.42±2.22	38.80±1.94
NGC5322	997.50±18.38	1204.00±26.62	938.00±23.33	423.70±21.19	235.70±11.79	168.50±8.43	97.71±4.88
NGC5338	53.32±2.46	61.99±3.31	48.42±4.29	26.86±1.34	15.43±0.77	15.90±0.80	28.05±1.40
NGC5353	642.90±4.14	857.30±5.53	611.20±6.75	310.40±15.52	157.80±7.89	109.20±5.46	67.78±3.39
NGC5419	667.00±13.52	778.30±19.36	674.50±19.88	339.00±16.95	177.00±8.85	94.80±4.74	62.49±3.12
NGC5481	124.90±2.30	152.30±2.95	121.10±3.68	60.97±3.05	37.36±1.87	19.34±0.97	9.64±0.48
NGC5557	401.50±3.33	487.00±4.49	402.00±5.92	227.90±11.40	118.20±5.91	77.85±3.89	44.61±2.23
NGC5576	523.00±5.78	686.00±6.95	507.40±9.81	276.70±13.84	157.10±7.85	101.40±5.07	54.56±2.73
NGC5596	48.23±0.84	58.02±1.18	47.23±1.61	23.83±1.19	13.95±0.70	10.65±0.53	13.85±0.69
NGC5813	755.30±13.91	937.40±16.41	743.00±21.22	315.00±15.75	177.40±8.87	96.53±4.83	45.91±2.29
NGC5831	297.90±3.57	355.70±4.26	289.30±6.93	158.90±7.95	90.15±4.51	47.58±2.38	30.63±1.53
NGC5845	153.10±1.27	189.60±1.40	155.40±2.58	74.82±3.74	38.64±1.93	26.44±1.32	19.11±0.96
NGC5846	1147.00±19.02	1406.00±23.31	1139.00±27.28	522.70±26.13	299.00±14.95	161.70±8.09	77.68±3.88
NGC5866	1207.00±17.79	1482.00±23.20	1222.00±20.26	667.20±33.36	364.20±18.21	360.90±18.05	342.70±17.13
NGC5982	381.70±3.87	477.20±6.15	376.50±5.90	200.50±10.03	124.80±6.24	68.59±3.43	42.75±2.14
NGC6482	299.30±2.76	379.80±4.20	307.20±3.68	-	-	-	-
NGC6684	983.80±12.69	1476.00±20.39	1030.90±19.14	440.50±22.02	251.00±12.55	160.90±8.04	108.30±5.42
NGC6703	352.30±3.25	418.00±5.00	344.00±5.39	227.00±11.35	121.00±6.05	64.26±3.21	32.73±1.64
NGC6776	168.30±2.17	184.10±3.22	165.70±3.51	113.90±5.70	66.85±3.34	40.20±2.01	30.83±1.54
NGC6849	124.90±2.30	151.10±3.34	117.80±3.47	68.62±3.43	35.78±1.79	23.17±1.16	16.48±0.82
NGC7077	19.54±1.04	19.82±1.68	19.29±1.78	10.37±0.52	6.55±0.33	7.41±0.37	13.91±0.70
NGC7176	424.70±5.09	515.20±7.59	428.30±8.29	210.10±10.51	-	129.70±6.48	-
NGC7360	38.03±0.95	48.21±1.64	38.74±1.53	19.82±0.99	11.90±0.59	8.07±0.40	15.33±0.77
NGC7457	372.30±4.46	431.70±6.36	362.60±8.02	183.50±9.18	101.30±5.06	71.68±3.58	50.35±2.52
NGC7619	415.10±4.97	479.40±7.07	419.70±7.35	166.90±8.34	117.30±5.87	60.52±3.03	37.35±1.87
NGC7626	413.20±5.71	519.00±8.13	420.10±8.51	167.20±8.36	123.10±6.16	85.07±4.25	35.64±1.78
NGC7785	269.20±3.72	328.70±4.84	285.60±5.26	133.80±6.69	77.04±3.85	57.52±2.88	39.77±1.99
UGC01503	41.32±0.88	47.72±1.27	40.68±1.31	-	-	-	-
UGC06570	35.10±0.84	41.64±1.19	35.04±1.36	19.81±0.99	13.16±0.66	25.16±1.26	81.27±4.06
UGC06637	16.21±0.46	18.91±0.80	13.92±0.76	7.64±0.38	4.71±0.24	8.30±0.41	15.92±0.80

TABLE 4 — *Continued*

Name	<i>J</i> (mJy)	<i>H</i> (mJy)	<i>K_S</i> (mJy)	<i>i3.6</i> (mJy)	<i>i4.5</i> (mJy)	<i>i5.8</i> (mJy)	<i>i8.0</i> (mJy)
UGC06655	12.83±0.40	14.23±0.79	10.30±0.65	6.66±0.33	4.32±0.22	7.50±0.37	14.48±0.72
UGC06805	17.94±0.55	19.23±1.04	17.74±0.90	9.33±0.47	5.89±0.29	13.31±0.67	31.83±1.59
UGC07436	22.85±1.16	26.62±1.99	19.89±1.91	-	-	-	-
UGC07580	13.90±1.29	18.89±1.85	16.63±2.20	-	-	-	-
UGC07854	10.29±0.63	12.99±0.84	8.20±1.08	-	-	-	-
UGC08876	53.67±0.84	65.88±1.21	52.70±1.70	-	-	-	-

TABLE 5
FLUXES (24 μ M TO 160 μ M SPITZER MIPS, 12 μ M TO 100 μ M IRAS) USED IN THIS STUDY, DATA WERE COLLECTED ACCORDING TO SECTION 2

Name	24 μ m (mJy)	70 μ m (mJy)	160 μ m (mJy)	I12 μ m (mJy)	I25 μ m (mJy)	I60 μ m (mJy)	I100 μ m (mJy)	H α (erg/s/cm ²)
Eso103-35	1693.0±81.0	1774.0±112.0	-	360±73	40±59	410±321	15170±3886	-
Eso428-14	1448.0±80.0	4714.0±389.0	-	20±37	340±70	430±80	70±348	-
Eso462-15	6.1±0.7	0.0±19.4	0.0±26.8	810±21871	-	1790±1432	4960±774	-
Eso483-13	29.8±3.8	417.0±23.0	579.0±69.0	40±41	-	150±57	1310±228	-
IC0798	0.6±0.2	-	-	20±34	120±68	160±43	470±191	16.05±3.72
IC1144	1.4±0.3	-	-	-	120±35	160±103	-	-
IC1459	60.9±4.3	542.0±32.0	627.0±72.0	-	-	-	-	-
IC1639	3.7±0.4	-	-	20±35	160±50	280±44	1210±158	49.57±10.38
IC3032	0.0±0.1	-	-	100±60	-	10±78	270±222	-1.91±1.38
IC3101	0.0±0.1	-	-	-	670±70	270±57	700±180	3.56±1.38
IC3328	0.5±0.1	-	-	-	-	-	-	7.42±6.02
IC3370	32.8±3.4	680.0±51.0	958.0±128.0	30±346	30±143	0±67	-	-
IC3381	0.5±0.1	-	-	30±33	50±42	20±49	-	5.25±2.42
IC3383	0.0±0.1	-	-	30±27	-	-	-	-0.97±1.93
IC3461	0.0±0.1	-	-	240±27	250±32	480±43	1260±131	-3.22±3.38
IC3468	0.2±0.1	-	-	280±28	1100±47	4680±41	3250±121	9.64±2.68
IC3470	0.0±0.1	-	-	190±135	100±76	40±62	1020±330	17.69±3.10
IC3487	0.0±0.1	-	-	130±27	360±44	1520±44	1950±196	19.60±5.23
IC3501	0.2±0.1	-	-	20±39	130±40	-	-	10.73±2.85
IC3586	0.0±1.0	-	-	240±41	290±31	-	190±224	-0.53±1.73
IC3602	0.7±0.1	-	-	10±26	-	100±54	550±166	-
IC3633	0.0±0.1	-	-	240±27	1100±40	14360±48	16890±180	3.82±2.25
IC3652	0.2±0.1	-	-	550±29	430±28	3620±373	8340±1389	14.50±7.53
IC3653	0.8±0.1	-	-	80±23	-	70±32	260±92	34.98±5.64
IC3735	0.0±0.1	-	-	560±27	1980±37	7650±30	6020±117	-
IC3773	0.3±0.1	-	-	550±19	1500±20	6120±33	9070±92	-3.72±3.19
IC3779	0.0±0.1	-	-	220±23	60±26	110±31	290±92	4.93±1.70
IC4296	21.4±8.0	118.0±12.0	71.0±12.0	250±26	180±26	70±36	150±80	-
IC4329	7.2±1.5	0.0±18.5	0.0±25.8	100±31	80±22	70±38	30±111	-
IC5063	2170.0±78.0	4425.0±321.0	-	170±22	110±39	-	-	-
NGC0221	175.0±16.0	25.0±18.0	-	-	-	-	150±102	-
NGC0315	94.0±6.0	331.0±17.0	536.0±48.0	50±20	30±20	-	520±108	-
NGC0404	135.0±8.0	2919.0±202.0	3499.0±366.0	60±21	80±21	-	-	-
NGC0410	6.1±0.8	0.0±24.0	0.0±45.0	130±24	150±25	1160±39	1560±118	-
NGC0474	5.1±2.2	38.2±7.5	107.0±22.0	0±20	120±21	1010±35	1310±87	-
NGC0507	-	0.0±18.8	0.0±22.1	90±26	10±19	320±34	1440±95	-
NGC0516	1.2±0.3	-	-	120±16	110±16	120±26	900±104	-
NGC0526	307.0±28.0	294.0±41.0	-	260±18	220±16	580±28	650±90	-
NGC0533	7.2±3.1	24.8±4.9	28.7±5.6	0±27	110±33	-	960±231	-
NGC0584	48.5±7.6	52.3±6.9	0.0±18.9	240±34	680±43	3580±247	760±1414	-
NGC0596	16.2±4.6	22.5±5.1	18.4±7.3	0±23	-	170±48	1240±285	-
NGC0636	10.5±3.6	0.0±17.2	0.0±26.9	210±35	130±27	150±54	1910±335	-
NGC0720	26.1±5.1	19.2±4.9	0.0±23.1	20±15	10±16	-	250±172	-
NGC0777	8.2±2.7	6.3±2.8	0.0±18.4	120±24	20±31	350±47	1530±229	-
NGC0807	59.9±3.2	198.0±9.0	2233.0±235.0	140±20	50±24	340±43	1190±158	-
NGC0814	697.0±42.0	3007.0±265.0	1952.0±182.0	150±28	30±39	40±41	260±122	-
NGC0821	15.4±4.8	0.0±16.3	0.0±27.3	110±48	40±33	570±54	1490±572	-
NGC0855	87.8±8.5	1700.0±136.0	2486.0±246.0	260±27	-	400±43	1300±150	-
NGC1016	5.1±2.9	0.0±15.4	0.0±28.5	120±30	-	20±48	10±156	-
NGC1023	60.1±5.6	0.0±29.6	0.0±34.8	390±29	-	480±39	1860±184	-
NGC1199	10.5±1.2	88.0±13.0	-	-	100±27	-	290±234	-
NGC1266	872.0±32.0	12690.0±535.0	10300.0±843.0	-	40±40	320±35	200±118	-
NGC1316	430.0±21.0	5440.0±312.0	12610.0±886.0	210±26	160±43	1960±51	3690±116	-
NGC1374	9.2±1.4	0.0±18.5	0.0±28.0	-	-	230±46	500±240	-
NGC1377	1835.0±84.0	6350.0±371.0	3380.0±248.0	600±35	80±42	90±51	710±242	-
NGC1386	1211.0±66.0	6900.0±412.0	-	360±34	830±43	5610±89	7120±680	-
NGC1395	46.4±6.5	135.0±11.0	213.0±14.0	-	100±57	230±44	610±97	-
NGC1399	61.9±7.3	16.4±7.6	26.5±8.6	830±30	1540±54	7640±43	15070±116	-

TABLE 5 — *Continued*

Name	$24_{\mu m}$ (mJy)	$70_{\mu m}$ (mJy)	$160_{\mu m}$ (mJy)	$I12_{\mu m}$ (mJy)	$I25_{\mu m}$ (mJy)	$I60_{\mu m}$ (mJy)	$I100_{\mu m}$ (mJy)	H α (erg/s/cm 2)
NGC1404	56.6±6.3	32.6±6.3	0.0±32.2	60±30	480±45	2530±44	3180±105	-
NGC1407	43.4±6.4	0.0±21.1	0.0±38.9	180±41	40±58	70±59	870±129	-
NGC1426	8.3±2.1	0.0±14.4	0.0±21.4	60±51	-	-	-	-
NGC1427	9.5±1.4	27.3±1.1	0.0±13.3	160±32	110±118	90±49	190±153	-
NGC1439	8.2±0.8	72.0±6.2	37.5±8.0	-	-	-	-	-
NGC1510	126.0±13.0	862.0±35.0	1237.0±103.0	-	-	-	-	-
NGC1522	88.0±4.0	924.0±63.0	749.0±66.0	340±25	910±22	2080±50	2920±293	-
NGC1533	15.8±2.3	374.0±18.0	-	-	-	-	-	-
NGC1543	18.2±2.9	-	-	80±28	-	-	-	-
NGC1553	86.7±8.9	527.0±24.0	322.0±21.0	200±32	250±36	110±48	-	-
NGC1700	19.0±4.9	30.4±5.3	44.1±7.2	1690±68	2150±62	20550±59	35050±142	-
NGC2110	641.0±32.0	4966.0±422.0	-	-	-	-	-	-
NGC2300	13.3±2.1	-	-	-	-	-	-	-
NGC2325	27.5±4.4	38.3±6.8	23.9±6.4	50±45	40±26	-	210±103	-
NGC2434	11.3±0.4	47.3±6.9	0.0±16.8	220±65	260±72	-	-	-
NGC2685	-	-	-	140±32	-	-	-	-
NGC2768	47.5±5.2	728.0±26.0	414.0±29.0	150±35	210±49	1680±44	2790±150	-
NGC2778	4.1±1.3	0.0±18.4	0.0±28.2	70±24	120±28	1180±33	2240±135	-
NGC2787	36.0±5.0	1017.0±46.0	705.0±48.0	190±36	40±42	-	250±356	-
NGC2832	3.5±0.5	0.0±21.0	0.0±38.0	-	-	-	-	-
NGC2970	1.3±0.2	-	-	80±22	10±20	350±47	1550±320	106.07±5.51
NGC2974	63.7±4.4	716.0±48.0	2076.0±154.0	60±35	0±74	100±55	1000±224	-
NGC2986	13.9±3.8	0.0±9.8	0.0±18.5	130±19	200±30	-	-	-
NGC3011	19.2±3.2	-	-	50±45	140±75	240±49	350±174	1567.43±21.48
NGC3032	151.0±8.0	2772.0±184.0	3044.0±273.0	-	-	-	-	-
NGC3073	9.4±1.5	218.0±8.0	515.0±42.0	180±31	160±25	610±47	570±229	645.78±9.30
NGC3115	97.0±4.0	52.0±4.0	0.0±45.0	-	-	-	-	-
NGC3125	636.0±32.0	4714.0±273.0	4337.0±327.0	70±20	140±31	1350±97	2300±277	-
NGC3156	16.7±4.2	254.0±18.0	203.0±21.0	80±40	50±50	110±68	810±295	545.61±14.83
NGC3226	26.9±3.2	327.0±14.0	-	230±77	150±42	600±49	1870±140	-
NGC3265	292.0±17.0	2719.0±144.0	2692.0±159.0	-	240±55	140±57	540±220	12125.80±101.61
NGC3377	17.6±5.4	84.6±5.7	77.7±9.2	100±58	240±60	220±44	450±210	-
NGC3379	66.8±8.8	63.5±8.0	65.2±8.2	30±27	20±54	310±66	920±324	-
NGC3384	61.3±7.8	44.6±17.2	-	230±39	90±35	730±51	1760±148	-
NGC3412	14.9±1.9	0.0±18.0	0.0±24.0	50±19	130±19	-	200±119	-
NGC3489	91.6±6.7	1756.0±78.0	2814.0±128.0	20±28	60±44	-	-	-
NGC3516	712.0±32.0	-	-	170±46	200±38	480±44	2050±113	-
NGC3522	1.7±0.3	-	-	0±43	120±40	410±52	1030±142	446.04±19.25
NGC3557	30.6±4.5	276.0±19.0	271.0±28.0	40±36	80±55	-	-	-
NGC3585	37.2±3.8	80.2±5.2	38.2±8.2	240±31	30±78	-	-	-
NGC3593	1497.0±110.0	19400.0±88.0	-	150±38	40±60	140±49	1480±169	-
NGC3607	84.9±6.7	1761.0±98.0	2215.0±186.0	330±41	-	670±62	870±241	-
NGC3608	18.7±4.2	69.5±8.2	103.0±21.0	130±31	70±58	490±58	2070±239	-
NGC3610	18.4±4.5	21.1±7.3	36.5±16.5	-	40±43	-	-	-
NGC3640	19.6±1.6	0.0±18.3	0.0±26.8	160±29	670±51	-	-	-
NGC3706	16.5±4.4	0.0±18.6	0.0±22.3	150±19	130±23	80±33	760±158	-
NGC3773	139.0±9.0	1591.0±183.0	2379.0±232.0	60±86	-	-	-	-
NGC3870	92.1±5.1	-	-	50±39	-	300±51	760±163	9116.76±74.08
NGC3923	43.7±6.7	23.8±5.4	48.4±7.8	-	-	30±50	70±122	-
NGC3941	23.3±3.1	-	-	-	-	-	140±152	-
NGC3945	39.9±4.1	284.0±19.0	2836.0±216.0	90±37	100±59	2410±70	9520±189	-
NGC3962	21.8±5.6	392.0±18.0	544.0±24.0	0±39	-	-	-	-
NGC4026	23.7±3.0	141.0±13.0	106.0±23.0	110±28	-	-	-	-
NGC4073	5.3±3.0	0.0±17.7	0.0±22.6	880±36	290±68	2260±71	5010±307	51.83±34.01
NGC4117	31.4±3.4	-	-	20±58	-	3600±66	6210±462	2442.03±27.28
NGC4125	74.7±6.9	1105.0±98.0	1735.0±187.0	40±36	-	-	-	-
NGC4138	167.0±16.0	2505.0±162.0	6144.0±642.0	390±31	680±66	-	-	-
NGC4150	69.3±8.0	1522.0±121.0	1720.0±168.0	270±44	340±57	90±83	240±222	-
NGC4168	5.2±1.3	0.0±15.0	0.0±26.0	-	100±56	30±45	580±216	273.94±22.91
NGC4203	43.3±3.5	933.0±111.0	2701.0±259.0	280±54	200±50	720±52	1290±148	-
NGC4251	17.3±2.4	-	-	130±35	60±57	420±63	260±141	-
NGC4261	51.5±3.2	127.0±11.0	375.0±18.0	20±45	430±67	-	-	-
NGC4267	11.7±0.3	0.0±16.9	0.0±20.9	-	230±69	-	-	-
NGC4278	44.7±12.7	829.0±68.0	1491.0±128.0	80±29	-	-	80±297	-
NGC4291	-	0.0±18.0	-	30±29	-	-	-	-
NGC4308	1.5±0.3	-	-	440±34	200±61	510±42	0±198	51.31±6.62
NGC4344	40.2±4.5	779.0±62.0	1986.0±226.0	-	-	-	-	31.41±2.78
NGC4350	29.8±3.3	474.0±32.0	1168.0±112.0	130±32	280±41	310±43	340±145	-
NGC4352	1.7±0.3	-	-	260±33	-	140±47	610±150	58.63±7.16
NGC4365	22.2±4.7	67.0±8.0	58.2±7.3	550±449	500±203	6460±72	15390±167	-
NGC4371	13.6±0.7	24.5±2.7	14.1±7.0	230±29	-	210±58	1150±317	-
NGC4374	66.6±8.6	617.0±41.0	535.0±61.0	200±36	130±55	300±54	870±306	-
NGC4377	3.2±0.3	-	-	20±34	10±51	-	420±265	-
NGC4379	4.3±0.3	-	-	40±32	10±54	-	-	-
NGC4382	52.4±6.7	23.6±6.5	24.7±9.0	10±44	0±47	-	500±141	-

TABLE 5 — *Continued*

Name	$24\mu m$ (mJy)	$70\mu m$ (mJy)	$160\mu m$ (mJy)	$I12\mu m$ (mJy)	$I25\mu m$ (mJy)	$I60\mu m$ (mJy)	$I100\mu m$ (mJy)	$H\alpha$ (erg/s/cm 2)
NGC4386	-	178.0±14.0	-	0±22	50±28	120±47	-	-
NGC4406	27.5±3.2	64.0±8.0	90.0±12.0	-	100±56	20±51	-	-
NGC4417	8.8±1.2	-	-	170±32	380±55	340±50	1510±203	-
NGC4421	3.3±0.4	0.0±25.0	0.0±30.0	120±41	-	270±44	30±102	100.24±11.42
NGC4434	4.8±0.9	-	-	30±39	260±61	330±52	270±161	-
NGC4435	111.0±10.2	2210.0±186.0	3022.0±327.0	130±34	-	-	-	-
NGC4442	20.2±2.2	-	-	640±28	1030±63	3520±59	10580±218	-
NGC4458	3.3±1.1	0.0±18.5	0.0±23.8	200±43	-	90±159	340±505	-
NGC4459	107.0±8.0	2400.0±175.0	3461.0±431.0	80±33	210±54	1250±111	1130±696	-
NGC4460	274.0±31.0	4413.0±389.0	4488.0±461.0	150±31	50±31	190±43	1120±265	-
NGC4464	2.0±0.3	-	-	230±36	540±54	620±55	640±264	-
NGC4472	74.7±8.6	61.1±7.6	66.4±7.8	70±29	-	80±80	2580±703	-
NGC4473	26.3±6.7	0.0±18.0	0.0±25.5	-	40±49	-	-	-
NGC4474	5.4±0.8	-	-	340±40	-	100±58	670±311	-
NGC4476	35.7±4.1	528.0±89.0	1323.0±135.0	140±31	220±50	390±163	410±595	289.65±11.54
NGC4477	39.0±0.8	507.0±12.0	514.0±29.0	150±32	-	-	-	-
NGC4478	12.6±3.9	0.0±17.9	0.0±23.7	200±29	-	400±182	1410±779	-
NGC4479	1.2±0.3	-	-	110±35	-	1150±62	2730±224	31.18±4.45
NGC4482	0.3±0.2	-	-	90±43	480±84	-	-	14.60±2.93
NGC4483	3.0±0.3	-	-	140±30	100±58	50±51	400±171	86.30±14.41
NGC4486	154.0±9.0	483.0±44.0	896.0±91.0	210±46	30±85	560±64	4670±174	-
NGC4489	3.2±0.3	-	-	60±33	-	190±66	-	90.15±11.65
NGC4494	34.5±4.5	316.0±12.5	235.0±19.6	140±28	310±44	880±40	950±168	-
NGC4515	1.9±0.2	-	-	110±22	180±22	450±30	640±66	118.99±10.28
NGC4526	267.0±12.0	8134.0±632.0	13710.0±1267.0	140±39	430±61	360±50	810±179	-
NGC4528	4.4±0.7	-	-	220±34	370±33	530±61	2480±142	-
NGC4552	58.5±7.8	96.3±10.2	188.0±16.0	220±28	-	60±56	260±226	-
NGC4564	23.9±3.7	-	-	80±21	120±19	450±42	1180±221	-
NGC4570	18.7±6.0	0.0±23.3	0.0±29.6	70±60	-	-	430±119	-
NGC4578	5.2±0.9	0.0±19.0	0.0±26.0	40±44	90±48	50±100	1160±513	-
NGC4589	15.3±4.5	275.0±16.0	396.0±21.0	100±27	170±29	90±43	440±143	-
NGC4612	6.0±0.8	-	-	230±32	50±44	270±39	630±112	-
NGC4621	34.9±6.3	33.7±5.7	47.4±6.6	50±30	20±43	190±43	880±163	-
NGC4623	1.8±0.2	-	-	10±28	-	20±50	-	-
NGC4636	31.8±5.6	197.0±12.0	185.0±24.0	160±25	100±38	30±40	-	-
NGC4638	12.7±0.1	4.3±1.1	0.8±1.3	340±19	340±15	5700±28	16170±73	-
NGC4649	108.0±10.0	48.6±6.8	0.0±30.4	80±20	10±19	100±37	-	-
NGC4660	15.5±4.3	38.3±6.2	59.1±8.2	30±20	-	620±63	2940±323	-
NGC4694	110.0±9.0	1545.0±112.0	3278.0±334.0	60±26	-	0±45	340±293	-
NGC4696	23.4±4.7	133.0±13.0	295.0±21.0	30±27	20±30	130±136	2280±936	-
NGC4697	44.7±6.7	618.0±55.0	830.0±68.0	-	-	310±74	-	-
NGC4709	8.2±0.2	0.0±15.5	0.0±27.0	70±36	40±48	10±55	600±231	-
NGC4754	17.1±2.9	0.0±12.2	0.0±22.2	160±38	100±50	450±52	660±180	-
NGC4762	39.1±6.5	12.1±2.6	0.0±24.2	280±46	390±72	3350±708	11680±2656	-
NGC4786	25.3±1.2	303.0±26.0	161.0±19.0	740±72	340±80	-	-	-
NGC4915	11.7±5.5	30.6±4.8	59.7±8.9	40±31	280±36	10±56	760±405	-
NGC4936	21.7±0.9	465.0±45.0	894.0±76.0	10±45	340±133	150±89	-	-
NGC5018	61.7±9.1	1174.0±134.0	1855.0±241.0	-	-	-	-	-
NGC5044	23.5±5.3	241.0±23.0	266.0±28.0	120±42	-	140±50	690±239	-
NGC5061	32.8±0.5	18.2±5.2	0.0±23.5	20±35	250±109	-	-	-
NGC5077	33.2±5.7	133.0±11.0	155.0±18.0	70±20	-	10±33	460±156	-
NGC5173	21.1±1.5	-	-	160±26	120±38	360±49	490±220	1572.38±29.91
NGC5273	83.1±4.5	657.0±44.0	836.0±79.0	40±29	30±59	110±72	900±430	4263.61±44.94
NGC5322	42.2±6.4	477.0±23.0	687.0±77.0	-	330±49	-	220±243	-
NGC5338	35.2±5.0	-	-	190±48	-	110±48	210±144	2388.48±25.11
NGC5353	24.7±3.3	492.0±38.0	490.0±52.0	-	-	20±47	400±129	-
NGC5419	12.9±0.1	0.0±18.3	0.0±21.7	220±32	-	740±47	3460±217	-
NGC5481	1.8±0.3	10.2±3.4	0.0±22.0	530±49	430±60	160±55	210±192	-
NGC5557	13.4±5.0	26.4±7.5	0.0±46.0	40±31	-	-	-	-
NGC5576	16.5±4.2	0.0±12.7	0.0±19.8	-	40±54	-	440±313	-
NGC5596	6.5±0.5	-	-	90±34	400±64	40±61	700±235	321.03±15.84
NGC5813	15.3±4.9	61.3±7.6	38.3±5.9	-	140±62	-	810±378	-
NGC5831	14.8±4.6	0.0±18.8	0.0±24.6	40±36	860±93	-	-	209.85±73.30
NGC5845	7.8±3.2	108.0±12.0	169.0±23.0	110±49	350±55	-	-	-
NGC5846	39.3±6.2	107.0±10.0	129.0±12.0	10±36	200±74	170±55	230±264	298.25±12.67
NGC5866	194.0±7.1	8753.0±605.0	17540.0±1297.0	-	160±49	210±39	230±179	-
NGC5982	13.8±5.1	39.0±7.2	65.8±11.7	210±43	-	-	430±142	-
NGC6482	9.5±0.8	33.6±12.1	0.0±45.2	80±33	220±72	220±47	770±192	-
NGC6684	17.7±2.0	-	-	-	-	-	0±170	-
NGC6703	20.3±4.5	43.5±6.4	21.7±5.1	20±30	-	0±54	170±209	-
NGC6776	16.4±1.3	126.0±12.0	58.1±19.3	-	0±59	200±57	470±286	-
NGC6849	3.3±0.1	0.0±12.6	0.0±19.8	10±37	260±56	-	50±157	-
NGC7077	28.7±3.1	411.0±37.0	452.0±42.0	90±44	60±60	-	640±263	-
NGC7176	2.6±0.4	-	-	210±29	380±46	120±93	-	-
NGC7360	9.6±0.6	-	-	1230±26	4110±35	5740±146	1870±561	-

TABLE 5 — *Continued*

Name	$24\mu m$ (mJy)	$70\mu m$ (mJy)	$160\mu m$ (mJy)	$I12\mu m$ (mJy)	$I25\mu m$ (mJy)	$I60\mu m$ (mJy)	$I100\mu m$ (mJy)	H α (erg/s/cm 2)
NGC7457	8.4 ± 2.5	0.0 ± 25.9	0.0 ± 33.5	660 ± 29	2460 ± 32	2730 ± 44	1480 ± 187	-
NGC7619	10.2 ± 4.7	0.0 ± 13.7	0.0 ± 23.5	410 ± 28	1870 ± 27	4790 ± 74	3980 ± 601	-
NGC7626	12.4 ± 3.6	18.0 ± 0.3	0.0 ± 25.3	110 ± 25	-	150 ± 48	-	-
NGC7785	8.2 ± 0.7	18.0 ± 0.9	0.0 ± 19.0	20 ± 24	70 ± 25	610 ± 40	1410 ± 131	-
UGC01503	39.6 ± 1.8	362.0 ± 66.0	1384.0 ± 139.0	110 ± 32	100 ± 33	690 ± 43	1620 ± 140	-
UGC06570	266.0 ± 33.0	-	-	140 ± 54	640 ± 84	1960 ± 131	2510 ± 210	8164.21 ± 64.04
UGC06637	18.0 ± 2.3	-	-	-	-	-	-	497.72 ± 7.42
UGC06655	18.4 ± 6.0	-	-	40 ± 32	450 ± 54	1650 ± 56	1540 ± 188	4977.99 ± 41.40
UGC06805	42.0 ± 3.6	-	-	40 ± 22	10 ± 36	350 ± 32	690 ± 119	7902.42 ± 63.48
UGC07436	0.0 ± 1.0	-	-	-	-	-	340 ± 141	5.34 ± 1.72
UGC07580	0.0 ± 0.1	-	-	70 ± 40	370 ± 67	10 ± 53	100 ± 152	1.49 ± 6.74
UGC07854	0.0 ± 0.1	-	-	-	-	60 ± 52	-	2.90 ± 1.59
UGC08876	1.5 ± 0.3	-	-	10 ± 30	-	-	-	274.75 ± 85.49

TABLE 6
HERSCHEL SPIRE FLUXES USED IN THIS WORK.

Name	$250\mu m$ (mJy)	$350\mu m$ (mJy)	$500\mu m$ (mJy)
IC3032	0.0 ± 3.2	0.0 ± 2.9	0.0 ± 2.1
IC3101	0.0 ± 3.4	0.0 ± 2.8	0.0 ± 2.1
IC3328	0.0 ± 3.8	0.0 ± 3.6	0.6 ± 2.6
IC3381	1.1 ± 5.4	0.6 ± 4.8	4.0 ± 3.9
IC3501	0.0 ± 3.7	0.0 ± 3.3	0.0 ± 2.6
IC5063	1723.8 ± 258.7	848.1 ± 134.0	279.4 ± 53.1
NGC0584	0.8 ± 13.9	6.2 ± 13.4	2.7 ± 9.7
NGC0855	788.2 ± 118.3	351.6 ± 53.0	139.9 ± 36.7
NGC1266	3610.5 ± 541.6	1479.6 ± 225.4	415.4 ± 70.3
NGC1316	3895.5 ± 584.4	1650.4 ± 249.6	502.9 ± 79.5
NGC1377	945.5 ± 141.9	361.7 ± 54.6	131.4 ± 35.1
NGC1386	3414.1 ± 512.2	1509.8 ± 229.9	460.8 ± 76.8
NGC1399	1.5 ± 35.3	17.1 ± 31.6	26.0 ± 4.8
NGC1404	0.7 ± 13.4	0.0 ± 12.5	0.0 ± 9.3
NGC3226	381.8 ± 57.5	159.0 ± 24.5	65.1 ± 10.7
NGC3265	926.6 ± 139.1	399.8 ± 60.2	137.6 ± 21.2
NGC3608	0.6 ± 10.3	6.2 ± 9.4	6.6 ± 7.8
NGC3640	0.7 ± 14.8	7.2 ± 14.4	6.1 ± 12.0
NGC3773	669.0 ± 100.5	286.1 ± 43.3	82.0 ± 13.0
NGC3941	14.0 ± 16.5	15.6 ± 13.2	5.8 ± 11.0
NGC3945	1974.2 ± 296.5	899.8 ± 137.8	290.8 ± 48.7
NGC4125	680.2 ± 102.4	374.8 ± 57.1	185.8 ± 38.5
NGC4138	3140.3 ± 471.1	1395.4 ± 213.2	463.3 ± 69.5
NGC4168	0.7 ± 9.3	4.6 ± 7.9	0.0 ± 5.5
NGC4203	1152.9 ± 173.2	526.1 ± 83.8	191.1 ± 30.4
NGC4251	0.1 ± 9.1	3.0 ± 8.6	3.2 ± 6.3
NGC4261	237.4 ± 35.9	309.0 ± 56.9	216.7 ± 33.0
NGC4267	20.6 ± 3.7	16.6 ± 13.0	7.4 ± 8.8
NGC4350	246.3 ± 37.0	64.6 ± 10.1	22.2 ± 4.0
NGC4352	0.5 ± 5.0	11.5 ± 4.9	9.2 ± 3.6
NGC4365	1.2 ± 23.2	13.5 ± 22.3	15.4 ± 15.3
NGC4371	0.7 ± 16.2	2.1 ± 13.3	0.0 ± 9.1
NGC4374	239.3 ± 36.1	146.1 ± 22.4	119.5 ± 18.4
NGC4377	275.0 ± 41.4	66.3 ± 10.4	28.9 ± 5.0
NGC4379	0.1 ± 12.4	3.9 ± 11.1	0.0 ± 7.7
NGC4406	1.0 ± 27.0	6.5 ± 27.0	7.6 ± 20.5
NGC4417	1.3 ± 9.9	10.2 ± 8.8	7.5 ± 7.0
NGC4434	0.0 ± 6.4	0.0 ± 5.6	0.0 ± 4.1
NGC4435	1621.1 ± 243.2	656.5 ± 98.7	186.8 ± 28.4
NGC4442	0.0 ± 11.1	0.0 ± 11.3	0.0 ± 8.3
NGC4458	0.0 ± 6.6	0.5 ± 5.8	1.1 ± 4.4
NGC4459	1451.5 ± 217.8	507.2 ± 76.2	154.3 ± 23.4
NGC4464	0.7 ± 4.5	2.9 ± 4.0	8.1 ± 3.3
NGC4472	12.9 ± 44.7	13.4 ± 41.5	11.8 ± 31.6
NGC4473	0.2 ± 16.2	2.5 ± 13.3	0.0 ± 9.6
NGC4474	0.1 ± 8.3	0.2 ± 7.1	5.6 ± 4.8
NGC4476	701.8 ± 105.4	270.4 ± 40.8	83.8 ± 13.1
NGC4477	414.8 ± 62.4	154.9 ± 23.8	42.2 ± 7.9
NGC4478	36.6 ± 5.9	29.5 ± 5.2	26.2 ± 4.7
NGC4479	0.0 ± 6.2	3.4 ± 5.5	3.9 ± 4.6
NGC4482	0.0 ± 4.3	0.0 ± 4.4	0.8 ± 3.6
NGC4483	0.0 ± 5.8	0.7 ± 5.1	0.7 ± 3.9

TABLE 6 — *Continued*

Name	$250_{\mu m}$ (mJy)	$350_{\mu m}$ (mJy)	$500_{\mu m}$ (mJy)
NGC4486	706.0 ± 106.0	1065.6 ± 163.1	1280.9 ± 194.0
NGC4494	74.2 ± 11.3	37.4 ± 6.3	13.3 ± 10.8
NGC4526	7884.3 ± 1183.4	3157.6 ± 475.0	994.8 ± 151.1
NGC4528	1.4 ± 7.9	8.6 ± 5.7	0.0 ± 5.3
NGC4552	2.2 ± 27.0	21.4 ± 4.0	18.4 ± 16.9
NGC4564	0.3 ± 10.5	0.0 ± 9.3	0.0 ± 6.5
NGC4570	0.1 ± 7.4	0.4 ± 6.6	0.0 ± 4.8
NGC4578	0.0 ± 10.7	7.4 ± 9.7	5.9 ± 7.3
NGC4612	0.8 ± 6.8	7.1 ± 6.5	12.4 ± 4.5
NGC4621	0.5 ± 17.4	0.0 ± 17.8	0.0 ± 15.0
NGC4636	87.5 ± 13.4	33.3 ± 5.7	11.2 ± 15.8
NGC4638	0.0 ± 6.4	0.0 ± 6.5	0.0 ± 4.1
NGC4649	0.1 ± 31.0	0.0 ± 28.5	0.0 ± 19.5
NGC4660	4.7 ± 7.1	12.4 ± 7.4	12.7 ± 5.8
NGC4696	112.8 ± 17.1	41.6 ± 6.7	25.2 ± 4.5
NGC4697	220.1 ± 33.1	65.6 ± 10.2	19.4 ± 17.8
NGC4754	0.0 ± 14.2	0.6 ± 13.3	0.0 ± 8.6
NGC4762	1.2 ± 13.8	2.0 ± 14.8	3.0 ± 10.9
NGC5273	266.2 ± 40.0	129.1 ± 19.7	52.8 ± 8.5
NGC5576	0.9 ± 9.7	8.4 ± 9.2	1.5 ± 7.2
NGC5866	7434.1 ± 1115.2	2983.6 ± 449.0	976.0 ± 149.3
UGC07436	0.0 ± 4.5	3.8 ± 3.9	0.0 ± 3.0
UGC07580	18.9 ± 4.4	5.5 ± 3.1	3.9 ± 2.5

TABLE 7
PARAMETERS FITTED BY CIGALEMC USING GALEX, SDSS, 2MASS, IRAC AND
MIPS DATAWHEN AVAILABLE.

Name	$\text{Log}(f_{\text{sys}})$	$\text{Log}(M_{\text{gal}})$ (M_{\odot})	$\text{Log}(M_{\star})$ (M_{\odot})	$\text{Log}(\text{SFR})$ (M_{\odot}/yr)	t_{D4000} (Gyr)	$\text{Log}(L_{\text{bol}})$ (L_{\odot})	$\text{Log}(L_d)$ (L_{\odot})
Eso462-15	-3.25 ± 0.83	11.65 ± 0.89	11.51 ± 0.89	-1.01 ± 0.28	9.27 ± 2.53	11.09 ± 0.61	8.66 ± 0.40
Eso483-13	-1.23 ± 0.57	9.10 ± 0.18	8.97 ± 0.18	-1.22 ± 0.09	0.59 ± 0.20	9.00 ± 0.07	8.04 ± 0.15
IC0798	-4.53 ± 0.93	9.63 ± 0.06	9.49 ± 0.06	-3.19 ± 0.64	9.09 ± 0.94	9.02 ± 0.06	6.41 ± 0.55
IC1144	-0.46 ± 0.45	7.77 ± 0.96	7.64 ± 0.96	-1.94 ± 0.94	0.37 ± 0.38	8.35 ± 0.84	8.24 ± 0.88
IC1459	-2.52 ± 1.05	11.04 ± 1.05	10.90 ± 1.04	-0.92 ± 0.22	7.39 ± 3.60	10.61 ± 0.66	8.87 ± 0.15
IC1639	-3.01 ± 0.42	11.09 ± 0.06	10.94 ± 0.06	-1.32 ± 0.23	8.91 ± 0.91	10.47 ± 0.05	8.53 ± 0.38
IC3328	-0.65 ± 0.55	6.44 ± 0.33	6.31 ± 0.33	-3.55 ± 0.40	0.53 ± 0.65	6.62 ± 0.29	6.48 ± 0.33
IC3370	-1.16 ± 0.72	11.40 ± 0.20	11.27 ± 0.19	1.04 ± 0.44	1.16 ± 1.52	11.32 ± 0.16	9.32 ± 0.20
IC3381	-3.63 ± 0.46	9.14 ± 0.06	8.99 ± 0.06	-3.91 ± 0.34	9.99 ± 0.44	8.51 ± 0.06	5.48 ± 0.54
IC3383	-3.23 ± 0.55	9.61 ± 0.07	9.46 ± 0.07	-3.03 ± 0.42	9.35 ± 0.85	8.98 ± 0.07	6.19 ± 0.56
IC3461	-2.77 ± 0.45	9.13 ± 0.06	8.99 ± 0.06	-2.98 ± 0.19	7.81 ± 1.07	8.53 ± 0.06	5.66 ± 0.57
IC3468	-2.36 ± 0.53	9.73 ± 0.07	9.59 ± 0.07	-1.89 ± 0.23	5.31 ± 1.28	9.17 ± 0.06	5.63 ± 0.59
IC3470	-3.02 ± 0.42	9.83 ± 0.06	9.68 ± 0.06	-2.57 ± 0.18	8.89 ± 0.79	9.21 ± 0.05	5.81 ± 0.57
IC3487	-3.34 ± 0.92	8.86 ± 0.88	8.71 ± 0.87	-3.97 ± 0.41	9.23 ± 2.93	8.28 ± 0.69	5.92 ± 0.46
IC3501	-3.90 ± 1.75	8.95 ± 1.24	8.81 ± 1.23	-3.56 ± 0.39	8.16 ± 3.67	8.48 ± 0.92	6.03 ± 0.68
IC3586	-2.92 ± 0.60	9.53 ± 0.07	9.38 ± 0.07	-2.82 ± 0.47	8.46 ± 1.64	8.92 ± 0.06	7.25 ± 0.53
IC3602	-3.21 ± 0.52	9.15 ± 0.06	9.00 ± 0.06	-3.47 ± 0.39	9.36 ± 0.89	8.53 ± 0.06	6.59 ± 0.43
IC3633	-3.27 ± 0.49	9.36 ± 0.07	9.22 ± 0.07	-3.28 ± 0.34	9.41 ± 0.77	8.74 ± 0.07	6.39 ± 0.55
IC3652	-3.52 ± 0.46	9.09 ± 0.06	8.94 ± 0.06	-3.83 ± 0.30	9.90 ± 0.48	8.46 ± 0.06	5.11 ± 0.60
IC3653	-3.50 ± 0.43	9.15 ± 0.06	9.01 ± 0.06	-3.76 ± 0.22	9.93 ± 0.45	8.52 ± 0.05	5.55 ± 0.54
IC3773	-3.25 ± 0.42	9.64 ± 0.06	9.50 ± 0.06	-3.03 ± 0.24	9.59 ± 0.56	9.02 ± 0.06	5.56 ± 0.58
IC3779	-3.52 ± 0.44	9.06 ± 0.07	8.92 ± 0.07	-3.87 ± 0.28	9.90 ± 0.45	8.43 ± 0.06	5.84 ± 0.58
IC4296	-3.27 ± 0.38	11.87 ± 0.07	11.72 ± 0.07	-0.80 ± 0.16	9.63 ± 0.48	11.25 ± 0.07	8.85 ± 0.29
IC4329	-3.28 ± 0.37	11.93 ± 0.06	11.79 ± 0.06	-0.76 ± 0.14	9.71 ± 0.44	11.31 ± 0.06	8.14 ± 0.50
IC5063	-1.41 ± 0.52	11.28 ± 0.18	11.14 ± 0.18	0.51 ± 0.23	1.65 ± 1.18	11.05 ± 0.06	10.80 ± 0.09
NGC0315	-2.87 ± 0.42	11.84 ± 0.07	11.69 ± 0.07	-0.47 ± 0.26	8.65 ± 1.06	11.22 ± 0.06	9.79 ± 0.14
NGC0404	-3.90 ± 1.08	9.77 ± 0.08	9.63 ± 0.08	-2.52 ± 0.27	8.03 ± 0.99	9.18 ± 0.07	7.69 ± 0.22
NGC0410	-3.22 ± 0.39	11.84 ± 0.06	11.69 ± 0.06	-0.80 ± 0.18	9.61 ± 0.50	11.21 ± 0.05	8.40 ± 0.48
NGC0474	-3.35 ± 0.40	11.09 ± 0.06	10.94 ± 0.06	-1.68 ± 0.23	9.76 ± 0.49	10.46 ± 0.06	8.06 ± 0.37
NGC0507	-3.10 ± 0.38	11.75 ± 0.06	11.61 ± 0.06	-0.77 ± 0.18	9.43 ± 0.60	11.13 ± 0.06	8.90 ± 0.52
NGC0516	-0.54 ± 0.51	6.93 ± 0.65	6.80 ± 0.64	-2.90 ± 0.62	0.46 ± 0.63	7.34 ± 0.53	7.21 ± 0.56
NGC0533	-3.10 ± 0.41	11.80 ± 0.07	11.65 ± 0.07	-0.70 ± 0.18	9.27 ± 0.66	11.17 ± 0.06	8.63 ± 0.36
NGC0584	-4.45 ± 0.79	11.23 ± 0.06	11.08 ± 0.06	-1.97 ± 0.41	9.90 ± 0.46	10.60 ± 0.06	7.84 ± 0.39
NGC0596	-4.41 ± 0.81	11.05 ± 0.06	10.90 ± 0.06	-2.11 ± 0.42	9.85 ± 0.48	10.42 ± 0.05	7.50 ± 0.44
NGC0636	-3.53 ± 0.46	11.00 ± 0.06	10.85 ± 0.06	-1.94 ± 0.28	9.93 ± 0.46	10.36 ± 0.05	7.76 ± 0.45
NGC0777	-2.98 ± 0.37	11.74 ± 0.06	11.59 ± 0.06	-0.68 ± 0.17	9.14 ± 0.72	11.11 ± 0.06	8.28 ± 0.45
NGC0807	-2.08 ± 0.48	11.09 ± 0.14	10.95 ± 0.14	-0.32 ± 0.20	4.33 ± 1.28	10.57 ± 0.10	9.72 ± 0.17
NGC0814	-0.38 ± 0.36	9.32 ± 0.20	9.19 ± 0.19	-0.38 ± 0.17	0.34 ± 0.10	9.70 ± 0.10	9.54 ± 0.14
NGC0855	-1.58 ± 0.50	9.32 ± 0.12	9.18 ± 0.12	-1.42 ± 0.13	1.42 ± 0.76	9.00 ± 0.06	8.26 ± 0.17
NGC1016	-3.40 ± 0.47	11.95 ± 0.06	11.80 ± 0.06	-0.90 ± 0.35	9.86 ± 0.52	11.32 ± 0.05	8.82 ± 0.46
NGC1023	-4.38 ± 0.79	11.26 ± 0.06	11.12 ± 0.06	-1.83 ± 0.24	9.84 ± 0.45	10.64 ± 0.05	7.20 ± 0.48
NGC1199	-3.23 ± 0.43	11.23 ± 0.06	11.08 ± 0.06	-1.42 ± 0.23	9.59 ± 0.60	10.60 ± 0.06	8.42 ± 0.39

TABLE 7 — *Continued*

Name	$\text{Log}(f_{\text{sys}})$	$\text{Log}(M_{\text{gal}})$ (M_{\odot})	$\text{Log}(M_{\star})$ (M_{\odot})	$\text{Log}(\text{SFR})$ (M_{\odot}/yr)	t_{D4000} (Gyr)	$\text{Log}(L_{\text{bol}})$ (L_{\odot})	$\text{Log}(L_d)$ (L_{\odot})
NGC1266	-1.02±0.54	10.52±0.22	10.38±0.21	0.12±0.23	0.82±0.82	10.38±0.08	10.21±0.12
NGC1316	-2.90±0.46	12.06±0.08	11.91±0.08	-0.28±0.29	8.66±1.13	11.44±0.08	9.92±0.17
NGC1374	-3.30±0.39	10.85±0.06	10.70±0.06	-1.86±0.14	9.71±0.44	10.22±0.06	7.14±0.48
NGC1377	-0.50±0.43	9.99±0.21	9.87±0.20	0.15±0.16	0.39±0.18	10.33±0.08	10.14±0.09
NGC1386	-1.74±0.48	10.48±0.11	10.33±0.11	-0.66±0.25	3.03±1.41	10.03±0.06	9.59±0.10
NGC1404	-3.28±0.37	11.75±0.06	11.60±0.06	-0.95±0.14	9.71±0.45	11.12±0.06	8.02±0.38
NGC1426	-3.47±0.40	10.78±0.06	10.64±0.06	-2.08±0.15	9.88±0.43	10.15±0.06	7.30±0.46
NGC1427	-3.20±0.37	10.94±0.06	10.79±0.06	-1.67±0.14	9.57±0.50	10.32±0.06	7.42±0.24
NGC1439	-2.51±1.30	10.01±1.44	9.86±1.43	-1.92±0.24	7.08±4.39	9.66±0.97	7.69±0.24
NGC1510	-0.50±0.37	9.13±0.18	9.00±0.18	-0.78±0.09	0.39±0.06	9.30±0.07	8.51±0.14
NGC1522	-0.34±0.32	8.64±0.20	8.52±0.20	-1.04±0.11	0.33±0.07	9.00±0.07	8.31±0.16
NGC1543	-3.66±0.40	11.11±0.06	10.97±0.06	-1.98±0.21	10.11±0.41	10.48±0.06	7.63±0.55
NGC1700	-2.66±0.62	11.66±0.08	11.51±0.08	-0.41±0.51	7.33±2.05	11.06±0.06	8.55±0.33
NGC2685	-1.29±0.68	10.23±0.14	10.09±0.13	-0.36±0.41	1.51±1.37	10.01±0.16	9.57±0.42
NGC2768	-3.08±0.41	11.03±0.07	10.89±0.07	-1.48±0.24	9.35±0.73	10.41±0.06	8.52±0.20
NGC2778	-3.35±0.46	10.69±0.06	10.54±0.06	-2.10±0.34	9.77±0.56	10.06±0.05	7.63±0.46
NGC2787	-3.37±0.44	10.66±0.07	10.52±0.07	-2.15±0.28	9.81±0.49	10.03±0.07	7.98±0.19
NGC2832	-3.10±0.89	11.53±0.90	11.39±0.89	-1.07±0.32	9.06±2.69	10.98±0.62	8.69±0.51
NGC2970	-2.84±0.42	9.92±0.06	9.77±0.06	-2.29±0.19	8.25±1.00	9.31±0.05	6.93±0.47
NGC2974	-3.21±0.43	11.69±0.07	11.55±0.07	-0.98±0.27	9.57±0.61	11.07±0.07	9.21±0.17
NGC3011	-1.58±0.53	9.65±0.12	9.50±0.12	-1.02±0.12	1.16±0.65	9.35±0.05	8.49±0.24
NGC3032	-1.44±0.51	10.19±0.13	10.05±0.13	-0.43±0.13	1.06±0.65	9.92±0.06	9.43±0.12
NGC3073	-1.88±0.46	9.61±0.10	9.47±0.10	-1.52±0.14	3.05±0.87	9.14±0.06	8.19±0.17
NGC3115	-3.44±0.35	11.19±0.06	11.04±0.06	-1.70±0.15	9.94±0.42	10.56±0.06	7.25±0.29
NGC3125	-0.29±0.26	9.10±0.20	8.98±0.19	-0.33±0.13	0.25±0.09	9.68±0.08	9.32±0.15
NGC3156	-2.77±0.45	10.31±0.07	10.16±0.07	-1.83±0.22	7.91±1.14	9.70±0.06	8.16±0.22
NGC3226	-2.51±0.61	10.49±0.08	10.34±0.08	-1.37±0.48	6.43±2.16	9.91±0.05	8.41±0.25
NGC3265	-0.99±0.55	9.67±0.16	9.53±0.15	-0.58±0.14	0.56±0.26	9.63±0.07	9.35±0.12
NGC3377	-3.36±0.39	10.45±0.07	10.30±0.07	-2.35±0.21	9.86±0.46	9.82±0.06	7.26±0.27
NGC3379	-3.02±0.38	10.86±0.07	10.71±0.07	-1.58±0.18	9.20±0.71	10.24±0.07	7.64±0.32
NGC3384	-3.26±0.40	10.56±0.07	10.41±0.07	-2.11±0.19	9.65±0.50	9.93±0.06	7.54±0.38
NGC3412	-3.47±0.40	10.62±0.05	10.47±0.05	-2.26±0.19	9.90±0.43	9.99±0.05	6.95±0.46
NGC3489	-2.63±0.46	10.43±0.07	10.28±0.07	-1.60±0.26	7.46±1.30	9.83±0.06	8.54±0.15
NGC3516	-1.59±0.50	11.18±0.12	11.04±0.12	0.32±0.18	1.90±1.00	10.83±0.06	10.35±0.13
NGC3522	-3.25±0.46	9.94±0.06	9.79±0.06	-2.63±0.21	9.34±0.64	9.32±0.06	6.78±0.51
NGC3557	-0.40±0.39	8.51±0.53	8.39±0.52	-1.14±0.36	0.34±0.32	9.04±0.28	8.95±0.28
NGC3585	-0.57±0.61	8.19±0.72	8.07±0.71	-1.60±0.41	0.53±1.06	8.60±0.39	8.09±0.20
NGC3593	-1.25±0.53	10.28±0.14	10.14±0.13	-0.32±0.21	1.13±0.87	10.02±0.07	9.80±0.10
NGC3607	-2.94±0.43	10.99±0.06	10.85±0.06	-1.38±0.25	8.90±0.93	10.37±0.06	8.70±0.23
NGC3608	-3.24±0.38	10.83±0.07	10.68±0.07	-1.82±0.16	9.61±0.49	10.20±0.06	7.77±0.28
NGC3610	-3.29±1.36	10.48±1.41	10.34±1.40	-1.92±0.37	8.04±3.47	10.05±0.99	7.89±0.41
NGC3640	-3.64±0.45	11.01±0.06	10.86±0.06	-2.02±0.24	10.01±0.44	10.38±0.05	7.42±0.43
NGC3706	-1.23±1.28	8.64±1.87	8.51±1.86	-1.91±0.79	2.83±4.06	8.90±1.33	7.96±0.64
NGC3773	-0.41±0.38	9.06±0.17	8.94±0.17	-0.73±0.09	0.36±0.07	9.34±0.06	8.74±0.15
NGC3870	-0.44±0.38	8.84±0.17	8.72±0.16	-0.99±0.10	0.37±0.06	9.08±0.06	8.48±0.18
NGC3923	-3.37±0.38	11.71±0.07	11.56±0.07	-1.07±0.15	9.78±0.45	11.08±0.06	7.78±0.35
NGC3941	-0.48±0.46	7.09±0.64	6.96±0.64	-2.68±0.64	0.39±0.36	7.60±0.51	7.50±0.55
NGC3945	-2.97±0.49	10.77±0.07	10.62±0.07	-1.64±0.37	8.86±1.15	10.15±0.06	8.66±0.21
NGC3962	-3.26±0.39	11.37±0.07	11.23±0.07	-1.32±0.20	9.65±0.50	10.75±0.07	8.73±0.13
NGC4026	-3.19±0.85	10.41±0.87	10.26±0.86	-2.30±0.25	9.22±2.61	9.86±0.58	7.67±0.29
NGC4073	-2.91±0.38	11.81±0.07	11.66±0.07	-0.54±0.18	8.98±0.80	11.19±0.06	8.71±0.46
NGC4117	-2.30±0.48	9.78±0.07	9.63±0.07	-1.89±0.24	5.60±1.36	9.21±0.05	8.11±0.26
NGC4125	-3.11±0.48	11.18±0.07	11.04±0.07	-1.38±0.35	9.30±0.87	10.56±0.06	8.95±0.21
NGC4138	-1.95±0.48	10.41±0.09	10.26±0.09	-0.82±0.17	3.45±1.01	9.92±0.06	9.12±0.15
NGC4150	-3.96±1.08	10.39±0.06	10.25±0.06	-2.17±0.50	8.76±1.18	9.79±0.05	8.60±0.25
NGC4168	-3.27±0.41	11.12±0.06	10.97±0.06	-1.54±0.20	9.58±0.54	10.49±0.05	7.56±0.50
NGC4203	-2.59±0.44	10.65±0.07	10.51±0.07	-1.33±0.24	7.26±1.32	10.05±0.06	8.72±0.24
NGC4251	-3.49±0.50	10.72±0.06	10.57±0.06	-2.19±0.35	9.90±0.53	10.09±0.05	7.85±0.47
NGC4261	-3.03±0.39	11.51±0.06	11.37±0.06	-0.93±0.19	9.16±0.71	10.89±0.06	8.78±0.17
NGC4267	-3.44±0.42	10.59±0.06	10.45±0.06	-2.27±0.21	9.92±0.44	9.96±0.05	7.08±0.42
NGC4278	-2.81±0.40	10.52±0.07	10.38±0.07	-1.71±0.20	8.45±0.99	9.91±0.06	8.18±0.26
NGC4308	-3.28±0.44	9.19±0.06	9.04±0.06	-3.48±0.26	9.57±0.56	8.56±0.05	6.12±0.49
NGC4344	-1.69±0.47	9.82±0.10	9.68±0.09	-1.17±0.19	2.37±1.04	9.39±0.06	8.66±0.24
NGC4350	-3.00±0.45	10.84±0.07	10.69±0.07	-1.60±0.30	9.02±0.98	10.22±0.06	8.53±0.26
NGC4352	-3.50±0.42	10.58±0.06	10.43±0.06	-2.33±0.25	9.89±0.45	9.95±0.06	6.97±0.52
NGC4365	-3.08±0.37	11.21±0.07	11.07±0.07	-1.30±0.18	9.37±0.63	10.59±0.06	7.67±0.32
NGC4371	-3.36±0.41	10.65±0.06	10.51±0.06	-2.13±0.21	9.81±0.46	10.02±0.06	7.01±0.34
NGC4374	-3.14±0.39	11.31±0.08	11.16±0.08	-1.24±0.16	9.42±0.54	10.68±0.07	8.30±0.24
NGC4377	-3.47±0.45	10.58±0.06	10.43±0.05	-2.30±0.28	9.88±0.47	9.95±0.05	6.68±0.55
NGC4379	-3.34±0.40	10.41±0.06	10.27±0.06	-2.34±0.17	9.81±0.44	9.78±0.05	6.66±0.52
NGC4382	-1.48±1.36	8.15±1.81	8.02±1.80	-2.61±0.69	3.45±4.17	8.27±1.26	7.15±0.41
NGC4417	-3.31±0.38	10.41±0.06	10.26±0.06	-2.31±0.16	9.71±0.46	9.78±0.05	7.01±0.51
NGC4421	-3.71±0.45	10.73±0.06	10.58±0.06	-2.37±0.24	10.11±0.43	10.09±0.05	7.04±0.53
NGC4434	-3.28±0.40	10.26±0.06	10.11±0.06	-2.44±0.19	9.67±0.51	9.63±0.05	7.10±0.51
NGC4435	-2.99±0.53	10.75±0.06	10.61±0.06	-1.71±0.39	8.95±1.12	10.13±0.06	8.60±0.24
NGC4442	-3.26±0.37	10.31±0.06	10.16±0.06	-2.40±0.21	9.74±0.48	9.68±0.05	7.09±0.49

TABLE 7 — *Continued*

Name	$\log(f_{ysp})$	$\log(M_{gal})$ (M_\odot)	$\log(M_*)$ (M_\odot)	$\log(\text{SFR})$ (M_\odot/yr)	t_{D4000} (Gyr)	$\log(L_{bol})$ (L_\odot)	$\log(L_d)$ (L_\odot)
NGC4458	-3.49±0.41	9.78±0.05	9.63±0.05	-3.14±0.22	9.95±0.43	9.15±0.05	6.48±0.48
NGC4459	-2.89±0.46	11.17±0.07	11.03±0.07	-1.15±0.30	8.60±1.15	10.56±0.07	9.08±0.18
NGC4460	-1.51±0.50	9.47±0.12	9.32±0.12	-1.25±0.14	1.34±0.75	9.15±0.06	8.59±0.13
NGC4464	-3.28±0.40	10.21±0.06	10.07±0.06	-2.46±0.17	9.65±0.48	9.59±0.05	6.63±0.53
NGC4472	-2.82±0.40	11.16±0.08	11.02±0.08	-1.07±0.20	8.46±1.01	10.55±0.07	7.70±0.32
NGC4473	-3.24±0.38	11.54±0.06	11.40±0.06	-1.13±0.18	9.68±0.49	10.92±0.05	8.06±0.47
NGC4474	-3.55±0.40	10.77±0.06	10.62±0.06	-2.18±0.22	9.94±0.44	10.14±0.05	7.38±0.53
NGC4476	-2.38±0.47	10.70±0.07	10.56±0.07	-1.11±0.29	6.38±1.53	10.12±0.06	9.00±0.24
NGC4477	-3.20±0.41	11.10±0.06	10.95±0.06	-1.53±0.23	9.59±0.55	10.47±0.06	8.47±0.18
NGC4478	-3.11±0.38	10.68±0.06	10.53±0.06	-1.85±0.17	9.43±0.62	10.06±0.06	7.54±0.44
NGC4479	-3.18±0.40	9.85±0.06	9.70±0.06	-2.73±0.19	9.46±0.58	9.22±0.05	6.19±0.56
NGC4482	-3.27±0.98	9.90±1.03	9.76±1.02	-2.79±0.45	9.21±2.80	9.34±0.76	6.47±0.55
NGC4483	-3.36±0.38	10.03±0.06	9.88±0.06	-2.74±0.15	9.78±0.44	9.40±0.05	6.43±0.52
NGC4486	-2.92±0.37	11.81±0.07	11.66±0.07	-0.52±0.13	8.84±0.77	11.19±0.06	8.72±0.18
NGC4489	-3.36±0.37	10.08±0.06	9.94±0.06	-2.73±0.17	9.87±0.43	9.45±0.05	6.62±0.50
NGC4494	-0.87±0.60	10.99±0.17	10.85±0.16	0.87±0.29	0.61±0.69	11.02±0.14	8.28±0.16
NGC4515	-3.24±0.41	9.89±0.06	9.75±0.06	-2.74±0.20	9.55±0.53	9.27±0.06	6.27±0.52
NGC4526	-2.43±0.52	10.31±0.08	10.17±0.08	-1.56±0.35	6.63±1.77	9.72±0.06	8.77±0.17
NGC4528	-2.98±0.86	10.22±0.84	10.08±0.84	-2.22±0.26	8.78±2.68	9.68±0.57	7.51±0.46
NGC4552	-4.25±0.89	11.19±0.06	11.04±0.06	-1.39±0.34	8.84±0.75	10.59±0.06	7.97±0.24
NGC4564	-3.11±0.41	10.73±0.06	10.58±0.06	-1.80±0.22	9.34±0.71	10.10±0.05	7.99±0.44
NGC4570	-3.31±0.38	11.22±0.06	11.08±0.06	-1.53±0.19	9.78±0.46	10.59±0.06	7.83±0.47
NGC4578	-0.52±0.50	7.13±0.61	7.00±0.61	-2.64±0.58	0.39±0.37	7.62±0.50	7.46±0.56
NGC4589	-1.74±1.26	9.99±1.33	9.86±1.32	-1.21±0.22	4.84±4.47	9.82±0.85	8.68±0.15
NGC4612	-3.50±0.42	10.93±0.06	10.79±0.06	-2.01±0.27	9.97±0.45	10.30±0.05	7.52±0.51
NGC4621	-4.24±0.88	11.20±0.06	11.06±0.06	-1.71±0.42	9.64±0.58	10.58±0.05	7.45±0.36
NGC4623	-3.40±0.43	10.58±0.06	10.43±0.06	-2.22±0.23	9.78±0.47	9.95±0.05	6.81±0.55
NGC4636	-3.06±0.41	10.85±0.07	10.70±0.07	-1.62±0.21	9.23±0.70	10.23±0.06	7.86±0.25
NGC4638	-1.78±1.81	8.03±1.89	7.90±1.88	-2.80±0.66	3.45±4.29	8.21±1.32	6.89±0.41
NGC4649	-3.12±0.38	11.64±0.06	11.49±0.06	-0.89±0.14	9.40±0.57	11.02±0.06	7.64±0.38
NGC4660	-3.26±0.38	10.65±0.06	10.50±0.06	-2.05±0.20	9.73±0.48	10.02±0.06	7.48±0.32
NGC4694	-1.85±0.46	10.34±0.09	10.19±0.09	-0.86±0.20	3.33±1.11	9.85±0.06	9.12±0.16
NGC4696	-0.50±0.48	8.65±0.57	8.53±0.56	-1.05±0.31	0.36±0.29	9.09±0.25	8.90±0.21
NGC4697	-1.05±1.06	9.15±1.08	9.02±1.07	-1.14±0.20	1.93±3.02	9.28±0.61	8.60±0.18
NGC4709	-0.46±0.45	8.15±0.79	8.03±0.78	-1.57±0.65	0.38±0.39	8.76±0.41	8.52±0.28
NGC4754	-3.44±0.40	11.02±0.06	10.87±0.06	-1.85±0.24	9.92±0.46	10.39±0.05	7.39±0.46
NGC4762	-3.55±0.43	10.80±0.06	10.65±0.06	-2.20±0.28	10.05±0.44	10.16±0.06	7.09±0.43
NGC4786	-3.06±0.81	11.54±0.69	11.40±0.68	-0.97±0.28	9.01±2.37	10.98±0.43	9.21±0.20
NGC4915	-1.42±1.34	9.09±1.66	8.95±1.64	-1.72±0.41	3.74±4.57	9.27±1.02	8.44±0.36
NGC4936	-0.96±1.00	9.61±1.14	9.48±1.13	-0.67±0.33	2.05±3.40	9.75±0.69	9.25±0.25
NGC5018	-2.98±0.50	11.70±0.07	11.56±0.07	-0.75±0.38	8.96±1.08	11.08±0.07	9.57±0.21
NGC5044	-3.08±0.39	11.68±0.07	11.53±0.07	-0.79±0.15	9.24±0.63	11.06±0.06	8.82±0.23
NGC5061	-1.45±1.36	9.16±1.82	9.02±1.80	-1.67±0.51	3.78±4.76	9.35±1.14	8.12±0.41
NGC5077	-0.98±0.67	11.14±0.18	11.01±0.17	0.96±0.33	0.74±0.90	11.14±0.15	8.80±0.16
NGC5173	-2.03±0.48	10.59±0.08	10.45±0.08	-0.72±0.17	3.86±1.01	10.08±0.05	8.93±0.31
NGC5273	-2.76±0.46	10.43±0.06	10.29±0.06	-1.76±0.30	8.07±1.26	9.83±0.06	8.51±0.16
NGC5322	-3.15±0.43	11.29±0.06	11.15±0.06	-1.30±0.26	9.51±0.68	10.67±0.06	8.82±0.22
NGC5338	-2.00±0.48	9.53±0.08	9.39±0.08	-1.81±0.22	3.98±1.21	9.02±0.06	8.11±0.24
NGC5353	-3.13±0.43	11.39±0.07	11.24±0.07	-1.16±0.26	9.38±0.73	10.76±0.06	8.83±0.28
NGC5419	-3.44±0.38	12.06±0.06	11.91±0.06	-0.82±0.21	9.94±0.44	11.42±0.06	8.06±0.48
NGC5481	-2.43±0.65	10.64±0.08	10.49±0.08	-1.13±0.52	5.95±2.36	10.07±0.05	7.11±0.51
NGC5557	-0.48±0.47	7.53±0.73	7.40±0.73	-2.20±0.68	0.38±0.37	8.12±0.66	7.97±0.73
NGC5576	-3.42±0.41	10.98±0.06	10.83±0.06	-1.87±0.20	9.92±0.45	10.34±0.06	7.55±0.46
NGC5596	-2.41±0.44	10.68±0.07	10.53±0.07	-1.09±0.17	6.14±1.03	10.09±0.05	8.50±0.36
NGC5813	-3.03±0.38	11.17±0.07	11.02±0.07	-1.28±0.20	9.21±0.71	10.55±0.06	8.06±0.33
NGC5831	-3.25±0.40	10.77±0.06	10.62±0.06	-1.91±0.21	9.69±0.51	10.14±0.06	7.80±0.44
NGC5845	-3.00±0.42	10.41±0.07	10.26±0.07	-2.04±0.26	9.11±0.85	9.79±0.06	8.03±0.27
NGC5846	-2.91±0.39	11.26±0.07	11.11±0.07	-1.06±0.18	8.77±0.89	10.64±0.06	8.30±0.24
NGC5866	-2.58±0.51	10.68±0.07	10.53±0.07	-1.36±0.38	7.41±1.70	10.07±0.06	8.96±0.22
NGC5982	-3.28±0.45	11.50±0.06	11.35±0.06	-1.16±0.21	9.58±0.54	10.87±0.06	8.41±0.34
NGC6703	-1.88±1.81	8.88±1.82	8.75±1.81	-2.37±0.48	4.43±4.96	9.08±1.13	8.28±0.42
NGC6776	-0.49±0.48	8.76±0.64	8.63±0.63	-0.97±0.42	0.38±0.33	9.26±0.29	9.08±0.27
NGC7077	-1.60±1.62	7.47±0.42	7.34±0.41	-2.25±0.46	0.46±0.92	8.06±0.16	7.98±0.20
NGC7360	-2.10±0.47	10.88±0.08	10.74±0.08	-0.48±0.16	4.08±0.98	10.36±0.05	9.11±0.31
NGC7457	-3.19±1.04	9.92±1.03	9.77±1.03	-2.76±0.45	8.93±3.07	9.39±0.73	7.25±0.40
NGC7619	-3.31±0.40	11.68±0.06	11.53±0.06	-1.05±0.19	9.76±0.48	11.05±0.05	8.36±0.46
NGC7626	-3.26±0.40	11.61±0.06	11.46±0.06	-1.09±0.20	9.73±0.48	10.98±0.06	8.26±0.27
NGC7785	-2.50±0.63	11.55±0.08	11.40±0.08	-0.34±0.51	6.54±2.27	10.96±0.05	8.25±0.25
UGC01503	-1.36±0.59	10.69±0.19	10.55±0.19	0.13±0.24	1.20±1.18	10.47±0.06	9.92±0.16
UGC06570	-1.18±0.52	9.84±0.13	9.70±0.13	-0.68±0.26	1.02±0.84	9.65±0.09	9.33±0.19
UGC06637	-1.11±0.58	9.45±0.13	9.31±0.13	-0.79±0.10	0.53±0.16	9.39±0.05	8.66±0.20
UGC06655	-0.72±0.51	8.49±0.15	8.35±0.15	-1.55±0.10	0.44±0.08	8.58±0.05	7.86±0.20
UGC06805	-1.02±0.55	9.09±0.14	8.96±0.14	-1.12±0.12	0.53±0.18	9.06±0.06	8.62±0.15
UGC07436	-3.13±0.50	9.44±0.06	9.30±0.06	-3.07±0.34	9.06±1.03	8.82±0.05	8.86±0.53
UGC07580	-2.92±0.42	8.82±0.07	8.67±0.07	-3.46±0.14	8.58±0.85	8.21±0.06	5.17±0.57
UGC08876	-3.28±0.39	10.39±0.06	10.24±0.06	-2.32±0.19	9.71±0.49	9.76±0.06	7.12±0.52

TABLE 7 — *Continued*

Name	Log(f_{ysp})	Log(M_{gal}) (M_\odot)	Log(M_*) (M_\odot)	Log(SFR) (M_\odot/yr)	t_{D4000} (Gyr)	Log(L_{bol}) (L_\odot)	Log(L_d) (L_\odot)

TABLE 8
PARAMETERS FITTED WITH SINGLE TEMPERATURE MODEL AND EMISSIVITY $\beta=1.5$
ON FIR DATA.

Name	Log(L_d) (L_\odot)	T (K)	Log(M_d) (M_\odot)	χ^2/ndf
Eso103-35	10.57±0.05	88.33±4.40	4.90±0.06	10.10
Eso428-14	9.76±0.02	54.14±3.61	5.22±0.14	1.05
Eso483-13	8.12±0.02	31.45±1.40	4.87±0.11	50.00
IC1459	8.75±0.02	31.76±1.31	5.47±0.10	1.18
IC3032	6.23±0.82	61.10±21.56	2.71±2.20	0.06
IC3101	6.30±0.87	60.61±21.96	2.95±2.27	0.05
IC3328	6.28±0.79	61.56±21.29	2.66±2.40	3.12
IC3370	9.43±0.02	30.07±0.93	6.28±0.08	67.35
IC3381	6.22±0.77	61.96±21.38	2.55±2.38	0.94
IC3501	6.37±0.91	60.58±22.64	3.05±2.15	0.05
IC4296	8.69±0.05	39.12±3.32	4.94±0.16	2.39
IC4329	6.70±1.00	55.18±25.00	5.27±4.60	0.80
IC5063	10.57±0.07	70.45±6.49	5.43±0.15	22.78
NGC0221	5.65±0.46	12.20±1.60	5.21±0.77	16.03
NGC0315	9.47±0.02	28.57±0.85	6.45±0.08	5.92
NGC0404	5.94±0.02	30.63±1.14	2.74±0.09	0.31
NGC0410	7.31±1.19	56.10±24.00	5.40±5.19	19.31
NGC0474	8.00±0.07	25.28±2.05	5.32±0.21	7.27
NGC0507	6.72±1.04	54.32±24.43	5.14±3.97	1.19
NGC0526	9.94±0.11	21.62±1.94	7.69±0.33	11.36
NGC0533	8.38±0.07	31.84±3.54	5.16±0.22	0.63
NGC0584	8.16±0.20	76.06±13.59	2.96±0.51	5.32
NGC0636	6.24±0.76	55.95±24.94	4.59±4.78	1.26
NGC0720	7.43±0.31	63.23±19.00	3.21±1.57	9.92
NGC0777	7.20±0.86	55.01±22.94	5.01±4.98	5.18
NGC0807	9.84±0.04	18.17±0.38	7.90±0.09	47.69
NGC0814	9.71±0.01	55.91±1.12	5.07±0.04	27.90
NGC0821	6.25±0.74	53.97±24.80	4.53±4.50	4.93
NGC0855	8.36±0.01	34.96±0.74	4.84±0.06	8.41
NGC1016	6.75±1.03	53.93±24.44	5.52±8.51	1.81
NGC1023	5.88±0.54	55.71±24.57	3.84±3.17	0.52
NGC1199	8.80±0.41	31.89±22.27	7.35±0.76	2.65
NGC1266	10.43±0.00	42.42±0.22	6.45±0.01	24.33
NGC1316	9.80±0.02	28.75±0.45	6.75±0.04	5.98
NGC1374	6.48±0.76	57.36±23.60	4.27±4.49	5.59
NGC1377	9.99±0.00	51.26±0.49	5.56±0.02	8.40
NGC1386	9.28±0.00	38.04±0.19	5.56±0.01	10.54
NGC1395	8.17±0.02	28.48±0.81	5.14±0.06	0.85
NGC1399	6.89±0.11	12.66±1.41	5.87±0.19	2.78
NGC1404	7.86±0.24	66.18±17.02	3.21±0.78	0.18
NGC1407	6.08±0.66	52.92±24.99	4.76±3.75	7.10
NGC1426	6.11±0.66	54.77±24.36	4.18±3.66	1.21
NGC1427	7.37±0.18	55.84±14.95	3.08±0.58	11.60
NGC1439	7.77±0.05	41.42±4.20	3.90±0.18	3.95
NGC1510	8.50±0.05	49.25±5.59	4.24±0.24	84.27
NGC1522	8.47±0.01	40.53±1.12	4.61±0.06	17.03
NGC1533	8.34±0.05	20.46±0.67	6.12±0.13	24.34
NGC1553	8.34±0.02	42.28±1.32	4.37±0.06	14.66
NGC2110	9.91±0.04	47.10±5.50	5.76±0.26	6.42
NGC2434	7.51±0.19	52.98±15.07	3.33±0.52	5.73
NGC2768	8.58±0.01	37.40±0.87	4.90±0.05	10.80
NGC2787	8.14±0.02	35.67±0.90	4.58±0.06	1.76
NGC2832	9.72±0.14	87.51±6.85	4.09±0.13	63.60
NGC2974	9.14±0.02	25.00±0.54	6.42±0.06	4.65
NGC2986	6.16±0.70	54.06±25.14	4.59±3.98	5.56
NGC3032	9.33±0.01	34.04±0.53	5.88±0.04	2.77
NGC3073	8.11±0.02	25.65±0.62	5.34±0.07	3.47
NGC3115	7.01±0.18	55.33±15.71	2.90±0.96	4.21
NGC3156	8.14±0.03	35.20±1.47	4.62±0.09	5.56
NGC3226	8.26±0.02	26.19±0.50	5.43±0.06	0.17
NGC3265	9.24±0.01	38.76±0.50	5.48±0.03	12.43
NGC3377	7.06±0.03	33.27±1.49	3.68±0.10	17.23
NGC3379	7.20±0.04	32.07±1.93	3.91±0.13	2.42
NGC3384	7.03±0.42	57.97±22.92	5.55±6.88	1.88
NGC3557	8.89±0.03	31.84±1.22	5.60±0.09	12.57

TABLE 8 — *Continued*

Name	Log(L_d) (L_\odot)	T (K)	Log(M_d) (M_\odot)	χ^2/ndf
NGC3585	7.75±0.08	46.54±6.44	3.63±0.23	1.70
NGC3593	9.48±0.00	36.61±0.10	5.85±0.01	9674.29
NGC3608	7.53±0.08	38.06±7.02	3.93±0.24	3.33
NGC3610	7.30±0.33	40.96±19.20	4.39±2.05	2.29
NGC3640	6.10±0.67	56.90±24.45	3.68±2.85	0.17
NGC3773	8.84±0.01	36.08±0.55	5.24±0.04	6.24
NGC3923	7.45±0.06	26.27±2.18	4.66±0.21	2.36
NGC3941	6.79±1.05	55.79±24.01	3.77±1.64	1.10
NGC3945	8.69±0.02	19.84±0.25	6.53±0.04	8.44
NGC3962	8.65±0.01	29.07±0.53	5.57±0.04	3.57
NGC4125	8.83±0.02	28.75±0.63	5.78±0.06	6.21
NGC4138	8.93±0.02	25.89±0.45	6.13±0.05	0.84
NGC4150	7.44±0.02	33.76±1.15	4.02±0.08	5.33
NGC4168	6.29±0.78	56.17±24.16	3.78±2.36	0.11
NGC4203	8.71±0.02	26.28±0.48	5.88±0.05	1.92
NGC4251	6.39±0.93	59.76±23.06	3.25±2.18	0.31
NGC4261	8.52±0.02	23.69±0.55	5.94±0.05	10.66
NGC4267	6.44±0.23	17.36±5.00	4.94±0.49	6.14
NGC4278	8.18±0.02	29.32±0.79	5.08±0.07	9.31
NGC4291	6.38±0.89	49.74±26.08	6.50±3.89	3.29
NGC4344	8.72±0.02	25.18±0.62	5.99±0.07	3.34
NGC4350	8.36±0.02	33.41±0.74	4.95±0.05	11.57
NGC4352	6.80±0.99	44.94±27.44	4.91±0.99	8.75
NGC4365	7.49±0.05	34.11±2.04	4.05±0.12	0.51
NGC4371	7.07±0.25	60.92±19.77	2.71±0.57	16.13
NGC4374	8.37±0.02	33.36±0.87	4.96±0.06	8.42
NGC4377	8.65±0.04	36.56±1.03	5.02±0.05	10.30
NGC4379	6.46±0.96	59.60±23.13	3.29±2.09	0.11
NGC4382	6.58±0.19	40.15±15.01	3.30±2.12	3.10
NGC4386	8.76±0.19	19.50±2.22	6.84±0.45	0.19
NGC4406	5.02±0.02	93.40±1.34	-0.77±0.03	9.77
NGC4417	8.09±0.14	69.58±11.07	3.05±0.26	5.52
NGC4421	6.32±0.76	55.95±24.23	4.54±3.78	0.29
NGC4434	6.03±0.66	57.94±23.03	3.07±2.20	0.85
NGC4435	8.96±0.01	30.62±0.25	5.75±0.02	100.32
NGC4442	6.17±0.76	62.86±21.24	2.64±2.88	0.06
NGC4458	5.80±0.53	61.33±21.99	2.50±2.94	0.05
NGC4459	9.17±0.01	33.56±0.54	5.75±0.04	8.84
NGC4460	8.58±0.01	35.68±0.83	5.02±0.06	3.67
NGC4464	5.97±0.63	51.16±25.83	3.82±1.44	3.09
NGC4472	7.28±0.04	31.78±1.82	4.01±0.12	0.16
NGC4473	6.36±0.82	56.01±24.20	3.95±2.47	0.45
NGC4474	6.54±0.92	58.30±23.07	3.42±2.21	2.79
NGC4476	9.08±0.02	29.59±0.68	5.96±0.05	7.72
NGC4477	8.47±0.01	31.53±0.50	5.20±0.04	5.88
NGC4478	6.73±0.07	11.61±1.05	5.89±0.15	2.35
NGC4479	6.31±0.87	60.85±22.86	3.11±2.32	0.93
NGC4482	6.26±0.83	58.44±22.63	3.28±2.54	0.35
NGC4483	5.87±0.59	58.19±22.63	2.83±2.34	0.71
NGC4486	8.55±0.02	27.98±0.97	5.58±0.09	24.88
NGC4494	8.24±0.02	36.63±0.90	4.61±0.05	1.20
NGC4526	8.84±0.00	31.24±0.17	5.59±0.01	6.30
NGC4528	8.29±0.24	72.81±12.59	3.18±0.33	4.35
NGC4552	6.63±0.03	29.78±0.89	3.50±0.06	8.41
NGC4564	6.11±0.70	57.59±22.99	3.27±2.31	1.67
NGC4570	6.15±0.73	58.18±23.81	3.35±2.27	0.37
NGC4578	6.31±0.78	53.98±24.91	4.21±2.28	2.86
NGC4589	8.57±0.02	28.90±0.67	5.51±0.05	3.11
NGC4612	6.48±0.81	48.96±26.30	4.61±1.26	2.79
NGC4621	6.31±0.05	30.94±2.08	3.12±0.14	18.48
NGC4636	7.74±0.02	33.12±1.05	4.36±0.07	3.17
NGC4638	6.46±0.30	66.50±17.34	1.79±1.26	3.99
NGC4649	8.32±0.03	94.04±1.02	2.52±0.03	1117.45
NGC4660	7.18±0.05	30.50±1.88	4.01±0.13	2.08
NGC4694	8.93±0.03	28.26±1.07	5.93±0.10	10.20
NGC4696	8.69±0.02	27.67±0.60	5.73±0.05	5.55
NGC4697	8.53±0.02	35.69±0.88	4.97±0.05	6.49
NGC4709	6.68±0.98	54.58±24.57	5.22±4.27	7.20
NGC4754	6.00±0.62	56.26±24.22	3.52±2.24	0.24
NGC4762	6.73±0.23	57.48±18.47	2.77±1.07	1.39
NGC4786	9.31±0.05	41.32±2.73	5.41±0.12	0.53
NGC4915	8.04±0.05	26.93±1.66	5.18±0.15	0.90
NGC4936	9.26±0.03	26.88±0.94	6.38±0.08	0.61
NGC5018	9.63±0.02	31.77±1.02	6.35±0.09	11.19
NGC5044	8.76±0.03	31.18±1.40	5.53±0.10	4.06
NGC5061	7.56±0.37	61.88±20.01	3.54±1.58	2.85

TABLE 8 — *Continued*

Name	$\text{Log}(L_d)$ (L_\odot)	T (K)	$\text{Log}(M_d)$ (M_\odot)	χ^2/ndf
NGC5077	8.60±0.02	31.06±1.14	5.37±0.09	353.34
NGC5273	8.49±0.02	35.46±0.88	4.94±0.06	17.31
NGC5322	8.70±0.02	33.48±1.57	5.30±0.12	13.66
NGC5353	9.02±0.02	32.28±0.97	5.69±0.07	78.11
NGC5419	6.72±1.00	54.91±24.39	4.96±4.26	1.16
NGC5557	7.94±0.37	48.40±19.54	4.70±1.87	7.76
NGC5576	6.09±0.68	55.65±24.40	3.66±2.18	1.23
NGC5813	7.93±0.07	42.33±4.29	4.01±0.18	28.02
NGC5831	7.23±0.87	65.48±21.68	3.78±5.51	21.82
NGC5845	7.88±0.04	28.72±1.67	4.86±0.14	14.40
NGC5846	8.00±0.03	30.43±1.22	4.83±0.09	1.24
NGC5866	9.20±0.00	29.41±0.07	6.09±0.01	3.05
NGC5982	8.11±0.06	28.59±2.39	5.12±0.18	2.73
NGC6482	8.99±0.16	84.78±9.05	3.48±0.99	78.27
NGC6703	7.94±0.11	45.41±7.75	3.91±0.25	3.23
NGC6776	9.48±0.22	74.04±15.54	4.45±0.59	3.83
NGC6849	6.67±1.00	53.83±25.04	5.33±4.21	3.35
NGC7077	8.28±0.03	33.40±1.33	4.88±0.09	5.81
NGC7457	6.01±0.60	57.06±24.20	4.05±3.31	1.77
NGC7619	6.58±0.92	55.30±24.95	5.07±4.31	1.46
NGC7785	8.09±0.22	56.80±18.52	3.92±0.70	6.97
UGC01503	9.88±0.02	28.32±0.96	6.88±0.09	41.94
UGC07436	5.93±0.61	56.84±23.00	2.97±2.08	3.22
UGC07580	6.58±0.42	31.53±9.38	3.58±0.52	0.41

TABLE 9
PARAMETERS FITTED BY A 2 TEMPERATURE MODEL WITH AN EMISSIVITY $\beta=2$
USING FIR DATA.

Name	$\text{Log}(L_d)$ (L_\odot)	α	T_d^1 (K)	T_d^2 (K)	$\text{Log}(M_d)$ (M_\odot)	χ^2/ndf
IC3328	6.45±0.81	0.50±0.29	27.48±10.13	71.11±14.39	4.75±2.80	9.31
IC5063	10.63±0.07	1.00±0.00	16.53±1.48	70.67±5.36	8.63±0.35	2.15
NGC0584	8.34±0.21	0.46±0.27	26.86±10.03	79.91±11.67	6.11±1.43	8.44
NGC0855	8.36±0.07	0.99±0.01	22.61±1.12	57.17±7.27	5.48±0.13	2.52
NGC1266	10.56±0.03	0.99±0.00	27.60±0.59	70.13±3.06	7.15±0.06	12.83
NGC1316	9.61±0.07	1.00±0.00	24.11±0.65	55.17±8.73	6.56±0.13	5.55
NGC1377	10.17±0.04	0.98±0.00	29.83±1.07	72.82±4.15	6.55±0.09	2.46
NGC1386	9.34±0.04	0.99±0.00	24.18±0.64	62.96±4.13	6.27±0.07	0.40
NGC1399	7.40±0.32	1.00±0.00	11.52±0.97	65.41±14.85	6.43±0.40	2.65
NGC1404	8.02±0.27	0.48±0.28	27.25±10.09	71.84±14.05	5.79±1.59	0.18
NGC3265	9.31±0.10	0.99±0.01	24.43±1.09	61.03±10.47	6.21±0.08	1.19
NGC3640	6.23±0.74	0.50±0.29	27.54±10.13	71.33±14.29	4.53±3.32	0.56
NGC4125	8.66±0.04	0.99±0.00	20.34±1.26	48.98±3.51	6.07±0.18	7.41
NGC4138	8.75±0.16	1.00±0.00	21.62±0.93	58.67±12.09	6.04±0.29	0.37
NGC4168	6.44±0.85	0.49±0.29	27.45±10.10	71.60±14.50	4.87±3.10	0.38
NGC4203	8.55±0.10	1.00±0.00	21.62±0.61	67.69±13.69	5.79±0.14	0.79
NGC4267	7.23±0.42	1.00±0.00	16.95±4.24	68.92±14.54	5.76±0.80	10.01
NGC4350	8.26±0.11	1.00±0.01	27.34±0.84	59.71±13.42	4.90±0.19	14.76
NGC4365	7.48±0.15	0.98±0.02	27.10±3.20	56.06±10.45	4.34±0.59	1.06
NGC4371	7.18±0.27	0.55±0.30	28.46±9.58	67.60±14.46	4.88±1.74	27.19
NGC4374	8.46±0.11	0.99±0.00	18.13±1.94	53.27±7.67	6.21±0.26	5.56
NGC4377	8.54±0.06	0.99±0.01	30.36±1.03	57.29±12.21	4.89±0.13	24.45
NGC4406	5.04±0.03	1.00±0.00	19.48±2.07	92.08±2.34	2.65±0.42	2.10
NGC4417	8.02±0.17	0.46±0.28	28.22±10.70	60.45±12.15	5.77±1.44	16.05
NGC4434	6.14±0.71	0.50±0.29	27.60±10.09	70.88±14.32	4.34±2.62	2.59
NGC4435	8.71±0.01	1.00±0.00	26.93±0.22	56.53±11.44	5.36±0.02	133.75
NGC4458	5.92±0.58	0.50±0.29	27.34±10.15	72.13±14.35	4.05±2.62	0.15
NGC4459	9.24±0.11	1.00±0.00	25.87±0.74	74.82±13.39	6.01±0.14	6.87
NGC4464	6.14±0.70	0.50±0.29	27.37±10.07	71.04±14.27	4.36±3.37	10.08
NGC4472	7.33±0.21	0.99±0.01	24.58±3.49	59.94±12.69	4.63±0.90	0.39
NGC4473	6.54±0.90	0.49±0.29	27.19±10.12	71.49±14.29	5.01±3.10	0.75
NGC4474	6.71±0.94	0.49±0.29	27.50±10.01	70.42±14.41	5.08±2.62	8.42
NGC4476	9.29±0.13	1.00±0.00	22.02±0.76	80.71±10.37	6.49±0.16	3.10
NGC4477	8.52±0.07	0.99±0.00	19.35±1.00	51.66±4.36	6.06±0.14	3.41
NGC4478	6.77±0.53	1.00±0.00	11.03±0.85	60.33±12.82	6.05±0.56	4.90
NGC4483	6.04±0.64	0.50±0.29	27.39±10.12	71.59±14.46	4.20±2.88	2.22
NGC4486	8.58±0.11	1.00±0.00	12.67±0.91	56.17±7.32	7.24±0.20	13.78
NGC4494	8.36±0.17	0.98±0.02	26.75±2.49	63.40±14.30	5.14±0.35	0.80
NGC4528	8.30±0.30	0.49±0.28	27.69±10.39	69.08±13.78	6.07±1.44	13.01
NGC4552	6.59±0.21	1.00±0.00	24.83±1.24	64.23±13.99	3.57±0.41	12.15
NGC4564	6.17±0.74	0.52±0.29	27.26±10.20	71.24±14.27	4.48±3.22	5.06

TABLE 9 — *Continued*

Name	$\text{Log}(L_d)$ (L_\odot)	α	T_d^1 (K)	T_d^2 (K)	$\text{Log}(M_d)$ (M_\odot)	χ^2/ndf
NGC4570	6.26±0.77	0.50±0.29	27.42±10.20	71.56±14.37	4.63±3.03	0.61
NGC4578	6.43±0.86	0.50±0.28	27.35±10.07	71.06±14.27	4.90±3.45	4.85
NGC4612	6.65±0.93	0.50±0.29	27.55±10.11	70.82±14.22	5.12±3.10	9.67
NGC4621	6.52±0.29	0.99±0.01	23.42±3.26	67.98±14.92	3.91±0.67	30.17
NGC4638	6.57±0.30	0.49±0.28	27.46±10.13	68.90±14.26	4.37±1.56	6.64
NGC4649	8.53±0.03	0.42±0.28	21.70±8.31	94.25±0.75	6.48±1.02	1847.70
NGC4660	7.16±0.19	0.99±0.01	25.23±2.49	58.57±11.86	4.19±0.71	3.66
NGC4696	8.49±0.10	1.00±0.00	23.47±0.92	56.97±10.24	5.53±0.21	7.97
NGC4697	8.53±0.11	0.99±0.01	27.55±1.47	59.99±11.62	5.16±0.22	7.28
NGC4754	6.16±0.70	0.50±0.29	27.33±10.04	71.97±14.28	4.42±3.33	0.41
NGC4762	6.96±0.29	0.50±0.29	27.60±10.10	71.37±14.50	4.73±1.63	2.25
NGC5576	6.25±0.75	0.50±0.29	27.26±10.18	71.28±14.29	4.47±2.57	2.08
NGC5866	8.98±0.01	1.00±0.00	23.42±0.50	49.03±2.17	5.99±0.06	0.91
UGC07580	6.98±0.31	0.90±0.17	27.61±6.68	56.04±11.51	4.31±2.26	3.01